

# 2

## Global tropical cyclogenesis as a stochastic process

The methodological approach described in this chapter is based on the concept of tropical cyclogenesis evolution as stochastic flows of homogeneous events. The basic idea of the investigation and the formation of probability characteristics for global tropical cyclogenesis, as a signal of interdependent structure by the mathematical apparatus of random flow theory, was first proposed and developed by the present author. At first glance it would seem that there is no correlation between the proposed approach and the approaches commonly used with the aim of determining the quantitative characteristics of global cyclogenesis (e.g., year-averaged or month-averaged numbers of tropical cyclones or TCs). What actually happens is that this is not the case. The proposed method is a more generalized approach as the outlined approximations fit naturally into this scheme.

### 2.1 INFORMATION SIGNAL MODEL: SIMULATION, CUMULATION

The formation and accumulation of the analyzed process are produced as follows. By a uniform (indistinguishable) event in the given study we mean a functioning TC within its lifetime—from generation till the phase of dissipation—without detailed account of its energy and thermodynamic features. In such an event random flow is such a stochastic process, in which the temporal set consists of unit differences (impulses), taking non-negative integer values. The unit positive “jump” corresponds to a moment of onset of the unit event (generation of the TC) and the negative one is the disappearance of the event (dissipation of the TC), but the number of unit differences indicate the number of appearances (or disappearances) of events at these moments. The number of pulses occurring (events) in a time interval (24 hours in our case) is therefore a natural physical parameter, the “instantaneous”

intensity of cyclogenesis, which determines the energetics of the ocean–atmosphere interrelationship (Pokrovskaya and Sharkov, 1993a).

However, on the strength of this, the time domain of operation of a concrete TC (lifetime) is the stochastic process (possibly with its complex statistics), the probabilistic features of global cyclogenesis will to a certain degree be modified depending on accepted values of the temporal interval (temporal window of observations). In the language of statistical procedures, this approach is a method for counting the number of events and taking into account event lifetimes (Cox and Lewis, 1966; Apanasovich *et al.*, 1988).

It is important to note here that completion of the operation of a TC as a geophysical system—or, in other words, “refusal” of a system to function (work) in the terminology of popular service theory or the theory of queues—usually has external reasons (presence of land in the path of a TC or its involvement in more large-scale circulation), and such a flow of events is generally identified as a “censorial” process (Khinchin, 1963; Cox and Lewis, 1966; Cox and Oakes, 1984; Gnedenko and Kovalenko, 1987).

Since we are not interested in the detailed structure and dynamics of each individual tropical structure, on the time axis we shall represent each tropical disturbance as a pulse with unit amplitude and a random length (corresponding to the time over which the TC is active) with a random time of occurrence (generation of an individual TC).

Mathematically, this procedure for forming a signal may be written as follows:

$$N(t) = \sum \Theta(t - t_i; \tau_i) \quad (2.1)$$

where  $N(t)$  is the instantaneous intensity of cyclogenesis (the number of TCs active in a 24-hour period); and  $\Theta(t)$  is the bounded Heaviside function:

$$\Theta(t - t_i; \tau_i) = \begin{cases} 1 & t_i < t \leq t_i + \tau_i \\ 0 & t_i + \tau_i < t < t_i \end{cases} \quad (2.2)$$

where  $\tau_i$  is the lifetime of an individual TC;  $t_i$  is the time of its formation (generation); and  $t_i + \tau_i$  is the time of its dissipation.

From the physical standpoint, this procedure structures the temporal evolution of global tropical cyclogenesis as a sequence of impulses that are equal in absolute value and are shifted in time. At first glance it seems that this temporal construction of events is rather strange. However, as we will show below, it is possible to learn much about the internal (inherent) correlation features of global tropical cyclogenesis by the proposed mathematical procedure in forming such a temporal construction.

The sequence of pulses formed in this way is just an integer-valued random temporal flow of indistinguishable events. Thus, we shall proceed using a representation of the temporal sequence of the intensity of tropical cyclogenesis as a statistical signal with a complex structure. Of course, this approach is highly simplified especially when referred to actual conditions occurring in nature. Nevertheless, as noted later, it does enable us to identify the important statistical mechanisms

governing global cyclogenesis and its intra-annual variability and to detect the structural characteristics of this process on timescales from several days to 5 years (see Sections 2.2–2.4, 2.7).

To determine a concrete form of the probabilistic model of cyclogenesis (amplitude characteristics) for each studied basin for each year (in a 3-month interval), experimental histograms of the number of events  $N(t)$  were constructed and their statistical distributions approximated, with subsequent analysis of their degree of fit.

To study the possible systematic changes in time variation of the intensity of the flow of events, we shall use a graph of the function of the cumulative number of events—cumulative function (CF) (Cox and Lewis, 1966) of active TCs in a 24-hour interval)—over the period of observation (1 year):

$$F(t) = \sum_{k=1}^{N(t)} \Theta_0(t - t_k) \quad (2.3)$$

where  $N(t)$  corresponds to (2.1);  $t_k$  is the time of event generation; and  $\Theta_0(t - t_k)$  is the Heaviside function, given by:

$$\Theta_0(t - t_k) = \begin{cases} 1 & t \geq t_k \\ 0 & t < t_k \end{cases} \quad (2.4)$$

where event generation is defined as just a positive increment of  $N(t)$  ( $\Delta N(t_k) > 0$ ).

As we will indicate below, the application of the CF approach (Eqs. 2.3–2.4) in processing time series of events is highly advantageous for detecting and revealing the fine structure in the time evolution of a system's dynamics. However, there exist many such cases (e.g., economic and administrative problems during natural disasters; Pielke and Pielke, 1997) when one way of looking at a system's dynamics is more restricted—namely, under temporal averaging of the order of 1 month (or 1 year). Under these conditions, the fine dynamical features of temporal evolution (and thus the dynamical interactions that are responsible for it) can be eliminated using a proper averaging procedure.

As we have already indicated (in Chapter 1), to ascertain the number of problems of climatic interactions, it is just as necessary to obtain the quantitative values of intensities of cyclogenesis as for primary and mature forms under temporal averaging of the order of 1 month (or 1 year) or, in other words, performing the following procedure:

$$N_0(t_i; \Delta t) = \frac{1}{\Delta t} \int_{t_i}^{t_i + \Delta t} N(t) dt \quad (2.5)$$

where  $t_i$  is the beginning of the current month (year); and  $\Delta t$  is the duration of the corresponding month (year). When the life of each individual structure is less than the month, the value of the parameter for “instant” intensities of flows that occurred within the month studied will go into the simple individual tropical event amount. Thereby, information on dynamic interactions in the global system on

scales from 1 day up to 1–3 months will be lost. As we will show, with the help of wavelet analysis (Section 2.7), it is precisely these scales of interactions that are of great concern in the dynamics of global systems. Nevertheless, the monthly averaged (or yearly averaged) approach allows us to reveal a number of interesting moments that are commonly used (e.g., Elsner and Kara, 1999; Henderson-Sellers *et al.*, 1998; Gray *et al.*, 1997).

## 2.2 ANNUAL SINGLE-COMPONENT STOCHASTIC MODEL OF GLOBAL TROPICAL CYCLOGENESIS

On the basis of processing temporal sets of intensities of global cyclogenesis for annual cycles 1988–1992, the purpose of this section is to present experimental results pointing to the existence of firm Poisson laws of distribution in the annual cycle of tropical cyclogenesis and making possible determination of their parameters (Pokrovskaya and Sharkov, 1993a, 1994a).

### 2.2.1 Time series and cumulative functions of global tropical cyclogenesis

Figure 2.1 presents the graphs of temporal evolutions of flows of global cyclogenesis intensity (daily averaging) for a 5-year term from 1988 to 1992. The raw data for 1988–1992 for global tropical cyclogenesis were taken from the systematized dataset “Global-TC” (see Chapter 5 for details and Pokrovskaya *et al.*, 1993; Pokrovskaya and Sharkov, 1999d).

From Figure 2.1 it is not difficult to see that, despite external distinctions of concrete temporal sets, flows of intensity represent typical telegraphic processes from the standpoint of casual processes. Moreover, in the annual temporal cycle of tropical cyclogenesis we can recognize some general properties: between August and October of each year (for the explored 5-year cycle) there comes a period of obvious increased activity when in the World Ocean Basin there are six to ten TCs acting simultaneously (this has occurred every year since September 26, 1992). Such a high concentration of TCs in the process of tropical cyclogenesis suggests the possibility of space and time correlations as a result of the excitement and operation of vortical systems. In Section 2.2.2 we will show experimental findings of this. At the same time, it is not difficult to see that global cyclogenesis fades considerably from December on. But, despite specific intra-annual variability, it is possible to try and formulate a united probabilistic model of global cyclogenesis. The question of intra-annual variability in the flow of cyclogenesis intensity requires separate consideration (see Section 2.3).

All the mentioned temporal features of global tropical cyclogenesis have effectively emerged as a result of observations of cumulative functions (Figure 2.2a–e). To better understand the temporal behavior of tropical cyclogenesis, its time series have been on a reduced scale than those represented in Figure 2.1. We should note that the shape of the cumulative function has effectively revealed the large-scale structure of the temporal evolution of random flows.

### 2.2.2 Probability model and its parameters

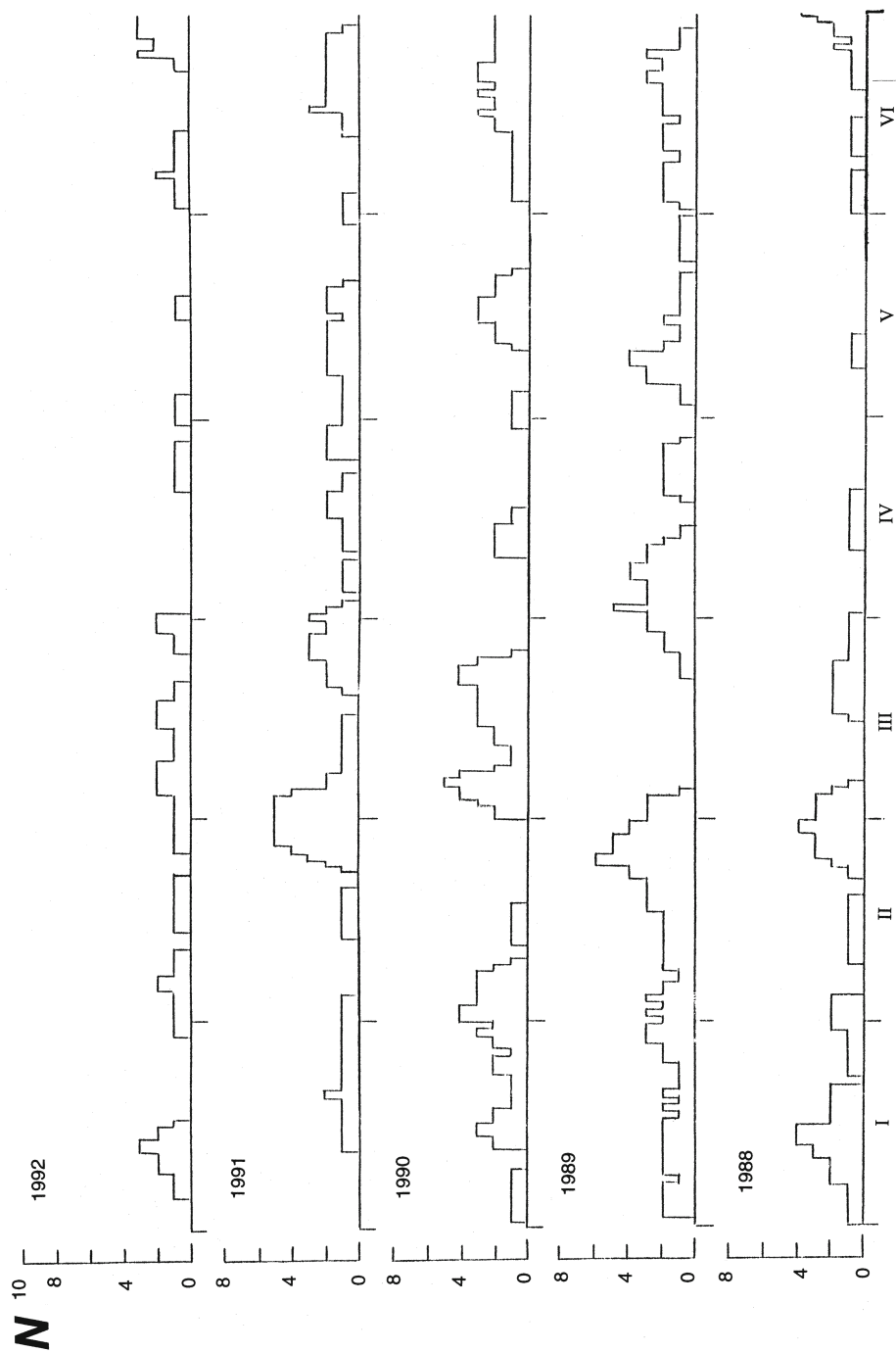
To get concrete-type probabilistic models of the physical process considered, histograms of integer parameter  $N(t)$  were built. Histograms are statistical analogues of the selective density of probability in accordance with known rules. For each group of arrays (1988–1992) sample averages and variances were calculated. The results of processing are presented in Table 2.1. External collation of sample histograms that possibly approximate the Poisson law (in the linear scale in Figure 2.3) already favor the hypothesis that the Poisson nature of the time sequence of tropical cyclogenesis can be calculated. So, in accordance with the Pearson criterion of agreement, the measure of divergence between the theoretical distribution and the experimental histogram (for 1991) is  $X^2 = 2.9$  (four degrees of freedom<sup>1</sup>) and satisfies the inequality  $X^2 < \chi^2(0.05; 4)$ . The last-mentioned fact indicates that the experimental sample set is compatible with the general set of Poisson distributions with  $\lambda = 1.7$ . In the same way, the theoretical Poisson distribution with  $\lambda = 2.0$  is satisfactorily compatible with experimental data for 1989. Here  $X^2 = 10.3$  and  $\chi^2(0.05; 6) = 12.6$ .

However, for other annual cycles (1988, 1990, and 1992 for which  $X^2$  are 34, 80, and 56, respectively), theoretical distributions are in poor agreement with observations (at the 5% confidence level). It is easy to find the reasons for divergences if we analyze the experimental histograms themselves (Figure 2.3a, c, e). Detailed consideration of histograms allows us to understand that divergences in theoretical and experimental distribution are attributable to histograms that show the number of days that are free from functioning TCs (i.e., days with  $N = 0$ ) and the lack of days when  $N = 1$  and 2. So, in 1988 there were 99 days free from TCs and in 1992, 84 days. If we rearrange the excess zeroes in the histograms to  $N = 1$ , it is possible to show that the theoretical Poisson distribution will satisfactorily be in agreement with experimental data. The physical explanation specified in the above divergences is connected with the strong inhomogeneity (understood, of course, in the statistical sense) in distributing the events (functioning TC). In other words, it is possible that the effects of clustering in the probabilistic structure of the event sequence may come into existence.

Study of the tails of the experimental distribution is of prime interest for the study of clustering effects in flows of Poisson type. Under the linear scale (Figure 2.3) these effects cannot practically be revealed. To resolve these questions we will use another presentation of experimental histograms—one on a semilogarithmic scale, as follows.

Comparison of experimental histograms and theoretical approximations executed on the semilogarithmic scale (Figure 2.4) shows that the Poisson character of the distribution of a value  $N$  is valid when the number of events (in the day) equal 6. At values  $N > 6$  the experimental histogram is greatly distinguished from Poisson distribution. This circumstance testifies to the fact that originally

<sup>1</sup> In accordance with statistical rules (Cox and Lewis, 1966), the number of degrees of freedom is defined as the number of categories in the experimental histogram minus the number of independent conditions (relationships), assessed on frequencies (for the Poisson process the number of relationships is two).



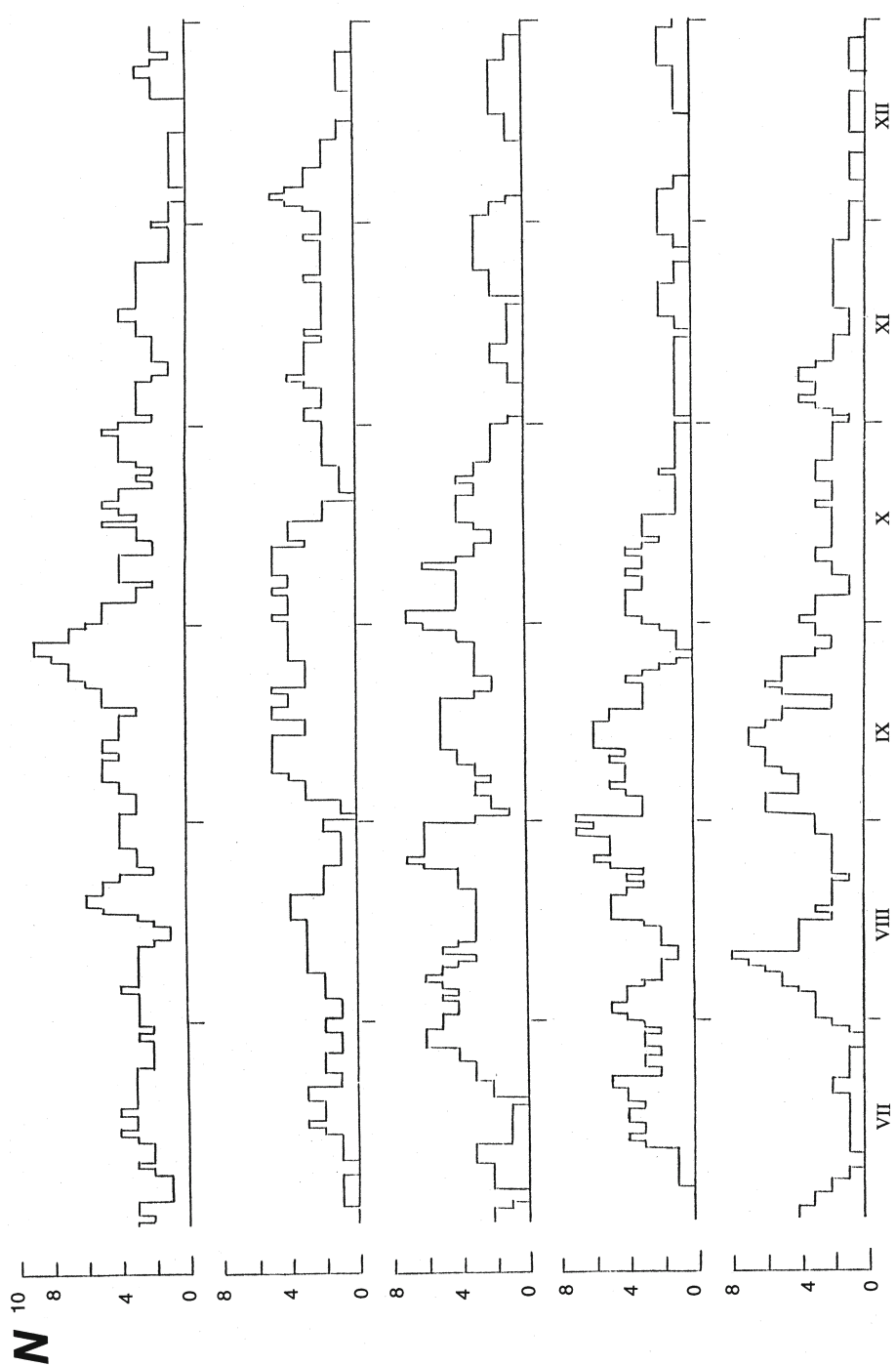


**Figure 2.1.** Annual time series of global tropical cyclogenesis intensity for 1988–1992 (from bottom to top) (from Pokrovskaya and Sharkov, 1994a).

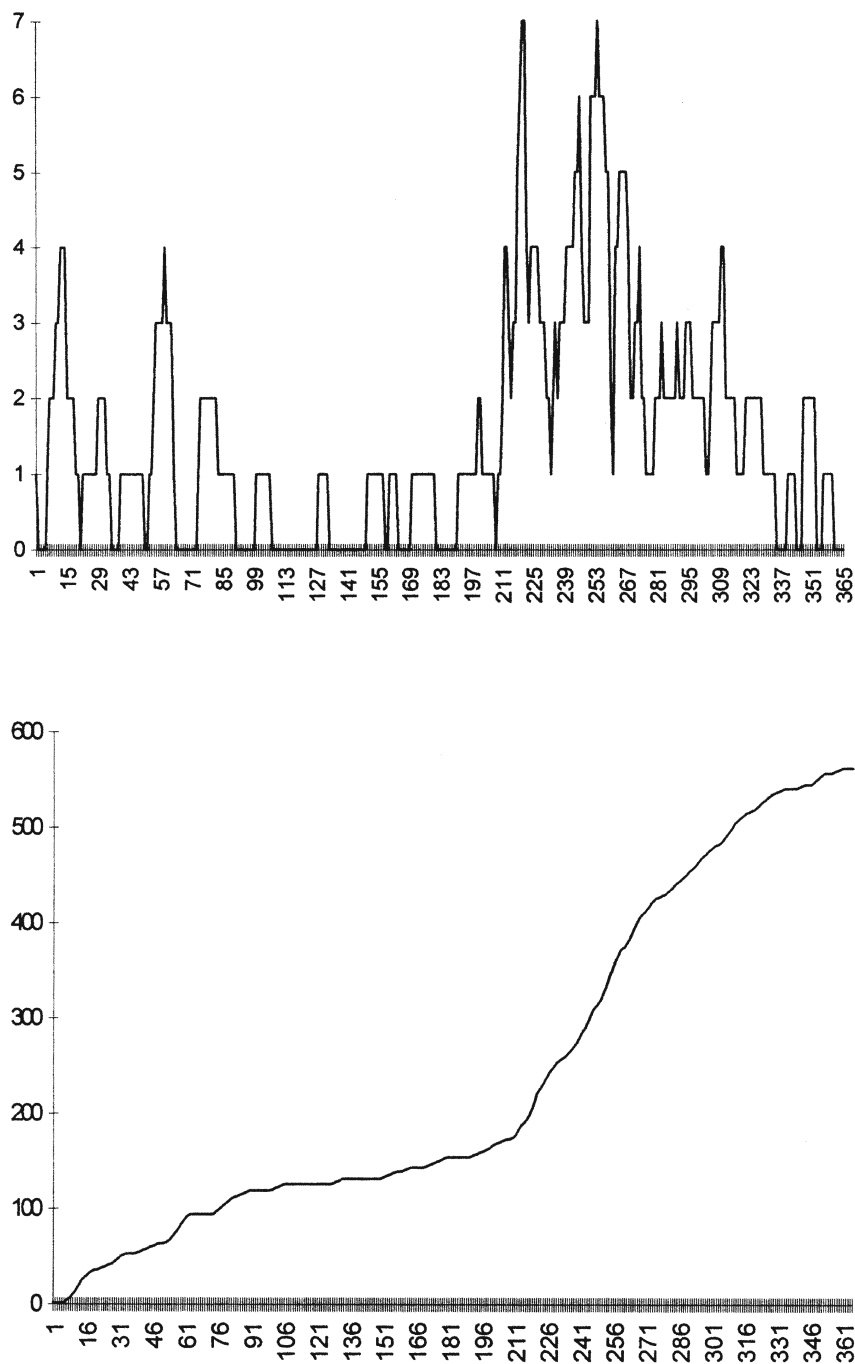


**Figure 2.2a.** Annual time series of the intensity (top) and cumulative function (bottom) of global tropical cyclogenesis for 1988.



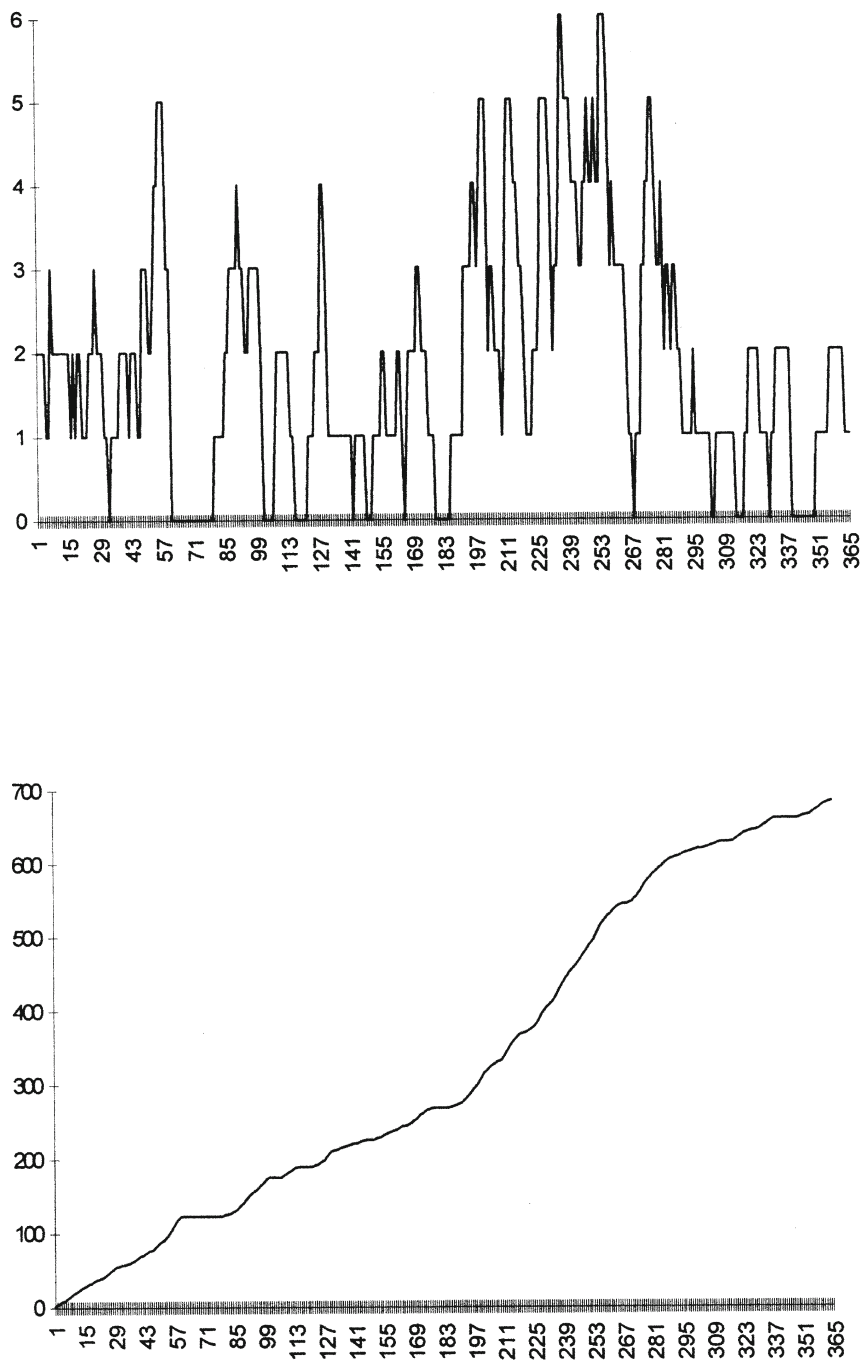


**Figure 2.2b.** Annual time series of the intensity (top) and cumulative function (bottom) of global tropical cyclogenesis for 1989.

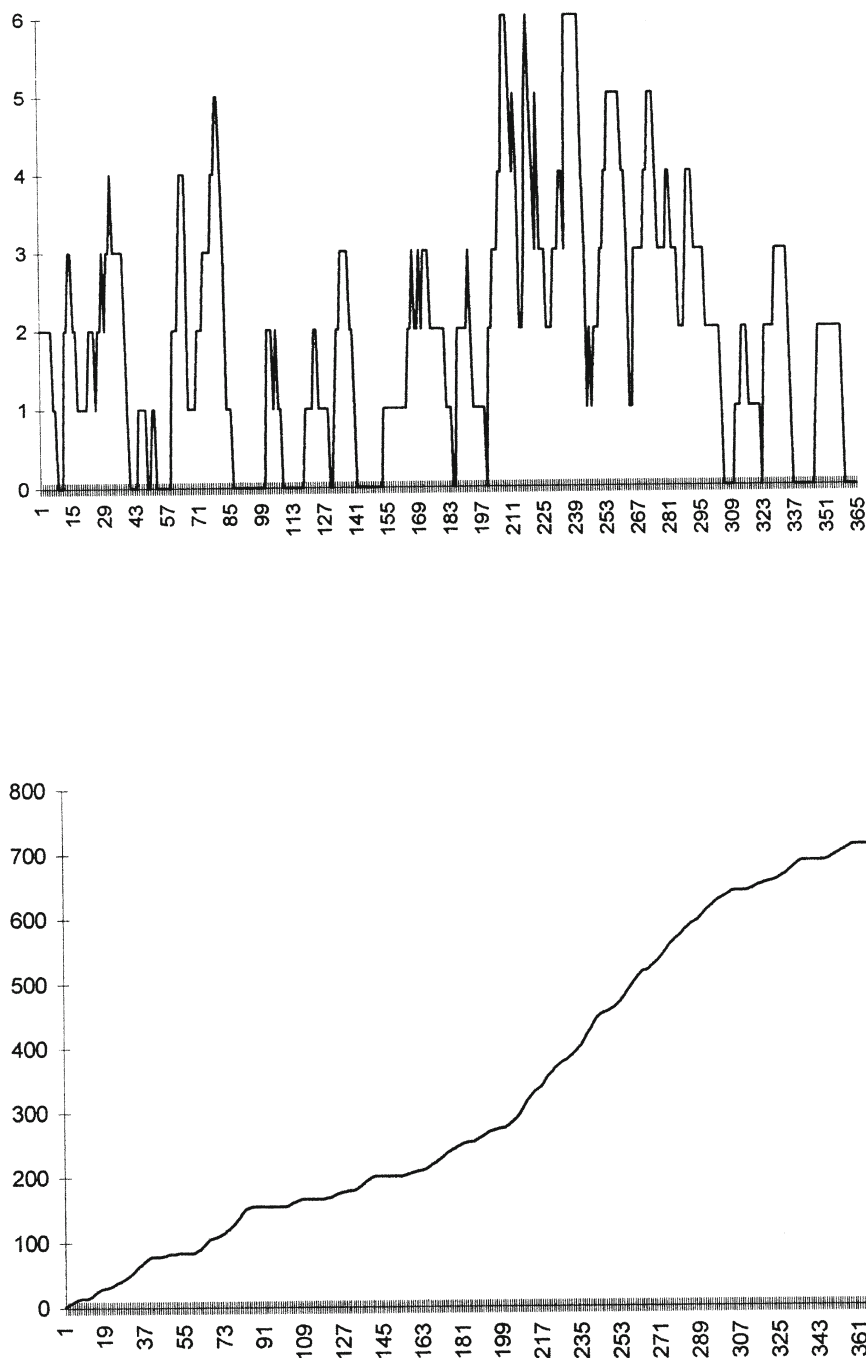


**Figure 2.2c.** Annual time series of the intensity (top) and cumulative function (bottom) of global tropical cyclogenesis for 1990.

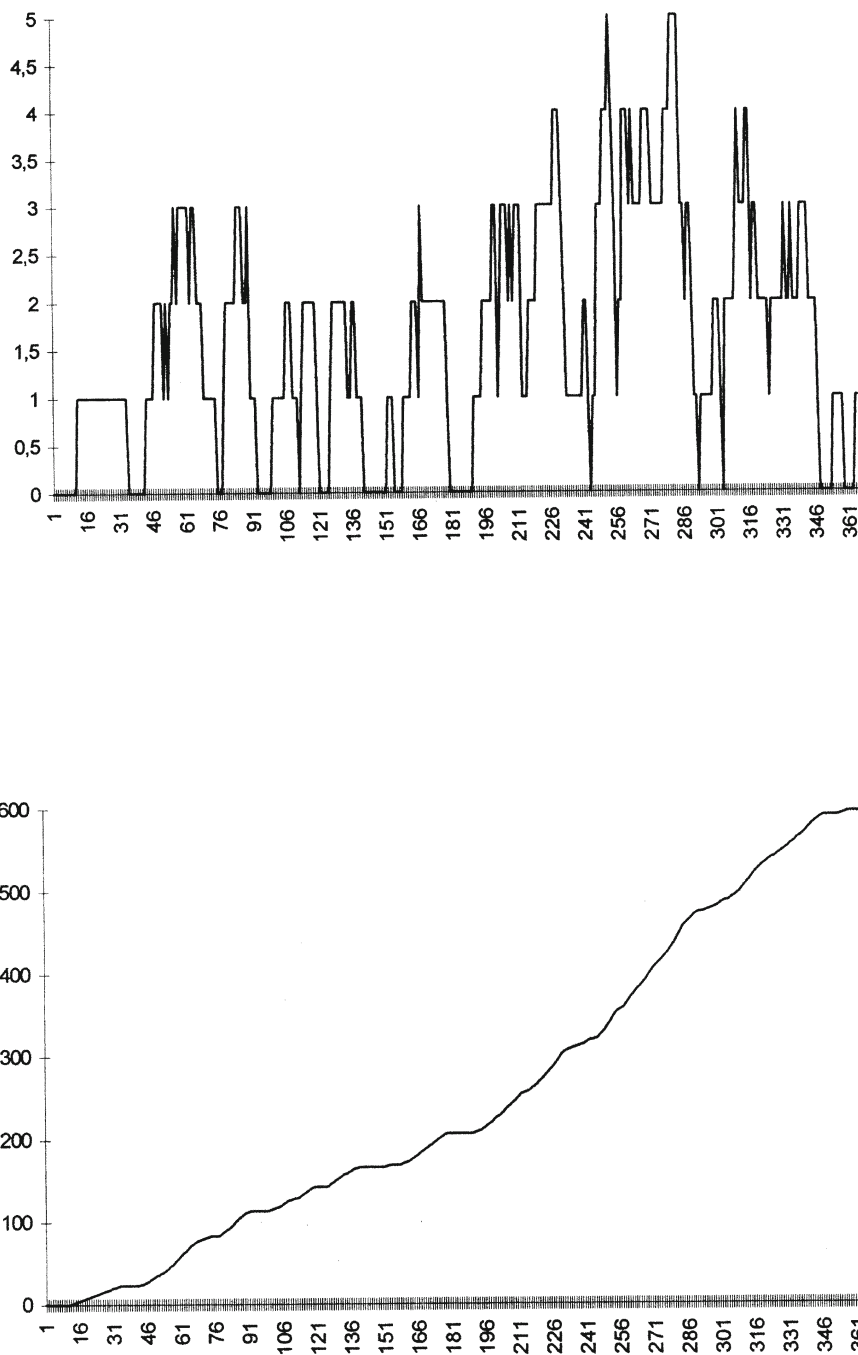


**Figure 2.2d.** Annual time series of the intensity (top) and cumulative function (bottom) of global tropical cyclogenesis for 1991.

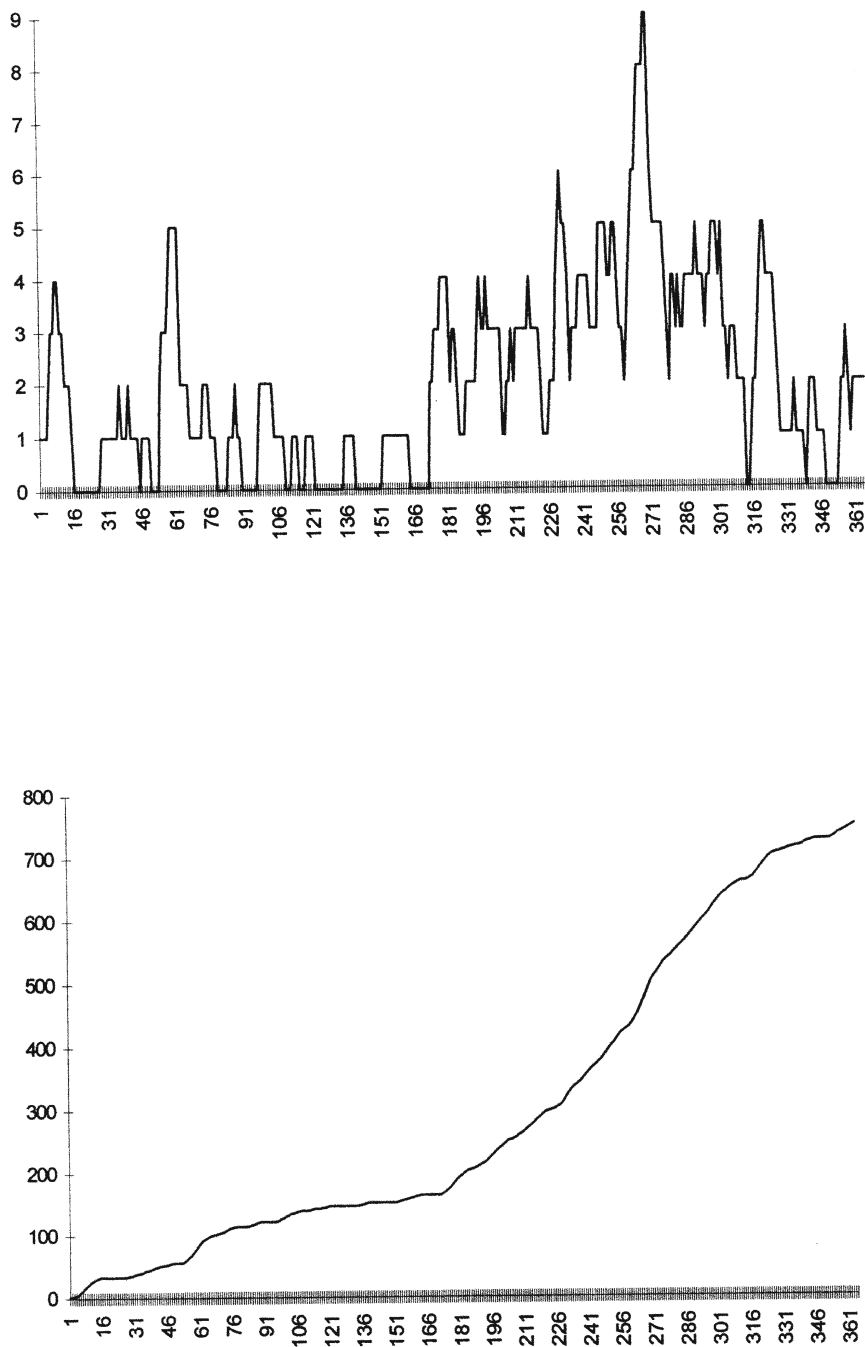


**Figure 2.2e.** Annual time series of the intensity (top) and cumulative function (bottom) of global tropical cyclogenesis for 1992.

**Table 2.1.** Parameters of distributions of global cyclogenesis intensity.

Year	Total number of occurrences	Main numerical characteristics of histograms		Parameter of approximating Poisson law
		Mean	Variance	
1988	571	1.57	2.30	1.6
1989	744	2.04	2.22	2.0
1990	741	2.03	2.75	2.0
1991	626	1.66	1.60	1.7
1992	722	1.97	3.10	2.0

*Note:* Total number of runs is 365 days. Parameter  $\lambda$  is the flow intensity. Total number of occurrences is the total amount of registered events (TCs per day) for the full period (365 days).

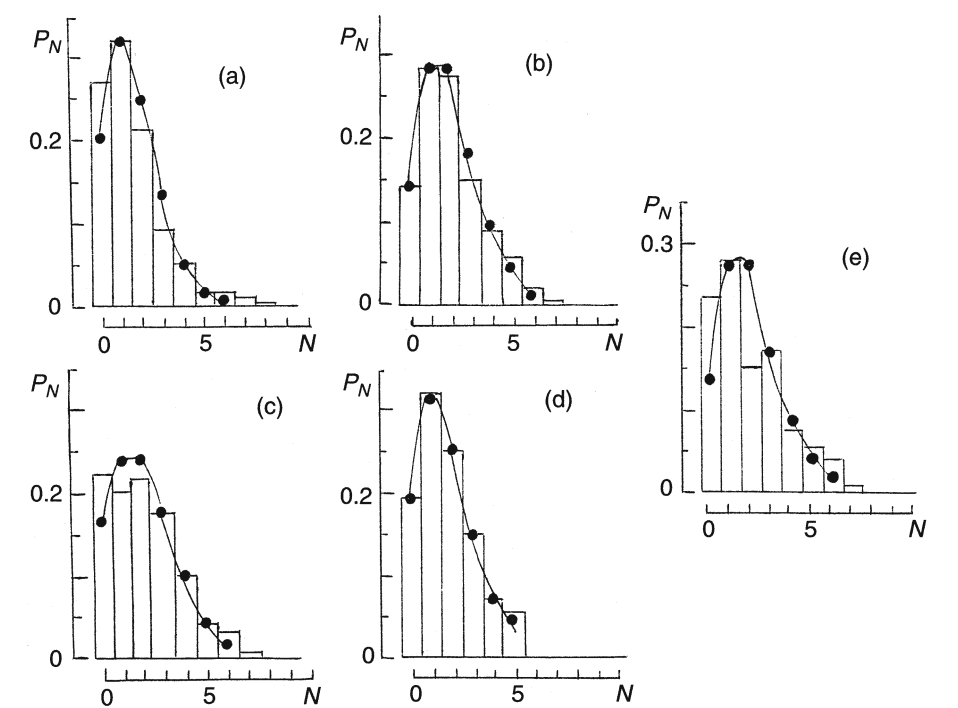


**Figure 2.3.** Sample probability densities (histograms) of cyclogenesis intensity and theoretic Poisson distributions on the linear scale. The stepped curves represent the experimental histograms. The full circles and the solid lines represent the theoretic Poisson law with the value given in Table 2.1. (a) Data for 1988; (b) for 1989; (c) for 1990; (d) for 1991; (e) for 1992 (from Pokrovskaya and Sharkov, 1994a).

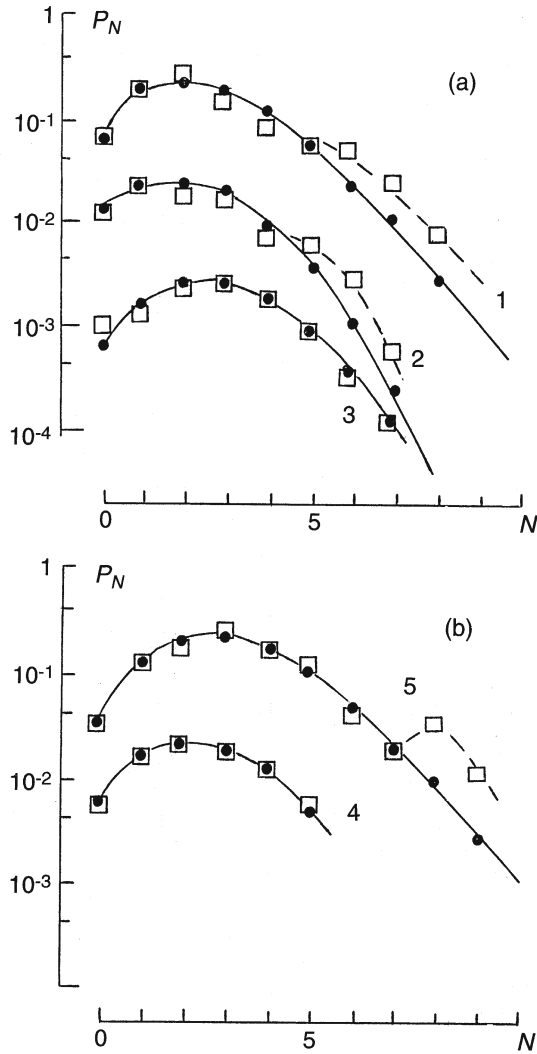


**Figure 2.4.** Sample probability densities of global cyclogenesis intensity and theoretic Poisson laws on semilogarithmic scales. The open squares and dotted lines represent the experimental histograms. The full circles and solid lines represent the theoretic Poisson law with the value given in Table 2.1. (a) Data for 1988–1990; (b) for 1991–1992; (1) data for 1988; (2) data multiplied by  $10^{-1}$  for 1989; (3) data multiplied by  $10^{-2}$  for 1990; (4) data multiplied by  $10^{-1}$  for 1991; (5) for 1992 (from Pokrovskaya and Sharkov, 1994a).

independent events (recall the functioning TC) gain correlation relationship (either in space or time). Under these circumstances the Poisson characteristic of the ordinarieness of flow breaks down (see Section 2.2.4). A similar situation (deviation from the Poisson distribution under  $N = 6$ ) is observed for the experimental histograms of 1988 and 1989 (for 1991  $N > 6$  was not observed). In both the process of develop-

ment and in the operation of tropical vortical systems clustering effects were discovered earlier by experiment (Minina, 1983; Pokhil, 1990, 1996; Carlowicz, 1995).

The particularities discovered require more detailed analysis of the structure of Poisson-type flows regarding not only amplitude but also temporal probabilistic features.

In view of the significant number of recorded events in experimental data ( $n > 500$ , see Table 2.1), point evaluation of the intensity of Poisson distribution flow  $\lambda$  and its confidence levels can be executed by means of a method based on normal approximation for the Poisson distribution with the equation:

$$\lambda t_0 = n + 1/2 C_{\alpha/2}^2 \pm C_{\alpha/2} n^{1/2} \quad (2.6)$$

where  $t_0$  is the total number of runs; and  $C_\alpha$  is the upper  $\alpha$ -quantile of unit normal distribution. Using this correlation under confidence levels of probability of 95%, we can evaluate the confidence level intervals for  $\lambda$ . They are equal to  $\pm(0.12-0.14)$ . Mean values of  $\lambda$  are provided in Table 2.1; the root-mean square (r.m.s.) of  $\lambda$  is 0.6–0.7.

### 2.2.3 Interannual variabilities

In this section we will consider the question of interannual variations in the intensity of Poisson flow, which is important from the standpoint of global energy exchange in the ocean–atmosphere system. Essentially, it is necessary to take or reject a hypothesis on the accessories of all revealed Poisson flows in the united general set. To resolve this problem we use a method that requires a fixed number of events when using dispersion relations and the F-distribution, respectively.

We know (Cox and Lewis, 1966) that if the total number of event occurrences of matching flows is great ( $n \gg 1$ ), it is possible to use a logarithmic transformation for the dispersion relation:

$$Z = \log R = \log(\lambda_2/\lambda_1) + \log(n'_0 t'_0''/t'_0 n''_0) \quad (2.7)$$

where  $\lambda_1$  and  $\lambda_2$  are the parameters of two independent Poisson processes; and  $t'_0$  and  $t''_0$  are observed time runs ( $t'_0 = t''_0 = 366$ ), for which  $n'_0$  and  $n''_0$  events have occurred accordingly. In this case the value  $Z$  will have a normal distribution with the average value and standard variance, respectively  $\frac{1}{2}(1/n'_0 - 1/n''_0)$  and  $(1/n'_0 + 1/n''_0)^{1/2}$ . Using this procedure to analyze most of the distinguishing intensities for 1988 and 1989 (see Table 2.1), we get 95% confidence levels for the correlation  $\lambda_2/\lambda_1$  as (1.62; 1.006). It is not difficult to see that the selective equation  $\lambda_2/\lambda_1$  is 1.29 and that it falls in the specified confidence interval. This means that the significant difference (within the framework of the specified approach) in correlations of the intensities of flows is not observed. A similar conclusion holds for correlations of the other annual intervals under investigation.

### 2.2.4 Poisson random model

We emphasize from the outset that the case in point is a measured parameter—the intensity of tropical cyclogenesis—possessing a sufficiently complex procedure of accumulation (shaping). The value of this parameter characterizes not only the intensity of processes of the birth and death of individual TCs but also contains the statistics of TC timescales. By the structured element of the time sequence under investigation is meant a variation in intensity of the unit ( $\Delta N = 1$ ). This change is not, generally speaking, associated directly with the generation of individual TCs.

In spite of the rather complicated structure of signal accumulation, as a whole the amplitude features of tropical cyclogenesis can be described within the framework of sufficiently simple physical Poisson-type models (e.g., fluctuation density in an ideal gas and fluctuation noise in electrical circuits). Of course, the process can be described within the framework of the univariate controlling probabilistic equation of birth–death (Bharucha-Reid, 1960). From equilibrium resolution it appears that the average value of the intensity of flow is the ratio of probabilities of both birth and death.

The Poisson approximation is useful for estimating probabilities associated with rare or extreme events (Bharucha-Reid, 1960; Feller, 1968; Zolotarev, 1983). The Poisson distribution describes the number of times that some event occurs as a function of time, where the events occur at random times.

The simplest whole number Poisson point process  $\{M(t), 0 \leq t < +\infty\}$  is specified by three conditions:

1. The process is ordinary (i.e., events must occur only once in any increasingly small time interval):

$$P\{M(\Delta t) = 1\} = \lambda \cdot \Delta t + o(\Delta t) \quad (2.8)$$

$$P\{M(\Delta t) > 1\} = o(\Delta t) \quad (2.9)$$

where  $\lambda$  is some positive quantity. The symbol  $o(\Delta t)$  represents the term that has a higher order value than  $\Delta t$ . In other words, this condition of Poisson flows means that the events in Poisson processes are very scarce and, hence, these events do not interact with each other.

2. The process is steady state (i.e., probability characteristics are independent of time).
3. The process possesses the following property: the number of events occurring in any time interval is independent of the number occurring in any other non-overlapping interval (“a lack of consequences”).

Based on these conditions it can be shown (Bharucha-Reid, 1960) that the probability  $P_k(t)$  of exactly  $k$  occurrences (points) over a time semi-interval  $(0, t]$  is given by the cumulative probability distribution function (Poisson law):

$$P_k(t) = P[M(t) = k] = \frac{(\lambda t)^k \cdot e^{-\lambda t}}{k!}, \quad k = 0, 1, 2, \dots, \infty \quad (2.10)$$

where the factorial  $k$  is denoted by  $k!$



From this equation it follows that the probability of the lack ( $k = 0$ ) of an event occurring in the semi-interval  $\tau$  is:

$$P_0(\tau) = \exp(-\lambda\tau) \quad (2.11)$$

The expected value  $m$  and the variance  $D$  of the Poisson distribution are equal to one another:

$$m = D = \lambda t \quad (2.12)$$

As  $m$  is the average number of occurrences in the time semi-interval  $(0, t]$ , so the parameter:

$$\lambda = \frac{m}{t} \quad (2.13)$$

may be considered as the average number of events occurring in the unit interval. Hence,  $\lambda$  is often denoted as the Poisson process intensity.

A number of various extensions of the Poisson distribution have been studied (Bharucha-Reid, 1960; Feller, 1968; Korn and Korn, 1961; Cox and Lewis, 1966). We consider two such extensions for the purpose of detailed processing of the global tropical cyclogenesis time series:

- an inhomogeneous Poisson process; and
- a filtered Poisson process.

The Poisson distribution is spoken of as an inhomogeneous process if its intensity is dependent on time  $\lambda(t)$ . For such an inhomogeneous process the probability  $P_k(t)$  of exactly  $k$  occurrences over a time semi-interval  $(0, t]$  is given by the following equation:

$$P_k(t) = \frac{1}{k!} \left( \int_0^t \lambda(\tau) d\tau \right)^k \cdot \exp \left( - \int_0^t \lambda(\tau) d\tau \right), \quad k \geq 1 \quad (2.14)$$

The expected value  $m(t)$  and the variance  $D(t)$  of this Poisson distribution are equal:

$$m(t) = D(t) = \int_0^t \lambda(\tau) d\tau \quad (2.15)$$

The filtered Poisson process  $\{\xi(t); t \geq 0\}$  can be expressed by the following equation:

$$\xi(t) = \sum_{i=1}^{M(t)} h(t, t_i, a_i) \quad (2.16)$$

where  $\{M(t), t \geq 0\}$  is, in the general case, an inhomogeneous Poisson process with inhomogeneous intensity  $\lambda(t)$ ;  $\{a_i\}$  is a sequence of random functions that are independent of  $\{N(t); t > 0\}$ ; and  $h(t, t_i, a_i)$  is a deterministic function of the three variables.

For practical implementation, the parameters of the equation  $\xi(t)$  allow the following interpretation:

- $t_i$  is the time when the random event occurs;
- $a_i$  is the amplitude of the elemental signal associated with this event;
- $h(t, t_i, a_i)$  is the value of the elemental signal (at time  $t$ ) governed by this event;

- $\xi(t)$  is the value (at  $t$ ) of the sum of elemental signals governed by the events that occurred over the temporal semi-interval  $(0, t]$ .

These processes are often termed “fluctuation noise” or “Schottky noise” (Bharucha-Reid, 1960; Korn and Korn, 1961).

This was the very same approach that was used to establish the information signal for global tropical cyclogenesis (see Section 2.1). For the instantaneous intensity of cyclogenesis (Eq. 2.1),  $h(t, t_i, a)$  was the bounded Heaviside function. The amplitude  $a_i$  of the elemental signal associated with the event is equal to 1 and the event’s time  $t_i$  is the time of TC onset.

For the cumulative function (Eq. 2.3),  $h(t, t_i, a)$  was the Heaviside function. The event time  $t_i$  is the time of positive increment of  $N(t)$  ( $\Delta N(t) > 0$ ) as distinct from the case of instantaneous intensity.

As mentioned in Section 2.1, the qualitative and quantitative analysis of cumulative functions has been applied with much success to the study of possible systematic variability in the temporal variation of time series intensity (Cox and Lewis, 1966). The efficiency of this method depends upon the fact that the shape of the cumulative function is acutely sensitive to temporal variation. Using time-dependent plots of cumulative functions, estimations of the integral and differential intensities of random processes may be determined from graphical displays of cumulative experimental data.

Striking examples of what can be achieved using analyses of cumulative functions are presented in Sections 2.2.1 and 2.6.1.

As a direct consequence of the Poisson approximation, tropical cyclogenesis possesses features known from the theory of Poisson flows: variation in intensities does not depend on the number of existing structured elements, on their previous history, or on the system’s condition. Also, the process satisfies ordinariness characteristics.

Variation in experimental histograms from the purely Poisson models explored above is highly symptomatic. There can be, as stated above, two types: an excess of zeroes and an excess of experimental tails of histograms above the Poisson branch of distribution. The first type of variation is connected with the time unsteady state of the process; the second can be interpreted as a break in ordinariness characteristics. In other words, the probability of the simultaneous origin of two or more events is not small and is finite. This is easily observable by analyzing the temporal sets of global cyclogenesis (Figures 2.1 and 2.2) for the July–September period of any annual cycle.

Note that the obtained results refer to daily interval partitioning of the time axis. By averaging for grid intervals, the statistics of the amplitude features of global cyclogenesis intensity can be greatly transformed so as to account for the change in the “contribution” statistics of lifetime (it can, in general, drop out of consideration) and to account for the statistics of time of TC genesis as well.

Besides the technique used in this approach for the accumulation of data employing a method that accumulates the number of events, there exist many other areas that need resolution. So, for example, the formation of a flow by

recording the moments of occurrence of separate events (TC generation)—the method of recording the births of events—is of concern in the solution of prognostic tasks. The flow generated by recording the births of events will contain more “pure” information on the statistics of TC generation and its properties as a whole will differ from the properties of the flows of intensity mentioned above.

## 2.3 ANNUAL TWO-COMPONENT STOCHASTIC MODEL OF GLOBAL TROPICAL CYCLOGENESIS

As we might expect, the attempt to generate unified (within the limits of a single year) probabilistic models of global tropical cyclogenesis meets with particular difficulties that can be bypassed, having considered two timeframes in the annual cycle that clearly have different intensities in the process of cyclogenesis: from January till July (interval I) and from August till December (interval II) (Pokrovskaya and Sharkov, 1994b).

### 2.3.1 Two-component probability model and its parameters

For detection of a particular kind of probabilistic model of the physical process under consideration, histograms of the integer parameter  $N(t)$ , being statistical images of the sample density of probabilities, were constructed according to known rules. For each group of sets for intervals I and II for each year (1988–1992) a sample mean and variances were calculated. Processing outcomes are shown in Table 2.2. External comparison of sample histograms with the possible (probable) approximating Poisson law (in a linear scale, see Figures 2.5 and 2.6) already favors the hypothesis that the Poisson character of the temporal sequence of tropical cyclogenesis can be considered. So, in line with a goodness-of-fit test of the Pearson criterion, the deviation of a theoretical distribution and experimental histogram for the data for interval II (1990–1991) satisfies the inequality  $X^2 < \chi^2(0.05)$ . This proves that experimental sampling is compatible with the general set of Poisson distributions having the values of  $\lambda$  indicated in Table 2.2. The satisfactorily theoretical Poisson distribution is in agreement with the experimental dataset for interval II (1988–1989), but at a broader window of reliability ( $\alpha = 0.01$ ).

As for the timeframe of interval I, the situation here is worse than with interval II. Here, the parent distributions of the Poisson distribution satisfactorily agreed with the experimental histograms for 1989 ( $\alpha = 0.05$ ) and 1990 ( $\alpha = 0.01$ ). But it poorly agreed with the outcomes of observations for 1988, 1991, and 1992.

It is an easy matter to find the reasons for divergences if we analyze experimental histograms (Figure 2.6). Detailed consideration of histograms allows us to understand that the divergences between theoretical distributions and the experimental dataset are explained by some kind of “non-uniformity” (understood in the statistical sense, of course) of the temporal distribution of events (operating TCs).

**Table 2.2.** Parameter of distribution of global tropical cyclogenesis (two-component model).

Year	Intra-annual interval	Total number of occurrences	Main numerical characteristics of histograms		Parameter approximating Poisson law	Measure of deviation of Pearson's criterion
			Mean	Variance		
1988	I	232	1.09	0.96	1.10	12.06
	II	376	2.46	3.17	2.50	17.23
1989	I	387	1.83	1.68	1.80	5.14
	II	337	2.20	2.55	2.20	12.21
1990	I	312	1.48	1.82	1.50	15.26
	II	387	2.53	3.01	2.50	10.28
1991	I	265	1.26	0.90	1.26	25.83
	II	373	2.45	1.80	2.50	4.13
	I	246	1.16	1.06	1.16	26.31
	II	495	3.21	3.09	3.20	9.86

*Note:* Total number of runs for interval I (January–July) is 213 days and for interval II (August–December) is 153 days.

In other words, the effect of some clusterization in a probabilistic temporal sequence of events is possible. So, in the data of 1988, the excess of the “four-in-hand” ( $N = 4$ ) structural elements of sampling is observed. In 1992, on the contrary, there is an excess of triple units ( $N = 3$ ) and disadvantage twin ( $N = 2$ ) units. In 1991 there was a grouping (clusterization) (Figure 2.5) of five units ( $N = 5$ ) within 1 week (end of February–beginning of March) or, in other words, an eruption in the activity of cyclogenesis against the background of a rather languid process. These effects are also responsible for the divergence of theoretical models and observational data (for interval I).

Studying the tails of experimental distributions, which at the linear scale (Figures 2.5 and 2.6) practically cannot be detected, is of most interest from the point of view of research into clusterization effects in Poisson-type flows. For the solution of these problems we shall take advantage of another representation of experimental histograms: namely, a semilogarithmic scale.

The study of comparability of experimental histograms and theoretical approximation models for the active period of the year, made on a semilogarithmic scale (Figure 2.7), has shown that the Poisson character of a density function of value  $N(t)$  is retained if the values of the number of events (per day) equal 6–7. At values  $N > 7$  experimental histograms differ essentially from the pure Poisson model. This proves that originally independent events (recall operating TCs) gain correlation connections (either in space or time) and, thus, the Poisson property of ordinarieness of flow (see Section 2.2.4) is upset. Such a clusterization of generation and operation of tropical vortical systems was earlier detected from observational

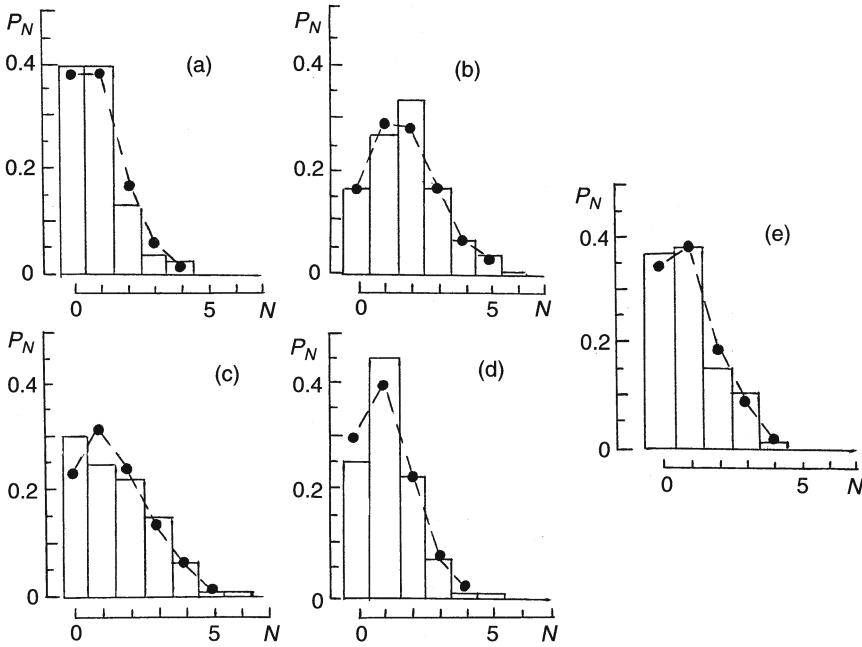


**Figure 2.5.** Sample probability densities of global cyclogenesis intensity and theoretic Poisson laws on linear scales for the intra-annual interval I. Stepped curves represent experimental histograms. Full circles and dotted lines represent theoretical Poisson laws with the values given in Table 2.2. (a) Data for 1988; (b) for 1989; (c) for 1990; (d) for 1991; (e) 1992 (from Pokrovskaya and Sharkov, 1994b).

data of the conditions for cyclogenesis in the Pacific Ocean (Minina, 1970; Pokhil, 1990, 1996).

These features require more detailed study not only of the amplitude but also the temporal probabilistic characteristics of Poisson-type flow patterns.

In view of the considerable sample size of the number of events in the experimental data ( $n > 200$ , see Table 2.2) point estimation of the intensity of a flow of Poisson distribution  $\lambda$  and its confidence level boundaries can be executed (made) by using a method grounded on the normal approximation of Poisson distributions (Cox and Lewis, 1966), by asking the question:

$$\lambda t_0 = n + \frac{1}{2} C_{\alpha/2}^2 \pm C_{\alpha/2} n^{1/2} \quad (2.17)$$

where  $t_0$  is the total number of runs (see Table 2.2); and  $C_\alpha$  is the upper  $\alpha$ -quantile of a unit normal distribution. Using this ratio at a confidence level probability of 95%, we get estimations of confidence intervals for  $\lambda$ . They were  $\pm(0.14-16)$  for interval I and  $\pm(0.22-0.28)$  for interval II. The average values of  $\lambda$  are listed in Table 2.2; the r.m.s of  $\lambda$  is equal to 0.06–0.07 for interval I and 0.11–0.14 for interval II.

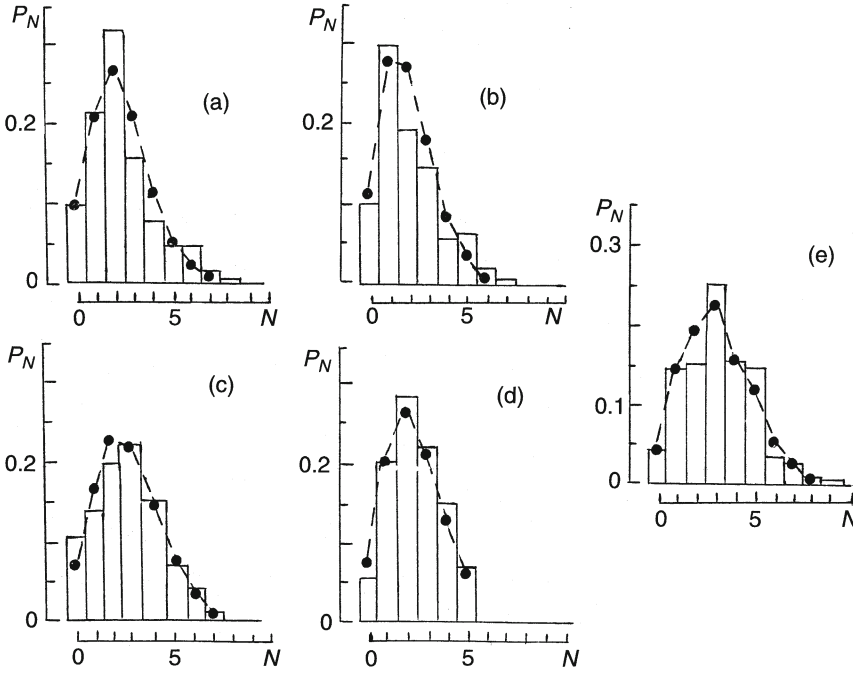


**Figure 2.6.** Sample probability densities of global cyclogenesis intensity and theoretic Poisson laws on linear scales for intra-annual interval II. See symbols and notations in [Figure 2.5](#) (from Pokrovskaya and Sharkov, 1994b).

### 2.3.2 Interannual variabilities for the two-component model

Let us consider the important problem of interannual variations in the intensity of a Poisson flow simulating tropical cyclogenesis from the point of view of global exchange in the ocean–atmosphere system. Essentially, it is necessary to accept (or reject) a hypothesis about fitting all Poisson models to a united (for 5 years) general set. To solve this we use a method based on the time of occurrence of a fixed number of events by using a variance ratio and F-distributions, respectively.

We know (Cox and Lewis, 1966) that if the sampling volume of the number of events for related flows is great ( $n \gg 1$ ), it is possible to take advantage of the logarithmic transformation for a variance ratio:

$$Z = \log R = \log(\lambda_2/\lambda_1) + \log(n'_0 t''_0 / t'_0 n''_0) \quad (2.18)$$

where  $\lambda_1$  and  $\lambda_2$  are the parameters of two Poisson independent processes; and  $t'_0$  and  $t''_0$  are the observable timeframes ( $t'_0 = t''_0 = 213$  for interval I and 153 for interval II), for which  $n'_0$  and  $n''_0$  events have also taken place, respectively. Thus,  $Z$  will have a normal distribution with average value and reference deviation of  $\frac{1}{2}(1/n'_0 - 1/n''_0)$  and  $(1/n'_0 + 1/n''_0)^{1/2}$ , respectively. Using this procedure for the

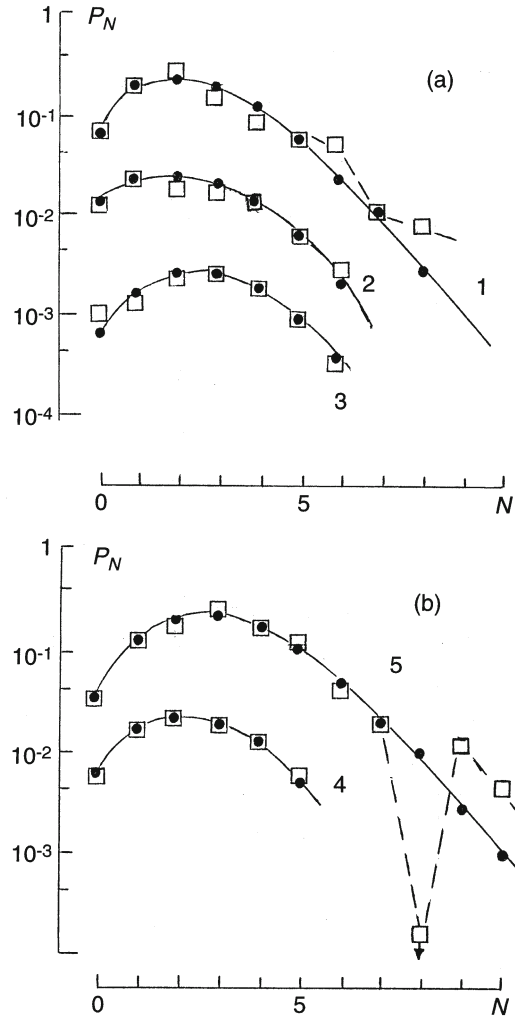


**Figure 2.7.** Sample probability densities of global cyclogenesis intensity and theoretic Poisson laws on semilogarithmic scales for intra-annual interval II. Open squares and dotted lines represent experimental histograms. Full circles and solid lines represent the theoretic Poisson law with the value given in Table 2.2. (a) Data for 1988–1990; (b) data for 1991–1992; (1) data for 1988; (2) data multiplied by  $10^{-1}$  for 1989; (2) data multiplied by  $10^{-2}$  for 1990; (4) data multiplied by  $10^{-1}$  for 1991; (5) data for 1992 (from Pokrovskaya and Sharkov, 1994b).

most different intensities for 1988 and 1989 (interval I) we find that the 95% confidence levels for ratio  $\lambda_2/\lambda_1$  are equal to (2.6; 1.2). It is not difficult to see that the sample relation  $\lambda_2/\lambda_1$  is equal to 1.63 and falls in the indicated confidence interval. By this we mean that no significant difference (within the framework of the indicated approach) in the ratio of the intensity of flow is observed.

For interval II the greatest differences in values of the intensity of flow are observed between 1989 and 1992. By following a similar procedure to Table 2.2, we find that the sample value  $\lambda_2/\lambda_1$  is equal to 1.43, whereas the 95% confidence interval is put in the range 2.18 and 1.14.

However, we emphasize that the criterion used to distinguish flow intensity is too “soft” and it makes sense to take advantage of other procedures. It is not difficult to see that application of the double  $t$ -criterion for the above-mentioned sampling would specify significant differences between the second intervals for 1988 and 1989. Thus, the problem of interannual variability requires further and more detailed analysis.

It has been found experimentally that the probabilistic characteristics of the amplitude of global cyclogenesis exhibit steady intra-annual variability and can be described within the framework of two series of Poisson approximations with steady parameters for flow intensity.

## 2.4 TROPICAL CYCLOGENESIS OF THE NORTHERN AND SOUTHERN HEMISPHERES

The first purposeful studies of cyclogenesis as a stochastic flow have shown a complex hierarchical structure of global tropical cyclogenesis and have allowed the formation of preliminary statistical–quantitative models (see Sections 2.2 and 2.3).

As for tropical cyclogenesis, considering each hemisphere separately, qualitative considerations can be applied over time to the non-uniform contribution to global cyclogenesis areas of northern hemisphere (NH) and southern hemisphere (SH) basins. At the present time, the problem of showing distinctions in the intensity of cyclogenesis of both hemispheres is currently connected with determination of the role of global circulations and ENSO (El Niño–Southern Oscillation) phenomena in forming tropical cyclogenesis (Henderson-Sellers *et al.*, 1998; Gray *et al.*, 1997).

On the basis of processing temporal sets of the intensity of tropical cyclogenesis, determined in the basins of the two hemispheres over a 15-year term (1983–1997), Pokrovskaya and Sharkov (1999b) have presented experimental findings on particularities in the structure of signals which reflect the operation of hemisphere cyclogenesis, as well as on intra-annual and interannual particularities of the contribution by both hemispheres to global tropical cyclogenesis.

For the procedure of accumulation and formation of a stochastic signal we use the approach developed in Section 2.1 and in Chapter 5.

Raw data for 1983–1997 on global cyclogenesis were selected from the systematized database Global-TC of remotely observed data on global tropical cyclogenesis (Pokrovskaya and Sharkov, 1999d).

### 2.4.1 Time series and cumulative functions for hemisphere cyclogenesis

Figure 2.8 presents graphs showing temporal evolutions of flows of intensity  $N(t)$  and of functions of an accumulating number of events  $F(t)$  for tropical cyclogenesis



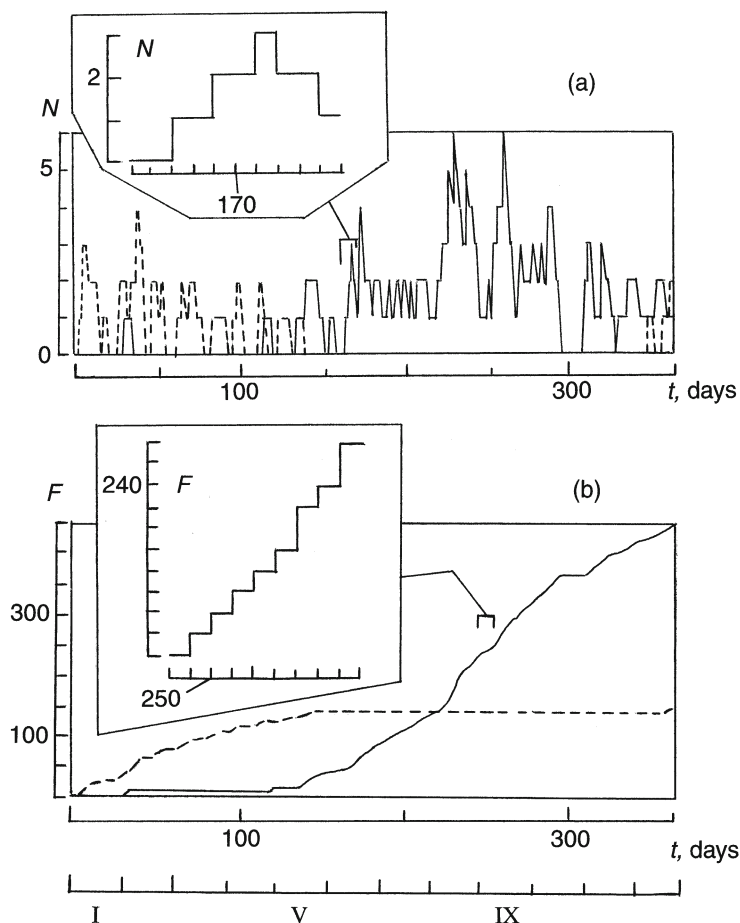


**Figure 2.8.** Annual time series of the intensity (a) and cumulative function (b) of tropical cyclogenesis for northern and southern hemispheres for 1986. Solid and dotted lines represent northern and southern hemisphere data accordingly (from Pokrovskaya and Sharkov, 1999b).

in the NH and SH (daily averaging) for 1986. This year is chosen as a distinctive example. Analysis of all 15-year (from 1983 to 1997) temporal cycles conducted by the present author shows that all explored annual samples of flows of intensity present themselves as typically telegraphic processes (Figure 2.8a). The detailed structure of the intensity and functions of a number of accumulating events are presented in increasing (daily) scale on insets to the corresponding graphs (Figure 2.8a–b).

In the annual cycle of hemispherical tropical cyclogenesis some general lines are tracked. So, in August–December of each year in NH basins a period of increased activity clearly exists, but for SH basins the activity is clearly reduced. For the first

half of a given year the reverse is true for NH basins where cyclogenesis is weak in comparison with its maximum in the second half of the year, but for SH basins the season of increased activity sets in. These particularities manifest themselves particularly graphically when considering the time evolutions of accumulation functions of a number of events (Figure 2.8a–b), where the time derivative of  $F(t)$  points to the differential intensity of the process.

Another important particularity of tropical cyclogenesis is its intermittent nature, which particularly graphically manifests itself in the analysis of temporal sets of accumulation functions of the number of events. Such an effect was first discovered during analysis of the time dynamics of tropical cyclogenesis in the Pacific for 1990–1991 (Pokrovskaya and Sharkov, 1996a).

Analysis of a 15-year period of the evolution of global cyclogenesis shows that intermittent effects in cyclogenesis on both a daily and monthly scale are universal phenomena that can be considered in the same way as global (or hemispherical) cyclogenesis (the same applies for their regional component). To show the quantitative features of this process, Pokrovskaya and Sharkov (1996a) proposed using two approaches: a differential one and an integral one (for corresponding time intervals). We will use these approaches in Section 2.4.3.

#### 2.4.2 Probability model and its parameters

To show a concrete type of probabilistic model for cyclogenesis (amplitude features) in the NH and SH and for each temporal interval (interval I from January to July and interval II from August to December during 1983–1997), experimental histograms showing integer numbers of events  $N(t)$  and approximating their statistical distribution—by subsequent analysis and degrees of agreement—were built. Moreover, the average and variances for each group of arrays were calculated. Processing results are presented in Tables 2.3–2.6.

Collation of selective histograms with the possible approximating Poisson law on linear and semilogarithmic scales (Figure 2.9) favors the hypothesis of the Poisson nature of amplitude fluctuations of intensity  $N(t)$  for tropical cyclogenesis. So, in accord with the Pearson criterion of agreement, analyzing the measure of divergence in the theoretical distribution and experimental histograms for a given cyclogenesis for NH and SH for 1983–1997 points to the fact that the experimental samples are compatible with the general set of Poisson distributions with values  $\lambda$ , as specified in Figure 2.9a–d. However, detailed analysis of the histograms has shown that in a number of cases unsatisfactory compatibility with theoretical approximations is observed.

Here we note that significant divergences occur exactly when the values of parameters reach their greater values (the tails of the experimental distribution). However, these areas of distribution are very interesting from the standpoint of the study of clusterization effects in Poisson-type flows. In the linear building of histograms, the tail branches of the distribution cannot practically be detected. To resolve these problems we will use another presentation of experimental histograms of a semilogarithmic type, as follows.

**Table 2.3.** Parameters of the distribution of cyclogenesis intensity over basins of the northern hemisphere for 1983–1997 (January to July of given year).

Year	Total number of occurrences	Main numerical characteristics of histograms		Parameter approximating Poisson law $\lambda$ (day <sup>-1</sup> )	Measure of deviation of Pearson's criterion
		Mean	Variance		
1983	73	0.34	0.46	0.3	28 (7.8)
1984	112	0.52	1.12	0.5	141 (11.1)
1985	132	0.61	1.0	0.6	46 (9.5)
1986	125	0.59	0.59	0.6	16 (7.8)
1987	121	0.57	0.89	0.6	63 (9.5)
1988	63	0.29	0.28	0.3	22 (9.5)
1989	142	0.67	1.19	0.7	59 (11.1)
1990	166	0.78	1.21	0.8	284 (12.6)
1991	132	0.62	0.59	0.6	19 (7.8)
1992	146	0.69	0.78	0.7	67 (9.5)
1993	87	0.41	0.62	0.4	42 (9.5)
1994	135	0.64	1.34	0.6	553 (12.6)
1995	92	0.43	0.85	0.4	140 (9.5)
1996	121	0.57	0.82	0.6	25 (9.5)
1997	220	1.03	1.67	1.0	63 (12.6)

*Note:* Total number of runs is 212 days. The figures in parens give the tabulated values of the function  $\chi^2(\alpha, f)$  for Pearson's criterion at the 95% confidence level for a corresponding number of degrees of freedom.

Study of the comparability between experimental histograms and theoretical approximations for an active period, executed on a semilogarithmic scale (Figure 2.9e–g), shows that the Poisson nature of density in sharing a value  $N(t)$  is retains if the values of a number of events (in the day) equal 4–6. At values  $N < 5$  the experimental histogram is distinguished from the Poisson distribution; moreover, both an “excess” and “deficit” of values of experimental histograms with respect to pure Poisson models are observed. Here the evident and significant excess of the experimental values of histograms about the theoretical distribution under  $N > 5$  are practically the same as the universal phenomena for cyclogenesis in both the NH and SH.

**Table 2.4.** Parameters of the distribution of cyclogenesis intensity over basins of the northern hemisphere for 1983–1997 (August to December of given year).

Year	Total number of occurrences	Main numerical characteristics of histograms		Parameter approximating Poisson law $\lambda$ (day <sup>-1</sup> )	Measure of deviation of Pearson's criterion
		Mean	Variance		
1983	279	1.80	1.68	1.8	8.4 (11.1)
1984	300	1.96	2.08	2.0	12.6 (12.6)
1985	339	2.21	2.90	2.2	45.0 (16.9)
1986	318	2.06	1.90	2.1	4.1 (12.6)
1987	304	1.99	2.31	2.0	24.0 (12.6)
1988	350	2.29	2.67	2.3	22.0 (14.1)
1989	325	2.13	2.89	2.1	28.0 (12.6)
1990	373	2.44	2.87	2.4	14.0 (14.1)
1991	290	1.88	2.03	1.9	15.0 (11.1)
1992	449	2.93	3.50	3.0	43.0 (16.9)
1993	308	2.01	2.99	2.0	75.0 (14.0)
1994	381	2.50	3.04	2.5	30.0 (12.6)
1995	339	2.21	3.69	2.2	70.0 (14.0)
1996	326	2.13	1.95	2.1	4.6 (11.0)
1997	426	2.78	3.16	2.8	30.0 (12.6)

*Note:* Total number of runs is 153 days. The figures in parens give the tabulated values of the function  $\chi^2(\alpha, f)$  for Pearson's criterion at the 95% confidence level for a corresponding number of degrees of freedom.

So, for instance, for cyclogenesis in the NH (for interval II in 1985) for values  $N = 6, 7, 9$  an excess of experimental values over theoretical ones exists, but for  $N = 8$  the reverse situation is true (the number of events with  $N = 8$  is zero and, accordingly, the experimental value of the density of distribution is also zero). For cyclogenesis in the SH a distinctive excess is also inherent in the experimental values of histograms over theoretical ones: so, for  $N = 5$  (SH, 1983, interval I and SH, 1992, interval I) experimental values are more than theoretical ones by a factor of 100 (Figure 2.9f, g). It is precisely this circumstance that may be responsible for significant divergences in the Pierson criterion.

**Table 2.5.** Parameters of the distribution of cyclogenesis intensity over basins of the southern hemisphere for 1983–1997 (January to July of given year).

Year	Total number of occurrences	Main numerical characteristics of histograms		Parameter approximating Poisson law $\lambda$ (day <sup>-1</sup> )	Measure of deviation of Pearson's criterion
		Mean	Variance		
1983	124	0.60	1.03	0.6	380.0 (11.1)
1984	175	0.82	1.30	0.8	107.0 (11.1)
1985	141	0.67	1.16	0.7	84.0 (9.5)
1986	126	0.60	0.75	0.6	13.8 (9.5)
1987	121	0.57	0.81	0.6	26.0 (9.5)
1988	119	0.55	0.78	0.5	207.0 (9.5)
1989	200	0.83	1.38	0.8	57.0 (11.1)
1990	156	0.74	1.22	0.7	64.0 (9.5)
1991	122	0.58	0.59	0.6	1.7 (7.8)
1992	121	0.57	1.10	0.6	281.0 (11.1)
1993	125	0.60	0.66	0.6	4.2 (7.8)
1994	156	0.73	0.22	0.7	42.0 (7.8)
1995	110	0.52	0.12	0.5	21.0 (9.5)
1996	137	0.64	0.82	0.6	25.0 (7.8)
1997	260	1.22	2.06	1.2	108.0 (12.6)

*Note:* Total number of runs is 212 days. The figures in parens give the tabulated values of the function  $\chi^2(\alpha, f)$  for Pearson's criterion at the 95% confidence level for a corresponding number of degrees of freedom.

We can show that exactly such a situation is also true for the remaining samples (e.g., for SH, 1984, interval I; SH, 1988, interval I; NH, 1994, interval I; and so on).

In view of the significant volume of the number of events in experimental data ( $n > 150$ ), point evaluations of the intensity of flow of Poisson distribution  $\lambda$  and its confidence level can be executed by means of a method based on normal approximation for the Poisson distribution (Cox and Lewis, 1966). With a confidence level probability of 95%, we can evaluate the confidence level intervals for  $\lambda$ . They reach  $\pm 0.14$  for interval I and  $\pm 0.16$  for interval II. Point evaluations and confidence intervals of the average value of  $\lambda$  for tropical cyclogenesis hemispheres for 1983–1997 are shown in [Figure 2.11](#) (p. 46).

**Table 2.6.** Parameters of the distribution of cyclogenesis intensity over basins of the southern hemisphere for 1983–1997 (August to December of given year).

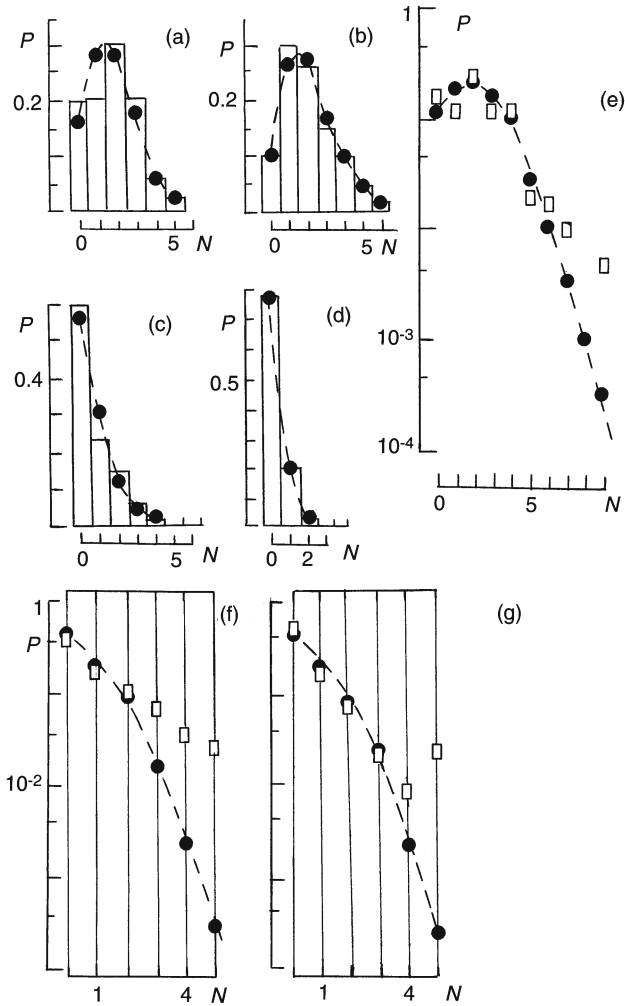
Year	Total number of occurrences	Main numerical characteristics of histograms		Parameter approximating Poisson law $\lambda$ (day <sup>-1</sup> )	Measure of deviation of Pearson's criterion
		Mean	Variance		
1983	50	0.32	0.33	0.30	5.20 (6.0)
1984	26	0.17	0.16	0.17	0.34 (6.0)
1985	13	0.08	0.08	0.10	0.18 (3.8)
1986	15	0.10	0.13	0.10	2.50 (6.0)
1987	31	0.20	0.23	0.20	1.90 (6.0)
1988	30	0.20	0.19	0.20	1.50 (6.0)
1989	16	0.10	0.09	0.10	0.18 (3.8)
1990	14	0.09	0.08	0.10	0.02 (3.8)
1991	52	0.34	0.46	0.30	37.00 (7.8)
1992	32	0.21	0.23	0.20	25.00 (6.0)
1993	24	0.16	0.13	0.16	0.05 (3.8)
1994	22	0.14	0.12	0.14	0.03 (3.8)
1995	34	0.22	0.25	0.20	8.80 (6.0)
1996	82	0.53	0.74	0.50	1.60 (7.8)
1997	48	0.31	0.28	0.30	0.68 (6.0)

*Note:* Total number of runs is 153 days. The figures in parens give the tabulated values of the function  $\chi^2(\alpha, f)$  for Pearson's criterion at the 95% confidence level for a corresponding number of degrees of freedom.

**2.4.3 Intermittency coefficient and “true” intensity**

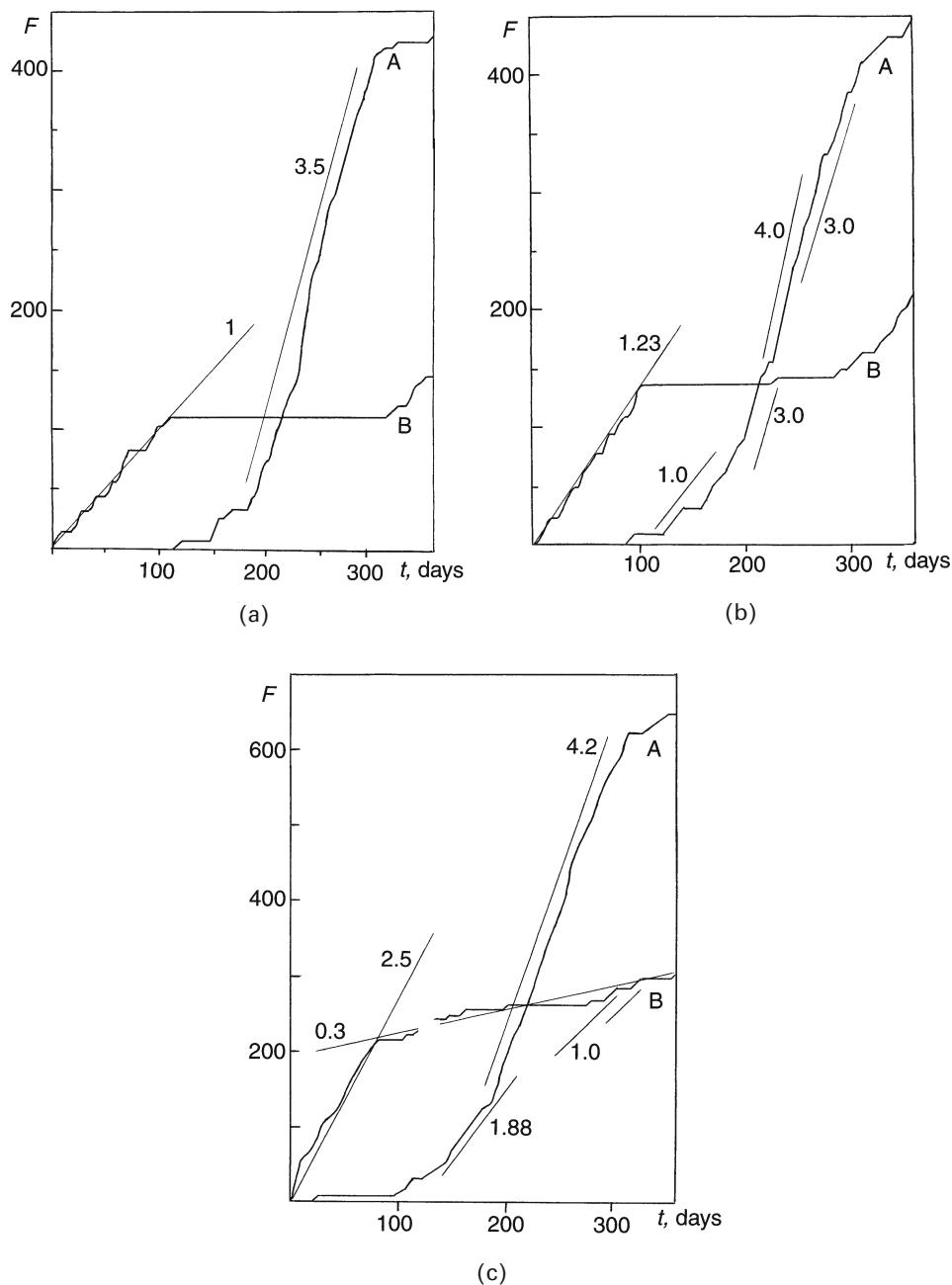
As already noted, to show the physical reasons for significant differences between average values of the intensity of the process, it is necessary to undertake a more detailed analysis of the temporal set of the sequence of events and, primarily, analyze the functions of the accumulating number of events (see Eq. 2.3).

Figure 2.10a–c presents (on a specially increased scale) the functions of a number of accumulating events for tropical cyclogenesis of the NH and SH for 1995–1997. Analysis of the data shown in Figure 2.10, as well as functions  $F(t)$  for all other explored periods (not shown in the drawing because of insufficient



**Figure 2.9.** Sample probability densities of cyclogenesis in the northern hemisphere (NH) and southern hemisphere (SH) and theoretic Poisson laws on linear scales (a–d) and on semilogarithmic scales (e–g). Stepped curves and open squares represent the experimental histograms. Dotted lines and full circles represent the Poisson distributions with values given in Tables 2.3–2.6. (a) Data of NH for 1983, II interval; (b) data of NH for 1986, II interval; (c) data of SH for 1986, I interval; (d) data of SH for 1988, II interval; (e) data of NH for 1985, II interval; (f) data of SH for 1983, I interval; (g) data of SH for 1992, I interval (from Pokrovskaya and Sharkov, 1999b).

room) shows that the behavior of  $F(t)$  for 1995–1997 is highly characteristic of the whole explored 15 years (1983–1997). The main particularity of the temporal set of the functions of the accumulation of events is its intermittent nature. In other words, intervals of generation and operation of cyclogenesis—where the derivative on a time



**Figure 2.10.** Annual time series of cumulative functions for northern (A) and southern (B) hemisphere cyclogenesis. (a) Data for 1995; (b) data for 1996; (c) data for 1997. Figures next to the straight lines represent the values of the intensity of Poisson processes (from Pokrovskaya and Sharkov, 1999b).



from  $F(t)$  is different to zero—alternate in a random manner with the intervals of “silence”—where  $dF(t)/dt = 0$ . Moreover, these intervals can range greatly in size—from days to months (the so-called “languid” season). So, analysis of the temporal set of accumulation functions for 1986 (Figure 2.8b) and for 1995–1996 (Figure 2.10a–c) shows that the active season for the NH is from May to November of the current year, while for the SH it is from December to March, and in the following winter (for the SH) it shows the silence area from March to November (the languid season). As a whole, such a structure for cyclogenesis is sufficiently well known. However, this methodology of building accumulation functions allows us to get new information on the modes of generation and operation of cyclogenesis.

Hence, we know (Cox and Lewis, 1966) that the ratio of the increment of accumulation functions  $\Delta F$  for the Poisson process to the time of observing ( $\Delta F/\Delta t$ ) is more or less the average value of the intensity of a Poisson flow of events (for the given time of observing  $\Delta t$ ). Of course, the time of observing (averaging) will correspond to the scale of events over which the studies are conducted. So, the values of intensity shown in Table 2.3 correspond to periods of accumulations in interval I (212 days) and interval II (153 days). But, if the time of accumulation is chosen sufficiently small, it is possible to speak of a kind of differential mode of values having an intensity of flows of  $\lambda_0$  and their temporal evolutions during  $\lambda_0(t)$  up to the integral value if for  $\Delta t$  we take the whole term of observations. So, analysis of Figure 2.10a–b shows that cyclogenesis in the NH during its active period (May–October) is highly irregular in its rate of generation: periods with a high rate of generation (for 1995  $\lambda_d = 3.5 \text{ day}^{-1}$ ) alternate with relatively small rates (over 5–7 days) of sharply lowered intensity (for 1995  $\lambda_d = 1.0 \text{ day}^{-1}$ ). The reverse holds for cyclogenesis in 1996 (Figure 2.10b), when there was an interval (230–274 days of the current year) with a sky-high rate of generation ( $\lambda_d = 4.0 \text{ day}^{-1}$ ) in between other intervals where activity dropped from  $3 \text{ day}^{-1}$  down to  $1 \text{ day}^{-1}$  inclusive of the silence season.

A qualitative change was observed for cyclogenesis in 1997 (Figure 2.10c). First, it is necessary to note the almost complete absence of winter silence areas, which are traditional for cyclogenesis in the SH. This distinctive branch is divided into small areas that include active periods with differential intensity of  $\lambda_d = 1.0 \text{ day}^{-1}$ . SH cyclogenesis is divided into two large periods (from January to March with integral intensity of  $\lambda_d = 2.5 \text{ day}^{-1}$  and from April to December with integral intensity of  $\lambda_d = 0.3 \text{ day}^{-1}$ ). As for NH cyclogenesis, it has its own particularities: cyclogenesis began much earlier (from the middle of January) and in its most active period (196–300 days of the year) it reached a sky-high (for the 15 years under discussion) differential rate of generation (it measured  $\lambda_d = 4.2 \text{ day}^{-1}$ ). Such a mode of cyclogenesis generation was called the “pipeline” of cyclones by Carlowicz (1995). Such high differential rates of generation are responsible for the greater values of accumulation functions—for the NH  $F(365) = 646$  and for the SH  $F(365) = 308$ —whereas in the “normal” mode these values are 1.5–2 times smaller (see Figures 2.8b and 2.10a, b). The physical reason for such serious global transformations in hemisphere cyclogenesis was probably the ENSO phenomena (the 1997–1998 episode), which actively developed during the whole of 1997 and at the

beginning of 1998. As is well known, during active ENSO episodes ocean temperature in the Pacific Ocean and the large-scale Walker circulation significantly increase and, in turn, this is greatly reflected in global cyclogenesis.

For a quantitative description of chaotic intermittent processes there are complex mathematical methods in common usage (Kadanov, 1993; Dubois, 1998). For our purpose we will use simpler approaches: we will define an intermittency coefficient and the true intensity. The first parameter  $\gamma$  will be defined as the ratio between the “clean” time of generation ( $t_g$ ) and the time of the full observation period ( $t_0$ ) or the volume of samples taken. The second parameter will be defined as the ratio of the number of events  $N$  to the time of clean generation of the process (i.e., where  $\Delta F/\Delta t$  is not zero). Hence,  $\lambda_t = N/t_g \text{ day}^{-1}$  is the value of the true intensity.

Calculated from experimental data for 1983–1997, the values of the intensity of the intermittency coefficient and the true intensity of flows of cyclogenesis of the NH and SH are presented in Table 2.7 and Figures 2.11–2.13.

Special calculations have shown that the values of the intensity of Poisson flows found earlier (Tables 2.3–2.6) are connected to the true intensity with a good degree of accuracy (better than 5%) by the equation  $\lambda_t = \lambda_0/\gamma$ . In other words, the physical sense of the true intensity is reached by recovering the average value of intensity of the condition of uniform generation for the whole period observed (or, in other words, without considering the contribution from the silence period).

These results, which might at first sight appear to be striking and uncommon, actually represent the usual and natural regime of the operation of tropical cyclogenesis under the assumption that this natural process can be conceived of as a radiophysical oscillator. For example, it can be a multivibrator that operates in pulse mode with equal amplitudes of pulses but with durations of pulses and a quenching oscillator (regime of intermittency) that are chaotic. In other words, for the case in point the compounded regime incorporates both a free-running and a triggered regime.

Thus, the intermittency coefficient is the ratio between the “pure” time of oscillations (a free-running regime) and the total interval of the operation. The term “true intensity” is the number of pulses in a unit time when the oscillator is operating (a free-running regime).

We will repeatedly use this demonstration and instructive analogue in other places in this book.

#### 2.4.4 Interannual variability between northern hemisphere and southern hemisphere cyclogenesis

The general picture of this temporal (15 years) set of values of cyclogenesis intensity (averaged on the temporal terms under investigation) in both hemispheres is presented in the Figure 2.11. Close inspection of these data shows that tropical cyclogenesis in both hemispheres possesses a clear time regularity and is determined by stability (of its intensities). In the NH maximum cyclogenesis is reached in the second half of the year, while in the SH the maximum is formed in the first half of the

**Table 2.7.** Intermittency coefficient ( $\gamma$ ) and the “true” intensity ( $\lambda_t$ ) of cyclogenesis over the basins of the northern and southern hemispheres for 1983–1997.

Year	Northern hemisphere				Southern hemisphere			
	Interval I		Interval II		Interval I		Interval II	
	$\lambda_t$	$\gamma$	$\lambda_t$	$\gamma$	$\lambda_t$	$\gamma$	$\lambda_t$	$\gamma$
1983	1.43	0.24	2.27	0.80	1.38	0.42	1.28	0.250
1984	2.07	0.25	2.34	0.84	1.96	0.42	1.00	0.170
1985	1.94	0.32	2.78	0.77	1.88	0.35	1.00	0.085
1986	1.56	0.38	2.36	0.91	1.56	0.38	1.25	0.078
1987	1.59	0.36	2.43	0.82	1.61	0.35	1.15	0.170
1988	1.10	0.27	2.63	0.87	1.48	0.37	1.07	0.180
1989	1.77	0.38	2.60	0.82	2.04	0.46	1.00	0.100
1990	1.76	0.44	2.87	0.85	1.92	0.38	1.00	0.092
1991	1.55	0.40	2.42	0.78	1.37	0.42	1.33	0.250
1992	1.78	0.39	3.51	0.83	1.66	0.35	1.45	0.140
1993	1.52	0.27	2.42	0.83	1.44	0.41	1.00	0.150
1994	1.98	0.32	3.05	0.83	1.79	0.41	1.00	0.140
1995	1.88	0.23	2.92	0.75	1.51	0.34	1.26	0.170
1996	1.57	0.36	2.45	0.87	1.61	0.40	1.34	0.400
1997	1.96	0.53	3.22	0.86	2.04	0.60	1.17	0.270

year. Based on the qualitative aspect of the problem, this statement is sufficiently well known. However, the quantitative evaluation of cyclogenesis intensity that we get is highly non-trivial: the intensities of NH and SH cyclogenesis for interval I practically coincide with annual values on average for 15 years, whereas for interval II they are different by a factor of 10 (on average). Moreover, attention is drawn to the fact that there is significant stability in the values of cyclogenesis intensity, with the probable exclusion of interval II of 1992 (NH), when cyclogenesis intensity sharply increased by more than 30% (on average).

Having expected a symmetrical distribution (normal type) for the values of intensity for these 15 years, it is possible to form a preliminary statistical model of a

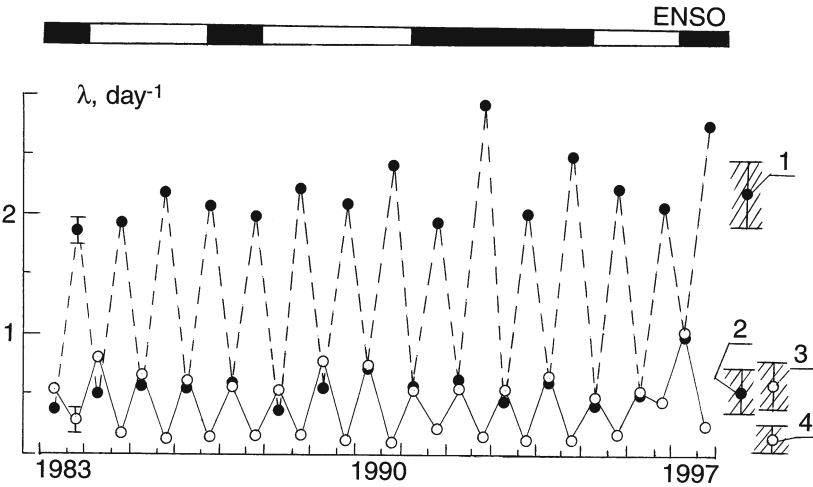


**Figure 2.11.** Intra-annual and interannual variability in experimental values of hemisphere cyclogenesis intensities for corresponding intervals (I and II) of the given year during 1983–1997. Full circles and dotted lines represent NH data. Open circles and solid lines represent SH data. Vertical line segments represent estimates of year-averaged intensity at the 95% confidence levels. (1) Multiyear (15 years) statistical model of NH cyclogenesis intensity (I interval); (3) model of SH cyclogenesis intensity (I interval); (4) SH, II interval. Solid and open bars indicate the active and suppressed periods of ENSO, respectively (from Pokrovskaya and Sharkov, 1999b).

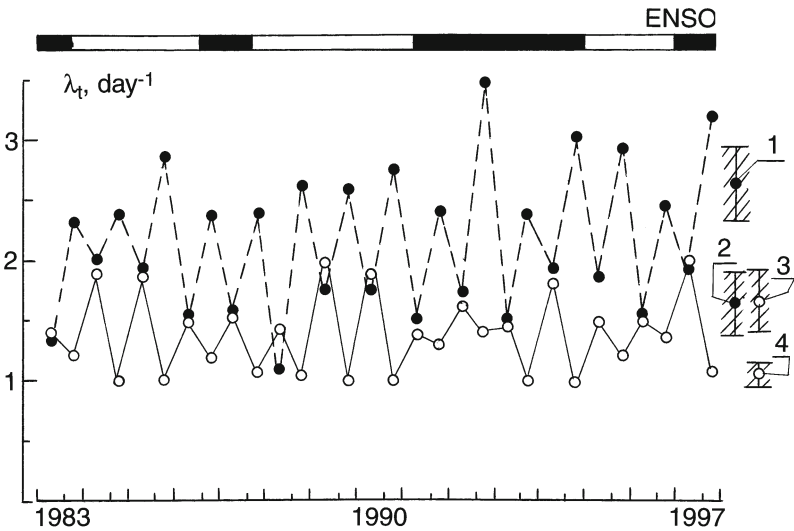


**Figure 2.12.** Intra-annual and interannual variability in experimental values of hemisphere cyclogenesis “true” intensities for corresponding intervals (I and II) of the given year during 1983–1997. See symbols and notations in [Figure 2.11](#) (from Pokrovskaya and Sharkov, 1999b).

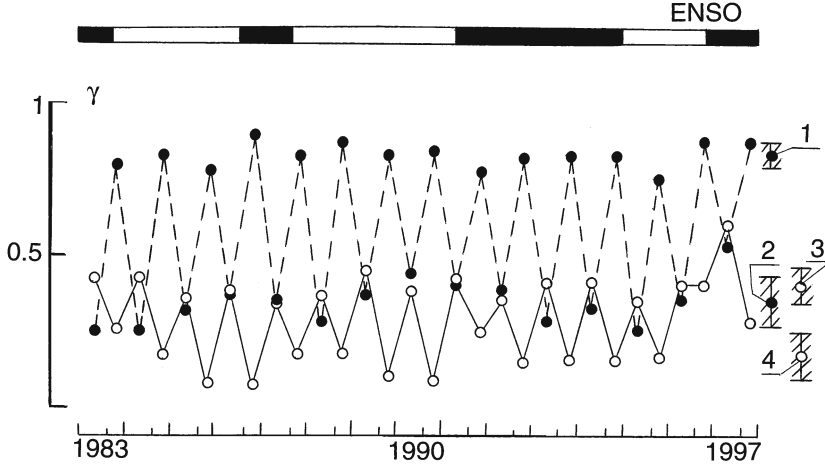


**Figure 2.13.** Intra-annual variability in the experimental value of the hemisphere cyclogenesis intermittency coefficient. See symbols and notations in [Figure 2.11](#) (from Pokrovsakya and Sharkov, 1999b).

long-standing sample set for the NH and SH:

$$\text{I interval} \begin{cases} \text{NH} & \lambda_0 = 0.58 & \sigma(\lambda) = 0.17 \\ \text{SH} & \lambda_0 = 0.68 & \sigma(\lambda) = 0.17 \end{cases} \quad (2.19)$$

$$\text{II interval} \begin{cases} \text{NH} & \lambda_0 = 2.22 & \sigma(\lambda) = 0.32 \\ \text{SH} & \lambda_0 = 0.21 & \sigma(\lambda) = 0.12 \end{cases} \quad (2.20)$$

where  $\sigma$  is the non-biased evaluation of r.m.s. These models are displayed in graphic form in [Figure 2.11](#).

Let us consider the important question of interannual variations in the intensity of Poisson flow in making a prototype for tropical cyclogenesis hemispheres. To do this, it is necessary to accept or reject the hypothesis that all annual Poisson models belong to the united (15-year) general collection set. Generally speaking, analysis can be done by using different approaches on the assumption that long-standing normal models of NH and SH tropical cyclogenesis exist (see Eqs. 2.19–2.20).

To check the hypothesis that the parameters of samples (taken on corresponding temporal terms) are comparable with the parameters of the general (15-year) set (Eqs. 2.19–2.20)  $H_0 : \lambda_i = \lambda_0$ , we will consider (following Feller, 1968) the sample function  $Z$ :

$$Z = \frac{\lambda_i - \lambda_0}{\sigma_0} \sqrt{t_i} \quad (2.21)$$

where  $t_i$  and  $\lambda_i$  are the total number and sample average set under study; and  $\sigma^2$  and  $\lambda_0$  are values of the variance and average of the general set. The formation and analysis of sample functions for the values of cyclogenesis parameters, over the considered period, for the NH and SH have shown that, under the given value

$\alpha = 0.05$ , hypothesis  $H_0$  has a 95% probability of being accepted for samples both for the NH and SH, with a few exceptions. So, samples from interval I for 1997 and 1990 (NH) and for 1984 and 1989 (SH), as well as from interval II for 1996 and 1983 (SH), cannot be referred to the general set (on the specified confidence level). This is very clear from analysis of Figure 2.11. The question of comparability of these samples with the general set requires more detailed consideration.

To resolve this problem, other statistical procedures—in particular, the double  $t$ -criterion (Feller, 1968) and the comparability of intensities of two Poisson processes method (Cox and Lewis, 1966)—were used. These approaches produced results similar to the ones we have just discussed.

Figures 2.12 and 2.13 show the temporal sets of values of the true intensity and the intermittency coefficient of cyclogenesis in the NH and SH for 1983–1997. As would be expected, just like the values of the true intensity, the temporal picture as a whole is similar to the one that corresponds to the average values of the intensity (Figure 2.11) with the difference that the values of the true intensity are greater than the values of the average intensity. The general regular picture of the time evolutions of the true intensity breaks down in the period 1991–1993, when a strong ENSO episode was observed. It is interesting to note that values of the true intensity in period I of the year under study for the NH and SH practically coincide, whereas in period II they are different by as much as 2.4–2.5 times. As for the time evolution of the intermittency coefficient, an amazing regularity and stability in the values of the intermittency is observed here. Any dependence on ENSO episodes were not observed.

Having expected a symmetrical distribution (normal type) for values of the true intensity and the intermittency coefficient for the 15-year period it is possible to form preliminary statistical models for samples from the NH and SH:

$$\text{I interval} \left\{ \begin{array}{lll} \text{NH} & \lambda_t = 1.68 & \sigma(\lambda_t) = 0.25 \\ \text{SH} & \lambda_t = 1.68 & \sigma(\lambda_t) = 0.24 \\ \text{NH} & \gamma = 0.34 & \sigma(\gamma) = 0.083 \\ \text{SH} & \gamma = 0.40 & \sigma(\gamma) = 0.064 \end{array} \right. \quad (2.22)$$

$$\text{II interval} \left\{ \begin{array}{lll} \text{NH} & \lambda_t = 2.69 & \sigma(\lambda_t) = 0.37 \\ \text{SH} & \lambda_t = 1.15 & \sigma(\lambda_t) = 0.15 \\ \text{NH} & \gamma = 0.83 & \sigma(\gamma) = 0.042 \\ \text{SH} & \gamma = 0.17 & \sigma(\gamma) = 0.086 \end{array} \right. \quad (2.23)$$

All these models are shown in graphic form in Figures 2.12 and 2.13.

In spite of the complex structure of signal accumulation, including the full lifetime of a single event (TC), it turns out that the amplitude features of the intensity of hemisphere tropical cyclogenesis can by and large be described within the framework of simple physical Poisson-type models (Brownian motion) with very clear parameters and weak interannual variability. As is clear from the Poisson

model, tropical cyclogenesis of both hemispheres possesses characteristics known from the theory of Poisson flows: changes in intensity do not depend on the number of existing structured elements, on their previous histories, or on the system's condition; moreover, the process satisfies the ordinariness characteristic (see Section 2.2.4).

Variations of experimental histograms from these purely Poisson models are highly symptomatic. This has to do with the fact that, from the standpoint of building physical models of cyclogenesis, these variations from the purely Poisson mode embody information on the structure of the object, because different-scale internal correlations in the system produce a break in Poisson characteristics. Note that these deflections reveal themselves as significant excesses by experimental tails in the histograms above the Poisson branch. In other words, these deflections manifest themselves by frequent and strong drops in cyclogenesis intensity. Such a type of clusterization of TC generation and operation (here separated in space by significant distances) was discovered earlier after experimental study of cyclogenesis in the Pacific and Atlantic Oceans (see Chapter 3).

As is the case with features of time series of cyclogenesis intensity, seasonal variability in cyclogenesis may possibly be interpreted as large-scale intermittency, while variability (with distinctive scales of the order of several day) within active seasons can be conceived of as small-scale intermittency. Such behavior of the time evolution of system parameters is characteristic of chaotic trigger systems. To demonstrate the comparability of cyclogenesis with a corresponding type of chaotic generator it is first necessary to make a detailed analysis of the particularities and the type of intermittencies.

## 2.5 EVOLUTION OF TROPICAL CYCLONE INITIAL FORMS AS A STOCHASTIC PROCESS

Remote-sensing study of the primary forms of TCs occupies a special place in programs that remotely monitor tropical disturbances (TDs) for a variety of reasons. First, there is a need to examine how medium-range (72 hours) forecasting transforms an individual primary TD into its developed stage (TC) and a need for detailed remote study of the structured, dynamic, and thermodynamic particularities of TDs at the moment of reaching maturity. Despite the obvious difficulty of making observations (in view of the multiscale process of dynamic interaction), the first successful attempts at complex study of the process of TC formation were carried out in the 1990s (Ritchie and Holland, 1997; Simpson *et al.*, 1988). Second, it is important to present another aspect of the problem regarding the structured particularities and correlation of temporal flows of the primary forms of TDs and the developed forms of TC that arise from them. Consideration of these questions is an important aspect of the study of the ocean–atmosphere system when studying the contribution that intensive vortical disturbances make to the thermodynamics and kinematics of the tropical atmosphere on different timescales. This problem is closely allied to the study of climate change and the study of the influence of large-scale

atmospheric circulation and ENSO phenomena on cyclogenesis (Henderson-Sellers *et al.*, 1998; Lighthill *et al.*, 1994).

However, attempts at remote-sensing investigation of primary forms of tropical disturbances have run into a variety of difficulties. In spite of significant efforts by researchers to observe and register separate (individual) tropical vortices (e.g., see Sharkov, 1998), final remote-sensing criteria about just how close an individual tropical disturbance is to its time of transition to the mature form are lacking. Difficulties emerge when we consider TDs as stochastic flows of events. They are associated with the absence of remote, meteorological, and chronological databases, created by the study of the primary forms (reasons for the cause of the last problem are discussed in Chapter 5). These databases must be formed, just as space–time stochastic crisis-situation models must be formed. Such models, in turn, can form the basis of resolving corresponding problems of ballistics provision for the remote experiments (Avanesov *et al.*, 1992; Anfimov *et al.*, 1995), and to resolve problems in predicting crisis situations.

The first goal-directed studies of mature forms of cyclogenesis (considered on the global scale as a stochastic flow of events) made possible the formation of preliminary statistical–quantitative models (see Sections 2.2 and 2.3).

As for cyclogenesis with respect to primary forms of TDs, semiquantitative considerations on the rates of generation of developing forms (TCs) from primary stages in different basins of the World Ocean have long been proposed (Khromov, 1948, 1966; Minina, 1970). However, it should be noted that no serious experimentally motivated proof of this has been cited. No absolute quantitative data on the intensity of the primary forms of cyclogenesis have been obtained.

On the basis of processing a time series of the intensity of the tropical cyclogenesis of both primary and mature forms, determined from the basins of both hemispheres for 1997, the purpose of this section is to present experimental results, pointing to features in the structure of the signal that reflect the temporal operation of hemisphere cyclogenesis, as well as to intra-annual particularities of the contribution to primary and mature forms in both hemispheres of tropical cyclogenesis, which in our view is important for understanding temporal variability in the correlation of primary and mature forms.

### 2.5.1 Simulation of an information signal

In this work we develop a methodical approach, based on presenting the temporal flow of the intensity of primary and mature forms of tropical cyclogenesis as a random flow of uniform events (see Section 2.1). The uninteresting detailed structure and track record of each individual tropical formation (in equal degrees either in its primary or mature form) will be placed on the time axis of each individual TD as a pulse of single amplitude with random duration (corresponding to the time of operation of TDs) and with random moments of TD appearances (generation of individual TDs). The number of received pulses (events) in a single temporal interval (here 1 day) is in such an event a natural physical parameter—an instant intensity in cyclogenesis, defining the energy of the interaction in the ocean—



atmosphere system. In the language of statistical procedures, this approach is identified as a means of calculating the number of events with due regard to the lifetime of an event (Apanasovich *et al.*, 1988).

The mathematically offered procedure of forming a signal may possibly be written in the same way as for mature forms (see Section 2.1).

Raw data for 1997 on the global cyclogenesis of developed forms (TCs) were not obtained from the systematized database Global-TC of remote observations for global tropical cyclogenesis (Pokrovskaya and Sharkov, 1999a). The database of primary forms of TDs in the World Ocean Basin for 1997 was put together on the computer platform Global-TC with analysis and systematization of source information on conditions in the tropical area, regularly (daily) updated during the whole of 1997 on the Internet (see Chapter 5).

### 2.5.2 Time series of the intensity of initial and mature forms

Figure 2.14 presents graphs of time series of the flows of intensity  $N(t)$  of tropical cyclogenesis in the NH and SH (daily averaging) for 1997 for primary forms of disturbances (Figure 2.14a) and for developed forms of TCs (Figure 2.14b). Note that on the graph of the intensity of primary forms (Figure 2.14a) the primary forms of mature forms of cyclones are not entered. They are, however, included as a natural period of evolutions when building up the time series of the intensity of mature forms. Analysis of Figure 2.14 shows that annual samples of the flows of intensity are presented as typical telegraphic processes both for primary and mature forms of cyclone. The detailed structure of the intensity of flows of primary forms is presented on an increased (daily) scale on the inset to the corresponding graph (Figure 2.14a). The main difference in the flow of intensity of primary forms from that of mature forms of cyclones is exemplified by the sharply fluctuating type of temporal set of signal. This is connected with the short (compared with mature forms of cyclones) lifetime of primary forms (1–3 days) and, accordingly, the reduced time of correlations of the process.

In the annual cycle of tropical cyclogenesis in both hemispheres some general lines are tracked. From August to November (day 170–day 320 of the year) in 1997 in NH basins, there is of course a period of increased activity both for primary forms and mature forms, but for SH basins there is correspondingly lowered activity. For the first half of the year (day 1–day 130) and end of the year (day 350–day 365), the inverse situation is observed: for NH basins cyclogenesis fades from its maximum in the second half of the year, but for SH basins there is a season of increased activity. In particular, graphically specified particularities reveal this when considering the time evolutions of the accumulation functions of a number of events (Figure 2.15a, b), where the derivative points to the differential intensity of the process. In essence, the question arises about how to collect two Poisson-type processes with greatly different intensities. For this reason we will select the annual temporal movement of these processes over two intervals (interval I is January–May and December and interval II is June–November) and use them to conduct some statistical procedures.

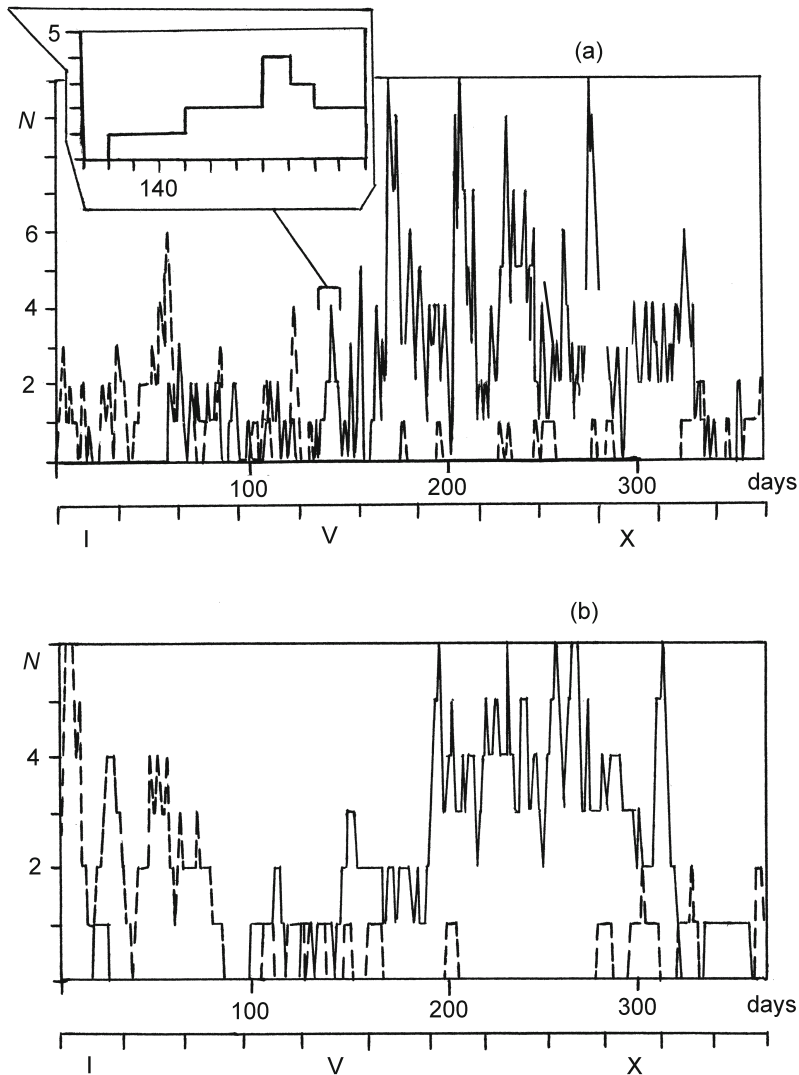


**Figure 2.14.** Annual time series of cyclogenesis intensity for initial forms (a) and for mature forms (b) for 1997. The solid line represents data from the northern hemisphere. The dotted line represents data from the southern hemisphere (from Pokrovskaya and Sharkov, 1999c).

Another important particularity of tropical cyclogenesis is the intermittent nature of generation that particularly graphically reveals itself when analyzing the temporal set of accumulated functions of a number of events. Pokrovskaya and Sharkov (1996a) first discovered such an effect when analyzing the time dynamics of tropical cyclogenesis in the Pacific for 1990–1991. To make the quantitative

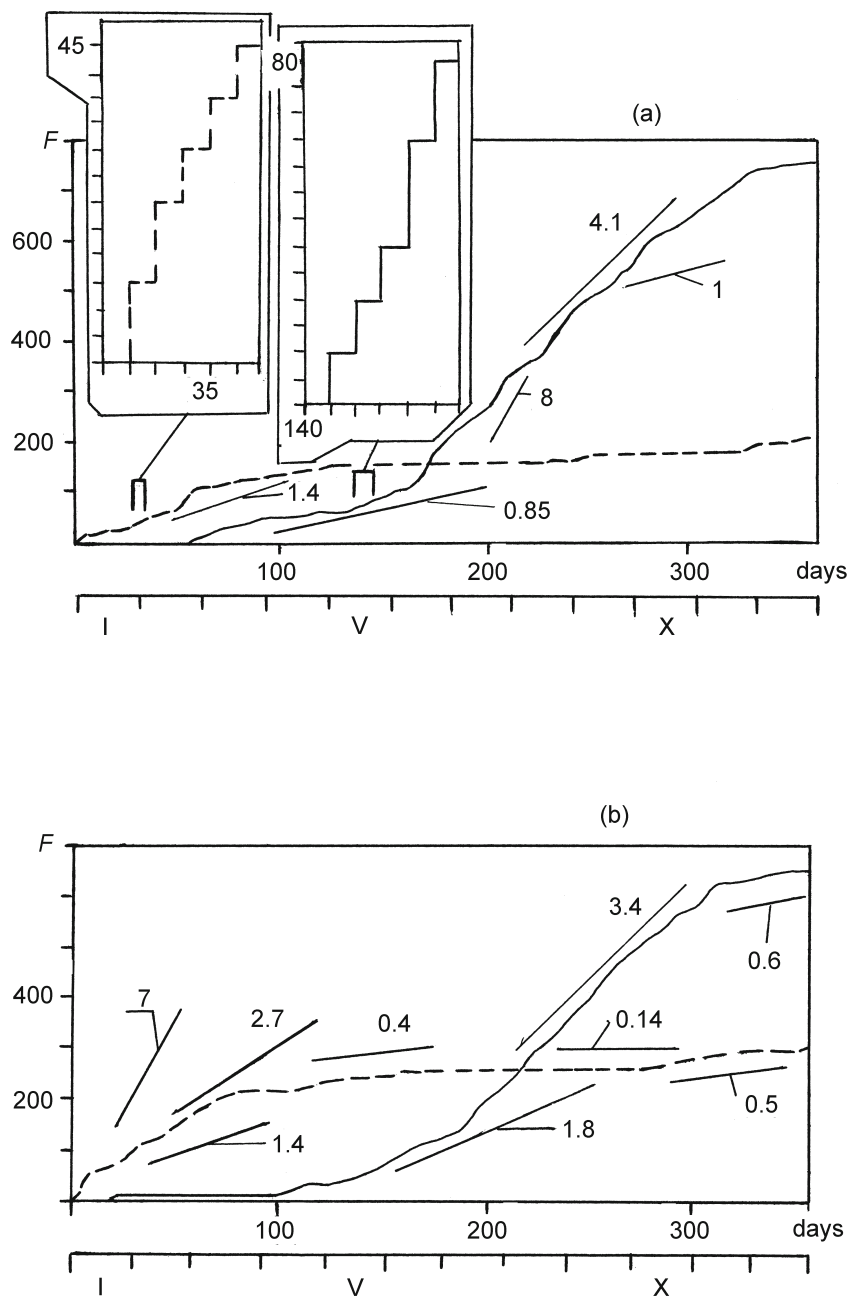


**Figure 2.15.** Annual time series of cumulative functions for initial forms (a) and for mature forms (b) for 1997. Solid and dotted lines represent data from the northern and southern hemispheres. The figures next to the straight lines represent values of the intensity of Poisson processes (from Pokrovskaya and Sharkov, 1999c).

features of this process known they proposed consideration of both a differential mode of cyclogenesis generation and an integral (for the considered time lag). We will use these approaches below.

Detailed analysis (at the pixel level) of the structures of accumulation functions (refer to insets on [Figure 2.15](#)) shows that the microstructure of accumulation functions possesses a non-uniformly step-like character that, strictly speaking, should be expected from microstructure intensities of cyclogenesis having both primary and mature forms of cyclones. Such a nature of temporary processes is well known in chaotic dynamics and is called the “devil’s staircase” process (see Section 2.7.1).

2.5.3 Probability models of the intensity of initial and mature forms

To demonstrate a concrete type of probabilistic model (amplitude features) for cyclogenesis of developed and primary forms for the NH and SH over interval I (January to July and December of the current year, 1997) and interval II (August to November of the current year) experimental histograms of the integer number of events  $N(t)$ —which approximate their statistical distribution by analyzing the degree to which they agree—were built. Moreover, sample averages and variances for each group of arrays were calculated. The numerical results of this are presented in [Table 2.8](#).

The collation of sample histograms using a Poisson-type approximating law and semilogarithmic scales ([Figure 2.16](#)) shows the possibility of using the hypothesis on

**Table 2.8.** Parameters of the distribution of the intensity of initial and mature forms of cyclogenesis over basins of the northern and southern hemispheres.

		Interval	Total number of occurrences	Main characteristics of histograms		Parameter of approximating Poisson law $\lambda$ (day <sup>-1</sup> )	Measure of deviation of Pearson's criterion
				Mean	Variance		
TCs	NH	I	86	0.47 (0.10)	0.42	0.5	8.03 (6.0)
		II	560	3.11 (0.25)	2.41	3.1	12.69 (11.1)
	SH	I	258	1.39 (0.17)	2.18	1.4	23.30 (11.1)
		II	50	0.27 (0.07)	0.21	0.3	3.10 (3.8)
TDs	NH	I	96	0.53 (0.10)	0.63	0.5	5.50 (7.8)
		II	650	3.58 (0.28)	4.83	3.6	11.80 (16.9)
	SH	I	171	0.93 (0.14)	1.23	0.9	4.00 (9.5)
		II	38	0.20 (0.06)	0.20	0.2	0.21 (3.8)

*Note:* Total number of runs is 182 days for interval I (January to May and December) and 183 days for interval II (June to November). Figures in parens give the tabulated values of the function  $\chi^2(\alpha, f)$  for Pearson’s criterion at the 95% confidence level for a corresponding number of degrees of freedom. In the “Mean” column the figures in parens give absolute values of confidence limits at the 95% confidence level.

the Poisson nature of the size of the fluctuation intensity  $N(t)$  of tropical cyclogenesis both for primary and developed forms. So, in accordance with the Pierson criterion of agreement, analysis of the measure of divergence between the theoretical distribution and experimental histograms of data on cyclogenesis for the NH and SH for 1997, proves (Table 2.8) that the experimental samples are by and large compatible with the general set of Poisson distributions with the parameter values shown in Table 2.8. This can be graphically demonstrated by collating the theoretical distribution and experimental histograms (Figure 2.16). It is important to note here that the statistical amplitude of the intensity of signal for tropical cyclogenesis for (strictly speaking) totally different physical systems (TDs and mature cyclones) practically coincide: in Figure 2.16 the left column of histograms presents the signal formed during the evolution of developing forms (TCs), and the remaining histograms present data on primary forms. It is easy to see that the statistical structure of signals and (interestingly) the numerical values when evaluating their parameters are very similar (see Table 2.8).

Here, detailed analysis of the histograms has shown that, in a number of primary forms, divergence between experimental histograms and theoretical distribution is observed; moreover, it will be necessary to note that such divergence (either for signals or developing mature forms) is defined at the greater values of the parameters (i.e., tails) of experimental distribution (Figure 2.16e,j).

Comparison between experimental histograms (primary forms) and theoretical approximations for intervals I and II of observation, executed on a semilogarithmic scale (Figure 2.16e,j), shows that the Poisson nature of the density of distributions of value  $N(t)$  is retained if the value of the number of events in a day equal 5. At values  $N > 5$  the experimental histogram is distinguished from the Poisson distribution; moreover, the significant excess of values of experimental histograms with respect to clean Poisson models for cyclogenesis is observed in both the NH and SH.

For instance, primary forms of cyclogenesis in the NH (for interval II of 1997) for values  $N = 8-9$  have an excess of experimental values over theoretical ones of 7–8 times. Cyclogenesis in the SH also has a clear excess of experimental values of histograms over theoretical ones: so for  $N = 6$  (SH, 1997, interval I) experimental values of the order of 1.5 above theoretical ones.

As a result of that, the effect of amplitude clusterization is inherent in both developed forms of TDs (this is the reason we repeatedly use experimental data, see Sections 2.2 and 2.3) and primary forms.

In view of the significant size of the sample number of events in experimental data ( $n > 180$ , see Table 2.8), point evaluation of the intensity of flow of the Poisson distribution  $\lambda$  and its confidence levels can be executed by means of a method based on the normal distribution drawing near a Poisson distribution (Cox and Lewis, 1966). With a confidence level probability of 95%, the evaluations of confidence intervals for  $\lambda$ , executed on the specified strategy, are presented in Table 2.8. It is interesting to note that in absolute values of the intensity of the time process both mature and primary forms practically coincide (with provision for confidence intervals).

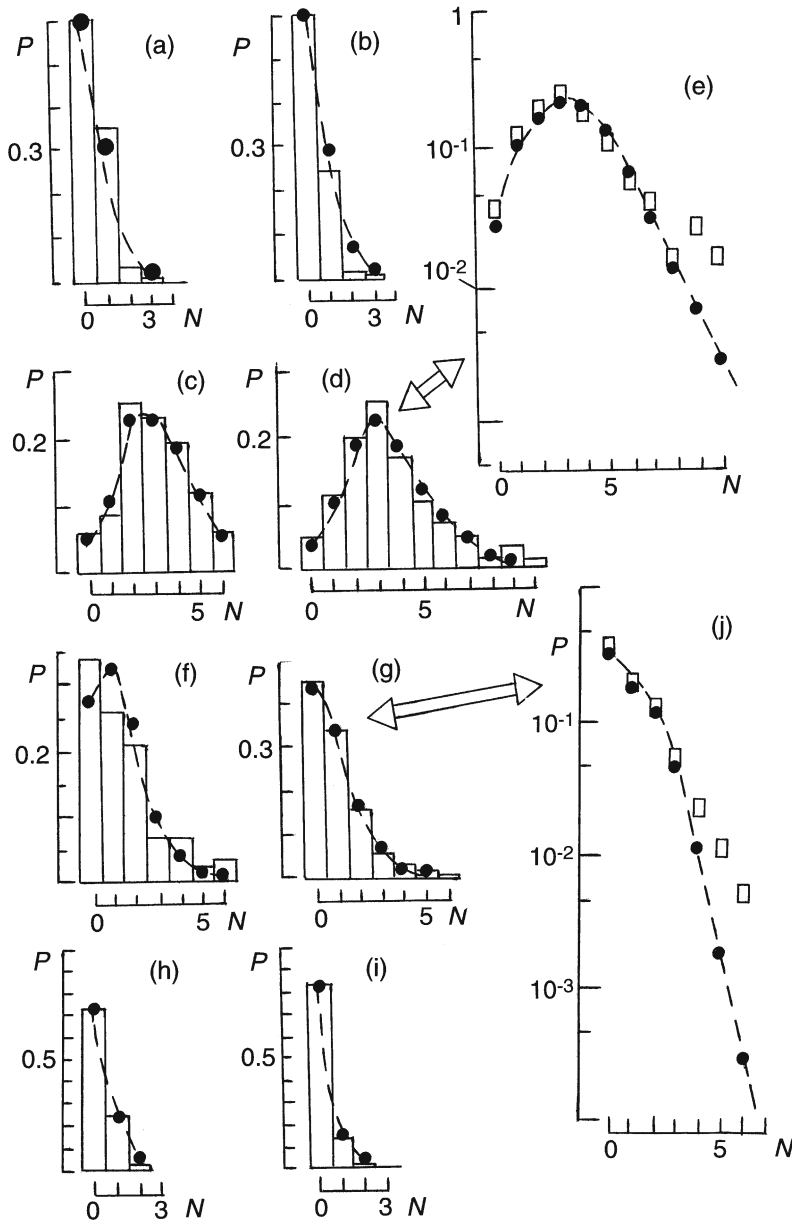


**Figure 2.16.** Sample probability densities of the cyclogenesis of initial and mature forms and the theoretical Poisson law on linear (a–d, f–i) and on semilogarithmic (e, j) scales. Stepped curves and open squares represent the experimental histograms. Full circles and dotted lines represent the Poisson distributions with the values given in Table 2.8. (a–b) Data of NH, I interval; (c–e) data of NH, II interval; (f–g, j) data of SH, I interval; (h–i) data of SH, II interval; (a), (c), (f), (h) represent the data of mature forms; (b), (d), (e), (g), (i), (j) represent the data of initial forms (from Pokrovskaya and Sharkov, 1999c).

#### 2.5.4 Integral intensity of processes

As already noted, to demonstrate the physical reasons for the significant difference in average values of intensities of process, it is necessary to subject the time series of the flow of events to more detailed analysis and at the same time to analyze the functions of the accumulating number of events.

The ratio between increases in the accumulation function  $\Delta F$  for the Poisson process and observation time ( $\Delta F/\Delta t$ ) is quite simply the average value of the intensity of the Poisson flow of events (for the given time of observation  $\Delta t$ ). Of course, the time of observation (averaging) will correspond to scaling of these events for which studies have been conducted. But if the time of accumulation is chosen sufficiently small, it is possible to speak of a kind of differential mode of values for the intensity of flows  $\lambda_0$  and their evolutions during  $\lambda_0(t)$ , up to integral value, if we take the whole term of observations for  $\Delta t$ .

Figure 2.15 presents the functions of the number of accumulating events of tropical cyclogenesis of primary and mature forms in the NH and SH for 1997. The main particularity of the temporal set of accumulation functions of events is the intermittent and non-uniform nature on scales of the order of several days and more. In other words, the intervals of generation and operation of cyclogenesis—where the derivative of  $F(t)$  to time is different from zero—alternate with the intervals of silence—when  $dF(t)/dt = 0$ . Moreover, these intervals can be highly significant—from days to months (the so-called “faded” season). Within the active season, we can observe the highly non-uniform structure of the signal, which is characterized by the scattering of values of differential intensity across rather broad intervals. As a whole, the large-scale behavior of accumulation functions both for primary and mature forms are very similar, though differences do exist in the details. So, analysis of the temporal set of accumulation functions for 1997 shows that the active season for primary forms (NH) began at the beginning of March and took place in two stages: the first stage includes March to the middle of June at an intensity of  $0.85 \text{ day}^{-1}$ ; the second stage begins in the middle of June and ends in November (day 339 of the current year). The differential intensity of the process in this period varies in a wide range from  $1 \text{ day}^{-1}$  to  $8 \text{ day}^{-1}$  with an average value of  $4.1 \text{ day}^{-1}$  (Figure 2.15a). The SH active stage occupies the period from January to April (day 1–day 120 of the year) with significant differential intensity fluctuations from  $0.5 \text{ day}^{-1}$  to  $6 \text{ day}^{-1}$  and later in the year (for the SH) by silence areas from June to November (faded season) with the values of differential intensities within  $0.1 \text{ day}^{-1}$  and  $0.3 \text{ day}^{-1}$  (Figure 2.15a).

The cyclogenesis of mature forms in the NH began in 1997 relatively early (at the end of January), then between April and June generation faded (the intensity over this term was  $1.8 \text{ day}^{-1}$ ), and then in July to November (day 196–day 326 of the year) experienced a high rate of generation (for this term the intensity was  $3.4 \text{ day}^{-1}$ ). In December 1997 generation dropped dramatically to the observed level of  $0.6 \text{ day}^{-1}$ . As for the cyclogenesis of developed forms for 1997 (SH), it is necessary to note the almost complete absence of winter silence areas, which are traditional for SH cyclogenesis. This winter silence area is divided into small areas

that have active periods with differential intensity of  $\lambda_d = 1.0 \text{ day}^{-1}$ . The cyclogenesis of developed forms in the SH is divided into two large areas: the first from January to March with integral intensity  $\lambda = 2.7 \text{ day}^{-1}$  and a broad range of variation in differential intensity from  $1.4 \text{ day}^{-1}$  to  $7 \text{ day}^{-1}$  and the second from April to the beginning of June with integral intensity  $\lambda = 0.4 \text{ day}^{-1}$  and from June to October with intensity  $0.14 \text{ day}^{-1}$ . In November and December cyclogenesis became more active with intensity reaching  $0.5 \text{ day}^{-1}$  (Figure 2.15b). Such an annual structure of variability in cyclogenesis of qualitative mature forms is by and large well known. However, for primary forms such experimental information is received first. Likewise, the large-scale structures of the annual cycle of cyclogenesis of developed and primary forms turn out to be similar (at least from 1997 data).

Analysis of the proposed structure of the accumulation signal, including the full lifetime of a single event (TC and primary form), has shown that the amplitude features of the intensity of tropical cyclogenesis (primary and developed forms) for both hemispheres can be described by simple physical Poisson-type models (Brownian motion) with very firm parameters. As a direct effect of the Poisson distribution drawing near, tropical cyclogenesis of both forms possesses characteristics known from the theory of Poisson flows: changing intensity does not depend on the number of existing structured elements, nor on their previous histories, nor on the system's condition; moreover, the process satisfies the ordinarieness characteristic.

These deviations of experimental histograms from purely Poisson models are highly symptomatic. This is connected with the fact that—from the standpoint of building physical models of cyclogenesis—it is exactly these deviations from purely Poisson mode that carry the main load, since internal correlation relationships of different scale in the system cause a break in Poisson characteristics. Note that these deviations reveal themselves basically as significant excesses (i.e., experimental tails) in histograms on the Poisson branch. In other words, these deviations reveal themselves as fairly frequent and strong short outbreaks of cyclogenesis intensity for developed and primary forms. For developed forms (TCs) such a kind of clusterization (space and time) is a well-known experimental fact (“pipeline” of cyclones; Carlowicz, 1995), but for primary forms such an experimental fact is observed for the first time.

As for the particularities of temporal sets of cyclogenesis intensity, seasonal variability in cyclogenesis can certainly be interpreted as large-scale intermittency (two temporal intervals), while intermittency (with distinctive scales of the order of several days) within active seasons can possibly be interpreted as small scale. Such behavior in time evolution by the parameters of this system is highly characteristic of the chaotic trigger-type systems. To make the parameters of cyclogenesis correspond to a type of chaotic generator it is necessary to make a detailed analysis, primarily, of particularities and the type of intermittency.

It is also important to present a consideration of the physical reasons underlying the sharply different (1.5 times) efficiency in generating developing forms for SH and NH basins.



On the basis of the proposed and developed strategy of shaping and accumulating statistical signals on remote data of the tropical cyclogenesis of primary and developed forms, considered for each hemisphere separately, it has been experimentally shown that the amplitude features of cyclogenesis intensity can be satisfactorily described by Poisson processes of alternating type. The cyclogenesis of primary and developed forms possesses a sharp intra-annual variability (revealed as two terms) and can be described by two Poisson models with firm parameters. We have created numerical models for the intensities of primary and developed forms for 1997. As a result, we have discovered the experimental effect of the amplitude clusterization of the flow intensity of primary forms.

### 2.5.5 Rate of hurricane formation

For a number of problems relating to climate interaction, it is necessary to obtain quantitative values of the cyclogenesis intensities of primary and developed forms by time averaging of the order of months (or even years)  $N_0(t_i; \Delta t)$  or, in other words, by carrying out the following procedure:

$$N_0(t_i; \Delta t) = \frac{1}{\Delta t} \int_{t_i}^{t_i + \Delta t} N(t) dt \quad (2.24)$$

where  $t_i$  is the beginning of current month; and  $\Delta t$  is the duration of the corresponding month.

As already indicated (Section 2.1), the correct averaging procedure, as shown in Eq. (2.24), eliminates the fine small-scale features of the temporal evolution of the tropical cyclogenesis dynamical system from consideration and yet can reveal the presence of large-scale features. This can be illustrated by the ratio between developing and mature stages of TCs (Pokrovskaya and Sharkov, 2000).

Numerical expression of the rate of hurricane formation (RHF) of developed forms will be defined as follows:

$$G(t_i) = N_{TC}(t_i) / N_{\Sigma}(t_i) \quad (2.25)$$

where  $N_{TC}$  is the monthly average number of developing forms; and  $N_{\Sigma}(t_i)$  is the average monthly number of TDs at any stage of life.

The database of primary and developed forms of TDs in the World Ocean Basin for 1997–1998 was created on the Global-TC computing platform with the help of pre-processing, systematization, and archiving of raw information about conditions in the tropical area, regularly (daily) obtained during all of 1997 and 1998 from the Internet (Pokrovskaya and Sharkov, 1999a, d).

The main results of monthly averaging of the instant intensity of flows of both mature and primary forms observed for 1997 and considered for the basins of both hemispheres are shown in Figure 2.17. Figure 2.17a, b also shows the time series of monthly cyclogenesis intensity in the NH and SH for both mature and primary forms. An allowance is made in both tropical systems for primary forms that transform into mature forms and for systems that remain unchanged. It is

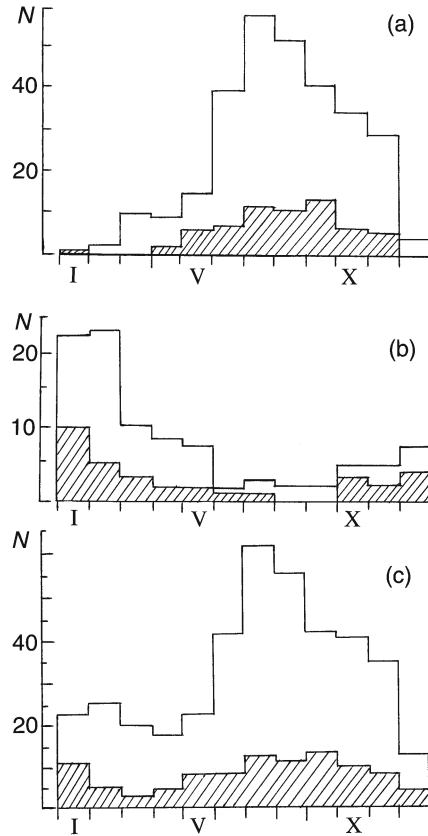


**Figure 2.17.** Annual time series of month-averaged intensities for mature and initial forms of tropical disturbances for 1997. Open stepped curves represent the data of initial forms. Stepped cross-hatched curves represent the data of mature forms. (a) Data of NH cyclogenesis; (b) data of SH cyclogenesis; (c) data of global tropical cyclogenesis (from Pokrovskaya and Sharkov, 1999c).

important to note that the time series of the intensity of developing forms almost exactly corresponds to the time series of primary forms, though there are determined particularities. There is also a determined number of primary forms (5–10 disturbances) in time intervals when TCs did not generally form: worthy of note are February, March, and December 1997 (for the NH) and August–September 1997 (for the SH). Moreover, we note that primary forms in both the NH and SH are generated every month, despite being statistically very lumpy. So, for the NH the maximum number of primary forms are observed between June and September and for the SH they are observed in January–February and October–December (Figure 17a,b). These are the times that maximum cyclogenesis of mature forms occur.

The picture throughout the World Ocean of the correlation between primary forms (where primary forms are born and subsequently when they become mature

**Table 2.9.** Monthly average rates of initial and mature form generation for 1997–1998.

	<i>Years</i>	<i>Basins of NH</i>	<i>Basins of SH</i>	<i>World Ocean basins</i>
Total number of TDs	1997	24.6	8.0	32.7
	1998	21.4	11.5	32.9
Initial forms of TDs	1997	19.7	5.2	25.0
	1998	17.1	8.5	25.6
TCs	1997	4.9	2.7	7.7
	1998	4.3	3.0	7.3

forms) and mature forms is shown in [Figure 2.17](#) and [Table 2.9](#). As would be expected, intra-annual variability in the cyclogenesis of mature forms has greatly smoothed out, whereas for primary forms it has remained observable. The total number of TCs for 1997 was 92 and, hence, the average number of cyclones per month was 7.7, the average number of primary forms that did not transform into mature forms was  $25 \text{ month}^{-1}$  (and so exceeds the rate of generation of mature forms by more than three times), and the average monthly number of all registered forms of tropical outbreaks was  $32.7 \text{ month}^{-1}$  (total number of TDs for 1997 was 392). Collation of these parameters into data for 1998 (see [Table 2.9](#)) shows a striking interannual (1997–1998) stability in monthly average rates of the generation of TDs: variations in the values of parameters, describing the rates of generation of disturbances at different stages, were less than 13%. However, in this case the asymmetry in the values of monthly average rates of TC generation in the basins of both the NH and SH (by 1.4–1.5 times) is noteworthy.

The total number of disturbances, however, do not yet fully represent the equilibrium of the global ocean–atmosphere system. In our opinion a more appropriate parameter of the stability study can serve as the correlation between mature and initial forms. Analysis of the data shown in [Figure 2.17](#) shows that seasonal variability determined in the general number of disturbances that appear in the World Ocean Basin per month is greatly flattened when the rate of births (Eq. 2.25) of mature forms from primary ones is considered. The results of calculating the generation factor are shown in [Figure 2.18](#) (for 1997 data). Analysis of the results leads to a number of interesting conclusions. The annual birth rate of mature forms in both the NH and SH has denominated periods: active and break (faded) periods ([Figures 2.18a, b](#)). In this case it is important to note that during active periods the generation factor has a stable value. In the NH its value is 0.2 and in the SH it is 0.3 with a very small monthly variation.

The total pattern throughout the World Ocean is shown in [Figure 2.18c](#). From analysis of the data it follows that the annual value of the generation factor—which is considered the process of generation of developing forms in all active basins of the World Ocean (in other words, cyclogenesis is presented as a united global process)—is amazingly stable. The average value for 1997 is 0.23 with very small monthly

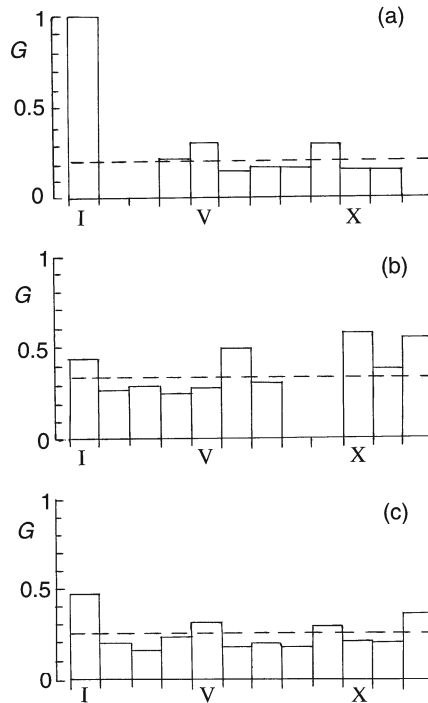


**Figure 2.18.** Annual time series of the month-averaged coefficient of hurricane formation for 1997. (a) Data of NH cyclogenesis; (b) data of SH cyclogenesis; (c) data of global tropical cyclogenesis. Dotted lines represent values of the year-averaged coefficient of hurricane formation (from Pokrovskaya and Sharkov, 1999c).

variations and for 1998 it is 0.22. If cyclogenesis is considered separately for each hemisphere, the average (for 1997) value of the generation factor for cyclogenesis in the NH is 0.20, but in the SH it is 0.33. A very close situation is observed for 1998: in the NH the generation factor is 0.20 and in the SH it is 0.26. The significant asymmetry in the year-averaged values of the generation factor in basins of the NH and SH has caught our attention.

These models and numerical features of the intensity of cyclogenesis (not only regional but also hemispherical) can be used in the study of global interactions in the ocean–atmosphere system; they can also be used for the operative planning of space experiments alongside existing systems for monitoring crisis situations.

### 2.5.6 Regional features of Pacific cyclogenesis

Figure 2.19 presents graphs of the time evolutions of the flows of intensity  $N(t)$  of tropical cyclogenesis (monthly averaging) for 1997 for primary forms of disturbances and for mature forms (TCs) for three active areas of the Pacific Ocean: northwest Pacific (NWP), northeast Pacific (NEP), and southwest Pacific (SWP).

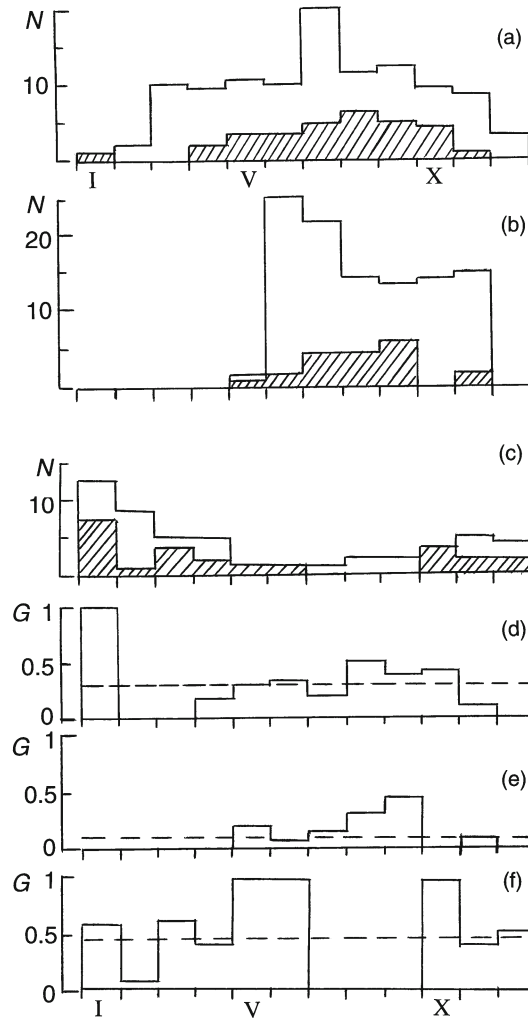


**Figure 2.19.** Annual time series of month-averaged intensities for mature and initial forms (a–c) and of the coefficient of hurricane formation (d–f) for cyclogenesis in the Pacific for 1997. (a, d) Data of northwest Pacific; (b, e) data of northeast Pacific; (c, f) data of southwest Pacific. Open stepped curves represent the data of initial forms. Stepped cross-hatched curves represent the data of mature forms. Dotted lines represent values of the year-averaged coefficient of hurricane formation.

Analysis of [Figure 2.19a–c](#) shows that annual samples of intensity flows present themselves as typically telegraphic processes (under corresponding time averaging) both for primary and mature forms of cyclones. The distinctive particularity of the temporal flow of the intensity of primary and mature forms is concluded by and large to have similar annual cycles of both forms of cyclogenesis. However, it

is easy to verify that the detailed structure of temporal flows has a variety of particularities.

So, there are both general lines and particularities found in the annual cycle of tropical cyclogenesis in the active area of the NWP. The active season of mature forms in the SWP was in April and continued until November 1997 (Figure 2.19a); moreover, it reached its maximum in August. By January 1997 the cyclogenesis of mature forms resulted in TC “Hannah” (9701) in the NWP. The average monthly rate of mature form generation in the active period was 3.2. At the same time, the cyclogenesis of primary forms in 1997 more or less existed throughout the whole calendar year and were intensive at 10 events (tropical depressions per month) reaching a maximum in July (20 events). The total number of TDs of both types in the SWP for 1997 was 108 and, as a result, the average monthly rate of generation of disturbances was 9.

In basins of the NEP the situation was very different: the cyclogenesis of primary and mature forms functioned synchronously and over a limited period (May–November). In this timegap the cyclogenesis of primary forms was very intensive with 15 to 25 events per month (Figure 2.19b) and the cyclogenesis of mature forms dropped to an average  $3 \text{ month}^{-1}$ . The total number of events in the NEP was 105, which means the average monthly rate of generation of disturbances was 8.75 (a numerical value close to the rate of generation in the NWP).

As is well known, in SH basins of the Pacific Ocean one season of increased activity occurs in summer and maximum activity is in January. These particularities are clearly shown in Figure 2.19c. However, it should be noted that the cyclogenesis of mature forms for 1997 was sufficiently extended throughout the year and lasted for large parts of the year (with the exclusion of May to September) with a sufficiently faded rate of generation of  $2.4 \text{ month}^{-1}$ . The cyclogenesis of primary forms in the SWP occurred throughout the year (without a break) with the evident maximum in January (12 events). The total number of outbreaks in the SWP in 1997 was 49 corresponding to an average rate of generation of  $4.08 \text{ month}^{-1}$ . Collation of the rates of generation in NH basins of the Pacific Ocean reveals that activity in southern parts of the Pacific with respect to the generation of TDs is twice as small.

Let us analyze annual variation in the generation factor of mature forms (Figure 2.19d–f). For basins in the NWP the nature of change is rendered sufficiently firm by the average value 0.3 (within an active period) and by small variation. The exception was January ( $G = 1$ ) when one TC occurred. The average annual generation factor of mature forms for the NWP reached 0.28. For basins in the NEP, temporal evolution of the rate of generation of mature forms was different and increased from May to September. The average value for an active period was 0.22; the average annual value was considerably less at 0.11. Unlike basins in the North Pacific Ocean, the time series of the generation factor for basins in the SWP exhibits a totally different nature. In spite of the faded cyclogenesis of mature forms, practically every second depression transforms into the mature form and, hence, a very intensive generation process is realized: in active periods the average value of the generation factor is 0.62 which is 2.5–3 times greater than for NH basins. The average annual value of the generation

factor for basins is 0.46, which is also significantly greater than similar features for northern basins of the Pacific Ocean.

### 2.5.7 Regional features of Indian Ocean cyclonic activity

The time series of the cyclogenesis intensity of primary and mature forms for 1997 that formed in the basins of the Indian Ocean are shown in Figure 2.20a, b. The active season of mature forms in basins in the southern part of the Indian Ocean (SIO) is from December to February which Figure 2.20a illustrates very well. For the

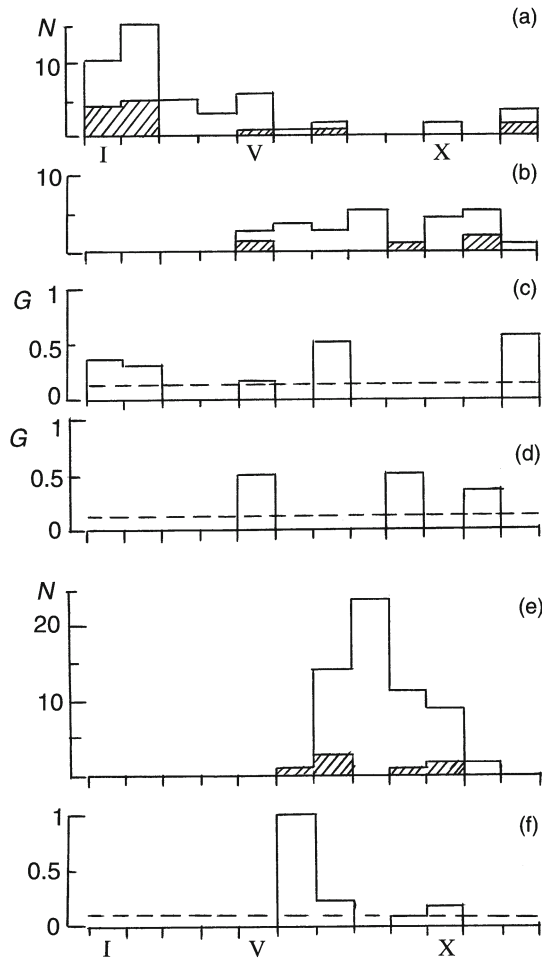


**Figure 2.20.** Annual time series of month-averaged intensities of mature and initial forms (a, b, e) and of the coefficient of hurricane formation (c, d, f) for cyclogenesis of the Atlantic (e, f), the North Indian Ocean (a, c), and South Indian Ocean (b, d). See symbols in Figure 2.19.

specific period, 9 events (TC) occurred causing the average monthly generation rate of mature forms to be 3. This value is close to the generation rate in the basins of the Pacific Ocean. The cyclogenesis of primary forms operated for large parts of the year (with the exclusion of August–September and November), though it was highly non-uniform: the maximum came in January–February (10 and 15 events, respectively). In the whole SIO for 1997, 47 events (TDs) occurred giving an average annual generation rate of disturbances of all forms of  $3.9 \text{ month}^{-1}$  and an average annual generation rate of mature forms of  $0.92 \text{ month}^{-1}$ .

Cyclogenesis of the northern part of the Indian Ocean (NIO) is significantly determined by the monsoon particularities of the regional climate. In 1997 in this part of the ocean four full-blown TCs occurred within 3 months (May, September, and November), giving a generation rate of developing forms of  $1.3 \text{ month}^{-1}$ . At the same time, the cyclogenesis of primary forms in the active season, corresponding to the period from December on gave a generation rate of  $3 \text{ month}^{-1}$  and “worked” continuously. In all the basins of the NIO for 1997, 24 events occurred. The average annual generation rate for disturbances was  $2 \text{ month}^{-1}$  and that of mature forms was  $0.3 \text{ month}^{-1}$ .

Let us analyze the generation rate of mature forms in the basins of the Indian Ocean (Figure 2.20c, d). The intermittent generation of mature forms in the basins of the Indian Ocean means the annual cycle of the generation factor breaks down into a number of separate (monthly averaged) areas with sufficiently high values of the generation factor: from 0.3 to 0.67 for the basins of the SIO and 0.4–0.5 for the basins of the NIO. The average annual values of the generation factor turn out to be moderate: 0.16 for basins of the SIO and 0.11 for basins of the NIO.

### 2.5.8 Regional features of Atlantic Ocean cyclogenesis

Figure 2.20e presents graphs of the time evolutions of the intensity flows  $N(t)$  of tropical cyclogenesis (monthly averaged) for 1997 for primary forms of TDs and for mature forms (TCs) for basins in the Atlantic Ocean.

The cyclogenesis of mature forms in the Atlantic in 1997 is worthy of note in that it had an unusually “faded” nature: cyclogenesis “worked” for as little as 4 months (June–July, September–October); moreover, the total number of TCs was 7 and, accordingly, the average monthly generation rate was 1.75. This value is twice as small as that of the basins of the Pacific Ocean. Unlike the cyclogenesis of mature forms, the cyclogenesis of primary forms in 1997 was highly “energetic” and compact from the temporal viewpoint: for 4 months (July–October) there were 57 events with most occurring in August (22 events). In other words, the average monthly generation rate of primary disturbances was 14.25 (in an active period) and the average annual rate was  $4.9 \text{ month}^{-1}$ .

Analysis of annual variation in the generation factor of mature forms (Figure 2.20f) shows that its annual cycle is divided into two areas: June–July and September–October with a moderate value of the generation factor of 0.1–0.2, as an exception in June, when one TC occurred ( $G = 1.0$ ). The average monthly value of the generation factor is 0.17 (in an active period) which, in general, should be



expected because of the intensive cyclogenesis of primary forms for the interval under investigation. The average annual (in 1997) value of the generation factor in the Atlantic was 0.12.

## **2.6 LARGE-SCALE STRUCTURE OF GLOBAL TROPICAL CYCLOGENESIS**

In this section the term “large-scale structure” is used to refer to the variability of global tropical cyclogenesis on the understanding that data are monthly (and yearly) averaged. As noted above, the different time-averaged sizes of readings for complicated fractal systems may, broadly speaking, give quite different results. We will demonstrate these intriguing features in the time series of global tropical cyclogenesis time below.

### **2.6.1 Spatiotemporal variability in global cyclogenesis**

Vortical structures in the tropical atmosphere may occur at any period of the year in tropical areas of oceans (with the exception of the southeast Pacific and the South Atlantic) given a certain combination of hydrometeorological settings in the atmosphere and on the Earth’s surface (see Chapter 4). This combination of settings substantially varies with each region and from year to year. Nonetheless, there exists a certain regularity, which is considered below.

The origination centers, frequency, and recurrence of TCs have all been determined—and basic pathways along which they advance have been predicted—as a result of climatological processing of satellite data.

The World Ocean (WO) Basin is rather conventionally subdivided into six regions, each with its own specific spatiotemporal features of tropical cyclogenesis (Minina, 1970; Neumann, 1993; Pielke and Pielke, 1997).

Four regions are in the NH:

- the NWP bounded by 0–40°N and 100–180°E;
- the NEP bounded by 0–40°N and 100–180°W;
- the northern part of the Atlantic Ocean (NA) bounded by 0–40°N and 20–100°W;
- the NIO bounded by 5–25° and 50–100°E.

Two regions are in the SH:

- the SWP bounded by 5–30°S and 30–130°E;
- the SIO bounded by 5–30°S and 30–130°E.

There are authors who hold the view that there should be a more detailed spatial separation of global cyclogenesis.

In this section we consider the distribution and contribution of each of the six basins of the World Ocean within a 10-year period of cyclogenesis based on the information provided by the Global-TC dataset (Pokrovskaya and Sharkov, 1994c, 1997a, 1999a,d). The major information parameter is the total number of TCs occurring monthly or yearly (the cyclogenesis rate) during a 10-year cycle (1983–1992) both over the entire basin of the World Ocean and certain active basins (expressed as a percentage of the total number of TCs on a global scale) (Pokrovskaya and Sharkov, 1995a).

Global cyclogenesis overall (annual average indices) and its regional components within the 27-year period of 1983–2010 is shown in Table A.1 (Appendix A). Analysis of the data presented shows that between 75 and 90 TCs per year (an average 86 TCs per year) occur throughout the World Ocean Basin, and two-thirds of these occur in the southern and eastern hemispheres. Cyclogenesis was abnormally intensive in 1992 (99) and weak in both 1988 (75) and 1993 (75). The number of TCs distributed (on average) throughout the six cyclogenesis regions is (per annum): NWP above 30 TCs; NEP 18; NA 9; NIO 4; SWP 15; and SIO 10 TCs (Figure 2.21).

Despite mass-media reports about the destructive consequences of TCs in the NIO basin, from the standpoint of cyclogenesis intensity the contribution of this basin is the lowest (4.6% over the 10 years). Cyclogenesis in this region is stable with slight annual variation. Cyclogenesis is predominantly controlled by the monsoon features of the regional climate.

The NA and SIO basins likewise provide a low contribution (NA 10.6% and SIO 11.6% on average) to global cyclogenesis. Annual variation is also similar and rather stable. The SWP basin provides a substantially higher contribution to cyclogenesis (17.9%) and is free of any considerable annual variation.

During the 10 years under consideration, it should be noted that we observed considerable stability in the cyclogenesis processes taking place in the NWP basin, which provides 32.9% of the total number of TCs to global cyclogenesis. The last basin (NEP), in our opinion, is the most interesting for two reasons: first, it provides a considerable contribution to cyclogenesis (22.1%) and, second, because of its peculiar destabilizing effect on global cyclogenesis variation. For instance, the above-mentioned abnormally weak (1988) and intensive (1992) cyclogenesis were mostly the consequence of sharp variation that occurred in this basin. Elucidation of the physical reasons for such a material variation in NEP cyclogenesis is a subject worthy of further investigation. One probable cause is the rather sharp change in the character of the atmospheric circulation in the SH which took place in 1987–1988 and 1991–1992 (ENSO phenomena) (Henderson-Sellers *et al.* 1998; Revell and Goulter, 1986).

Let us now consider the same 10-year time series of global tropical cyclogenesis in a different way using the cumulative function (Section 2.1). In the case being considered, all the timescales of interaction will be taken into account to depict the structure of the cumulative process. Figure 2.22 illustrates the 10-year temporal evolution of the cumulative functions of global tropical cyclogenesis and of NH and SH cyclogenesis.

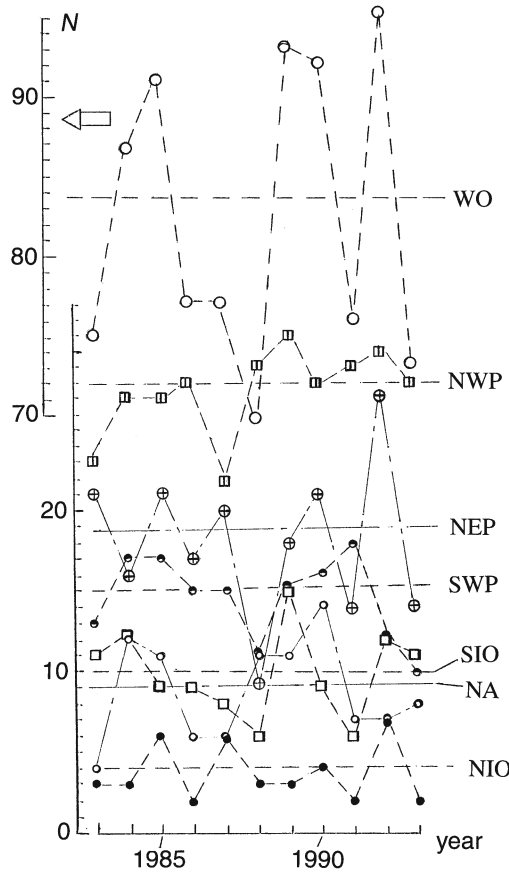


**Figure 2.21.** Temporal evolution of the year-averaged intensity of global and regional cyclogenesis for the 10-year period 1983–1992. See symbols in the text of Section 2.6.1 (from Pokrovskaya and Sharkov, 1994c).

As expected, the temporal evolution of cumulative functions differs fundamentally from year-averaged temporal patterns. The cumulative functions of both global cyclogenesis and hemisphere cyclogenesis are linear functions with small variation and are the consequence of intra-annual features.

These functions are best demonstrated by the NH pattern (Figure 2.22). Global and SH cumulative functions have less pronounced intra-annual features.

It is significant that the cumulative patterns exhibit the following characteristics:

- high degree of regularity;
- total absence of interannual variation of any values;
- stable values of averaged slopes of approximated straight lines.

This characteristic (i.e., averaged slope) is of great importance in cyclogenesis dynamics since it may be physically interpreted as the global rate of cyclogenesis

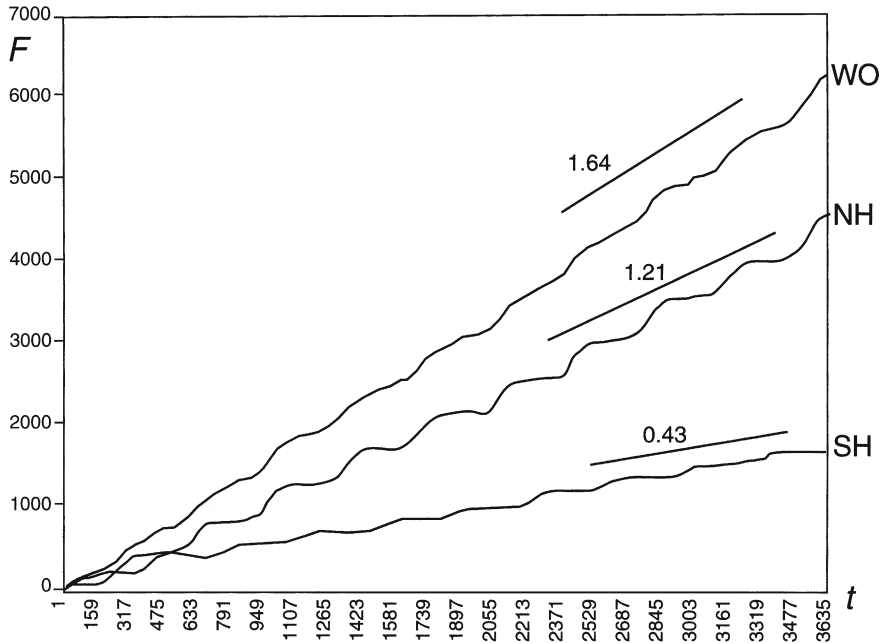


**Figure 2.22.** Ten-year time series of the cumulative functions ( $F$ ) of global tropical cyclogenesis (WO) and of NH and SH cyclogenesis. The timescale is in days. Figures next to the straight lines represent values of the intensity of the Poisson process.

generation. As for global tropical cyclogenesis for the 10-year period (1983–1992), the global rate of cyclogenesis generation is equal to 1.64 events/day, while the rates of NH and SH cyclogenesis equal 1.21 and 0.43 events/day, respectively. Thus, the global rate of NH cyclogenesis far exceeds (2.82 times as great) these characteristics for the SH.

Furthermore, it must be emphasized that the intra-annual variation for NH and SH cyclogenesis has the property of clearly defined harmonicity. The first harmonics for hemisphere cyclogenesis are phase-shifted by about half a year. This feature of global cyclogenesis is well known (Minina, 1970; Neumann, 1993; Pokrovskaya and Sharkov, 1994c, 1995a).

### 2.6.2 Intra-annual variation of global cyclogenesis

Let us now turn to considering (monthly averaged) annual variation of global cyclogenesis (Pokrovskaya and Sharkov, 1994c, 1995a). Analysis of the intensity of global cyclogenesis (monthly averaged) presented in Figure 2.23 provides evidence of some of its peculiarities. We can see that two maxima occurred in the 10-year period (in February and September). The first is due to activity in basins of the SWP and SIO and is as much as 5 TCs per month. We can see a sharp increase in cyclogenesis in August–September (up to 12 TCs per month) which is mainly due to

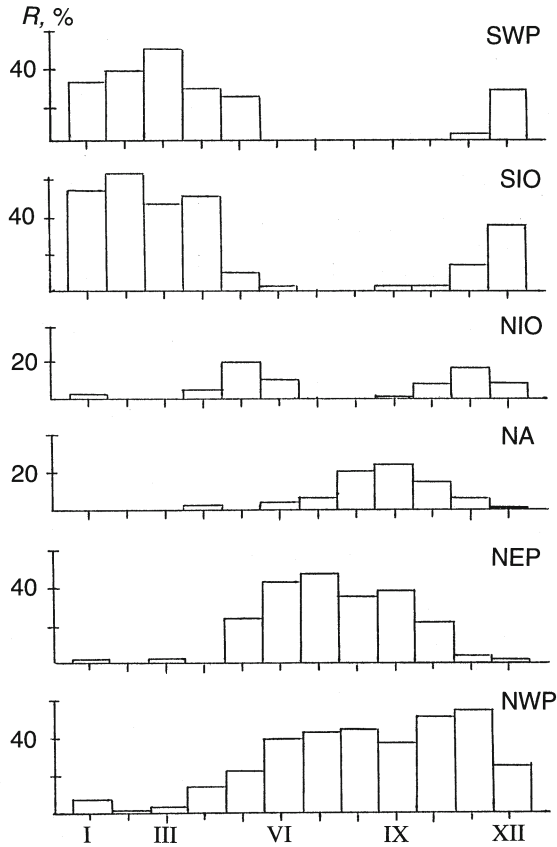


**Figure 2.23.** Relative contribution ( $R$ ) of the active basins of the World Ocean to global cyclogenesis (monthly averaged). See symbols in Section 2.6.1 (from Pokrovskaya and Sharkov, 1995a).

activity in the NEP and NWP. When considering the relative contribution to tropical cyclogenesis from oceans located in the NH and SH (Figure 2.24), we can see an interesting regularity in that the contribution from SH oceans dominates (more than 80%) in January to April, whereas in June to October the situation radically differs where contribution from the NH ocean predominates (more than 90%). May and December can be viewed as transition periods where the contribution of each hemisphere is about 50%.

### 2.6.3 Spatial structure of generation centers

In order to assess the TC generation capability of basins, let us introduce a quantitative parameter: the spatiotemporal rate (STR) of cyclogenesis  $K$  over a  $1,000 \times 1,000$  km basin per month in an active cyclogenesis season in a given

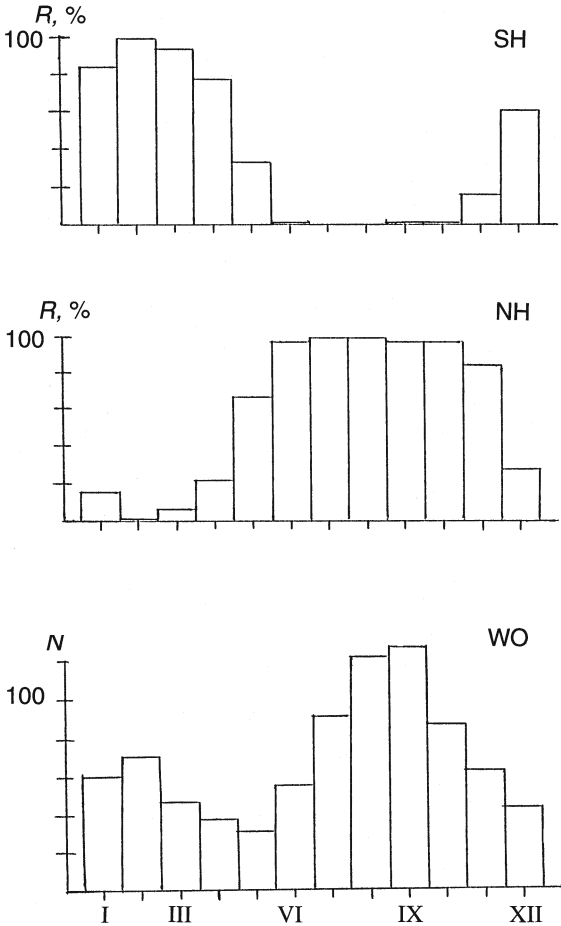


**Figure 2.24.** Global cyclogenesis intensity in 1983–1992 (monthly averaged) and the relative contributions ( $R$ ) of basins in the NH and SH. The values of  $N$  are given in absolute units (number of TCs per month from 1983 to 1992); the values of  $R$  are given as percentages (from Pokrovskaya and Sharkov, 1995a).

region (Pokrovskaya and Sharkov, 1995a). Based on the spatiotemporal characteristics of this parameter, we can make certain conclusions about space-monitoring strategy and tactics.

Let us start the analysis of spatial features of metastable zones with the NWP basin, which makes a large contribution to global cyclogenesis. [Figures 2.25](#) and [2.26](#) present spatial maps of tropical cyclogenesis origination centers in the eastern and western hemispheres. Blackened points designate the geographical locations of TC initial phases, which subsequently convert to tropical storms (TSs). Analysis of the geographical spatial distribution of origination centers shows the sharply irregular concentration of origination centers. We can clearly trace zones where there is an

**Table 2.10.** Values of the spatiotemporal rate parameter for cyclogenesis in the northwest Pacific Ocean basin.

<i>Block coordinates (°N, °E)</i>	<i>Parameter values</i>
10–20, 110–120	0.38
15–25, 130–140	0.36
15–25, 140–150	0.42
15–25, 150–160	0.22
5–15, 130–140	0.70
5–15, 140–150	0.67
5–15, 150–160	0.47

increased concentration of these centers: intensive cyclogenesis zones about  $300 \times 300$  km in size. For instance, we can distinguish at least three active zones in the NWP with the following centers:  $10^\circ\text{N}$ ,  $145^\circ\text{E}$ ;  $13^\circ\text{N}$ ,  $132^\circ\text{E}$ ; and  $17^\circ\text{N}$ ,  $133^\circ\text{E}$ .

Also noteworthy is the great number of TDs (27 of 274 within a 10-year period) that convert to advanced phases in the immediate vicinity of a coast, at a range of 20 km to 100 km. Table 2.10 presents estimates of the spatiotemporal rate for the most heavily filled blocks in the NWP basin. As expected, southern blocks in this basin turn out to be most informative. The cyclogenesis rate sharply decreases to the north and east of these blocks (by an order of magnitude). Note that a closed basin in the South China Sea also experiences intensive cyclogenesis ( $K = 0.38$ ).

A far higher concentration of origination centers is exhibited in regional cyclogenesis in the NEP (Figure 2.25), where a vast ( $500 \times 500$  km) active zone is found confined by the coordinates of  $15^\circ\text{N}$  and  $100^\circ\text{W}$ . It is as close as 250 km from the Mexican coastline. Moreover, the occurrence of TD effects in the immediate vicinity of North America has been likened to those in the NWP. So, in the offshore zone (200 km) of the NW basin of the Pacific Ocean nearly 30 TCs have originated (i.e., 17% of the total number of regional TCs).

When assessing the STR for the most heavily filled blocks—those with coordinates of  $10\text{--}20^\circ\text{N}$ ,  $100\text{--}110^\circ\text{W}$  (polygon A),  $10\text{--}20^\circ\text{N}$ ,  $110\text{--}120^\circ\text{W}$  (polygon B), and  $5\text{--}15^\circ\text{N}$ ,  $90\text{--}100^\circ\text{W}$  (polygon C)—we get the following values:  $K = 1.7$  for polygon A;  $K = 0.7$  for polygon B; and  $K = 0.76$  for polygon C. In other parts of this basin the STR sharply decreases by an order of magnitude or more (e.g.,  $K = 0.18$  for polygon D, with coordinates of  $10\text{--}20^\circ\text{N}$  and  $145\text{--}155^\circ\text{W}$ ). This suggests that blocks A, B, and C are of most interest to space monitoring. This is so because the frequency of spacecraft intersecting the possible origination center of a vortex structure is greatest here.

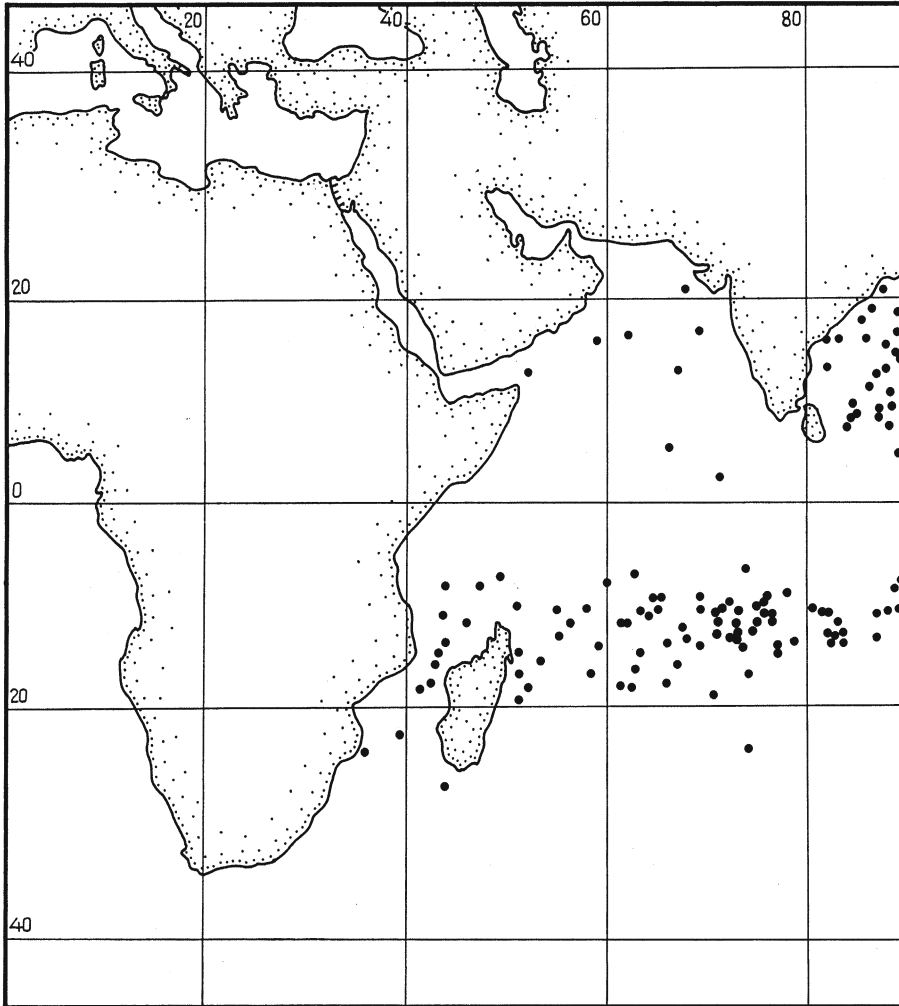
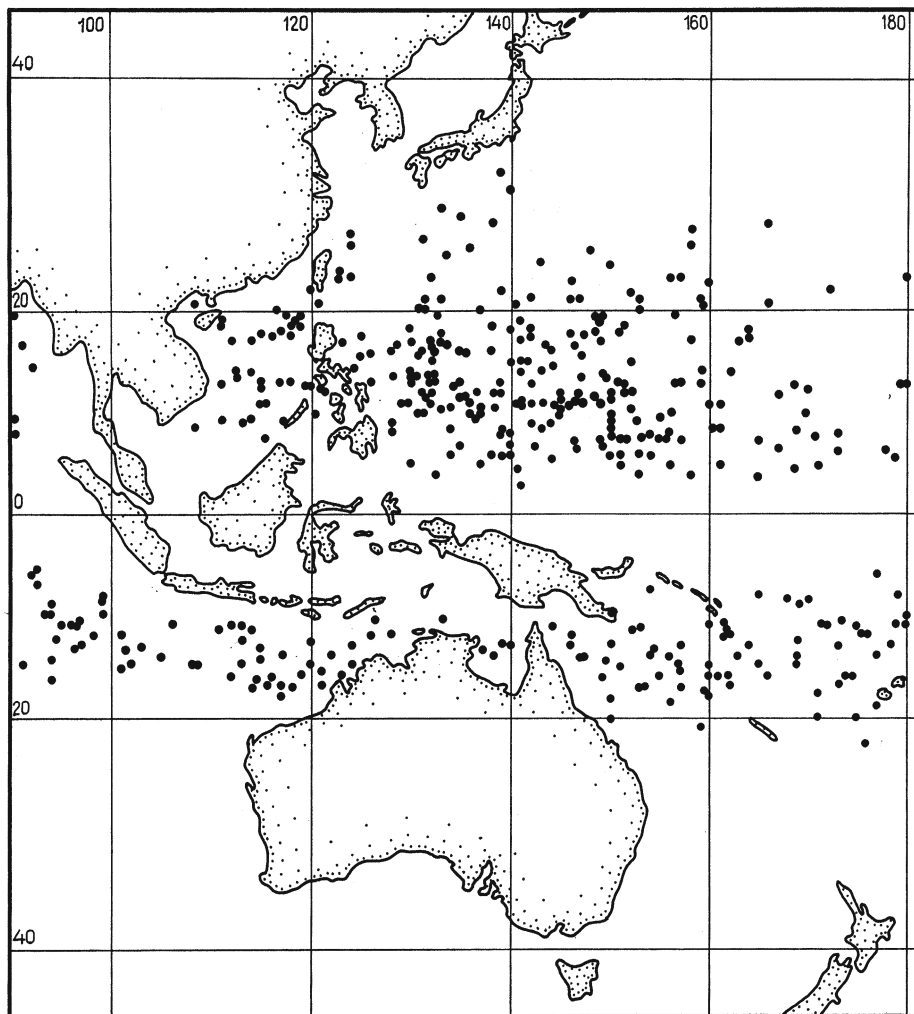


**Figure 2.25.** Spatial maps of tropical cyclone generation centers in the eastern hemisphere for 1983–1992. Points designate geographical locations of the generation stage of TCs (from Pokrovskaya and Sharkov, 1995a).

From the standpoint of tropical cyclogenesis, the Atlantic basin of the World Ocean (Figure 2.26) has the following features: advanced forms of TC occur only in its northern part (i.e., the North Atlantic); cyclogenesis is “scattered” rather uniformly throughout the vast basin; and no activity centers have revealed themselves (within a 10-year cycle). STR values are in the range  $K = 0.13$ – $0.3$  both in the open sea and in closed basins (e.g.,  $K = 0.26$  in the Gulf of Mexico). Much as in other active basins, in this basin a great number of TCs (up to 10% of the total) have originated in the immediate vicinity of a coast. This effect is most pronounced for TC





origination in closed basins (i.e., the Gulf of Mexico and the Caribbean Sea). The origination and formation of TCs at upper latitudes right up to  $37\text{--}38^\circ\text{N}$  are important and distinctive features of Atlantic cyclogenesis; they are most likely due to the Gulf Stream.

Though the NIO (Figure 2.26) is characterized by weakly defined cyclogenesis (4.5% of total number of TCs in the World Ocean over 10 years), we can clearly see an active zone located in the area with coordinates of  $9^\circ\text{N}$  and  $85^\circ\text{E}$  (Bay of Bengal). What is more, estimation of the STR in this basin provides a rather high value of

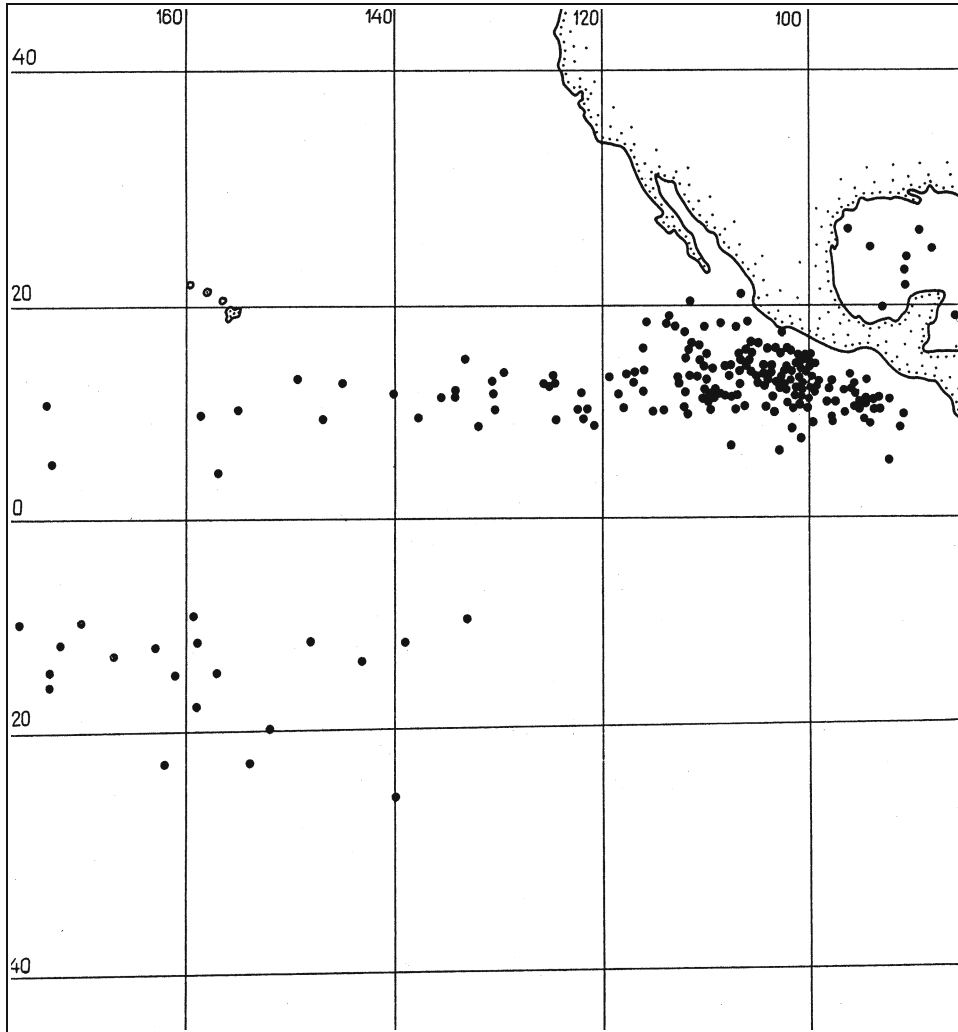
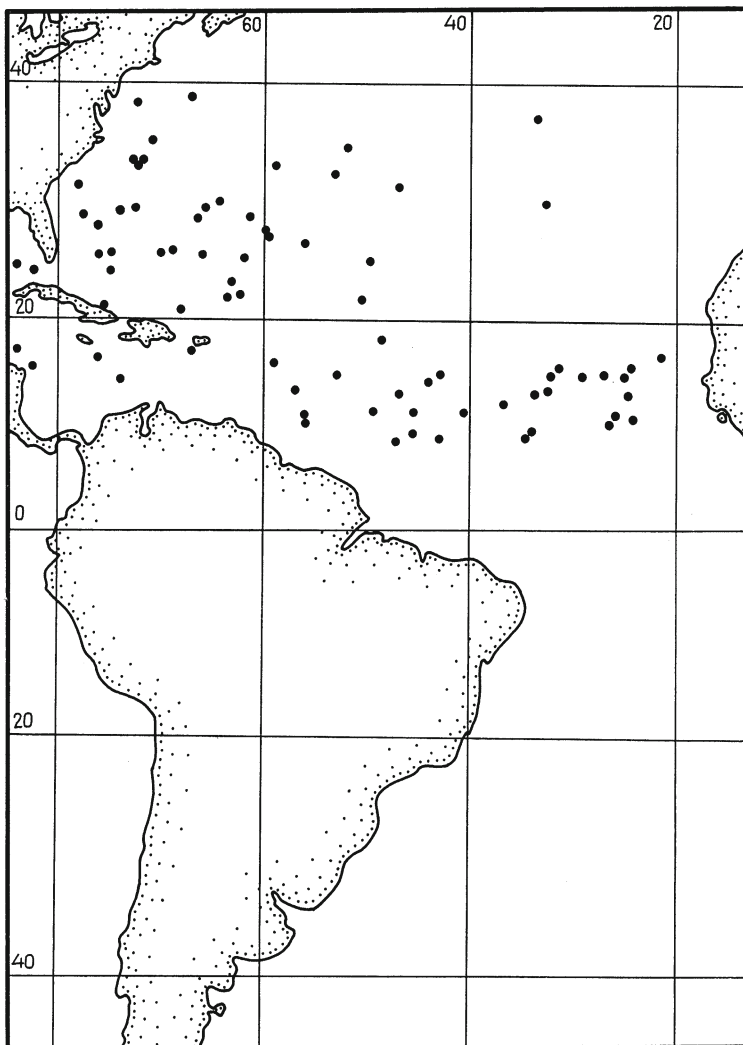


**Figure 2.26.** Spatial maps of tropical cyclone generation centers in the western hemisphere for 1983–1992. Symbols are the same as in [Figure 2.25](#) (from Pokrovskaya and Sharkov, 1995a).

parameter  $K$  ( $K = 0.65$ ) because of the short duration of cyclogenesis activity during monsoon periods. About 30% of TCs occur in the immediate vicinity of the coast (200 km). Practically all TCs that originate in the Bay of Bengal are serious hazards to the heavily populated areas of Bangladesh and India. Another noteworthy feature of NIO cyclogenesis is that, in particular cases, TCs have even originated near desert areas such as the Arabian Desert (i.e., in regions with distinctly reduced humidity).



In southwestern parts of the Pacific and Indian Oceans, TC origination centers are distributed more or less uniformly, without sharply defined active zones. Estimates of the STR are  $K = 0.1-0.4$  for the SWP and  $K = 0.2-0.4$  for the SIO. From the observational standpoint, of most interest are studies of intensive cyclogenesis ( $K = 0.6$ ) in the offshore zone of the Indian Ocean near the western coast of Australia (Great Sand Desert), in closed and shallow seas (Timor and Arafura Seas), and the closed shallow Gulf of Carpentaria.

## 2.7 HIERARCHICAL STRUCTURE OF GLOBAL TROPICAL CYCLOGENESIS

Global tropical cyclogenesis is a good example of a chaotic process, in which the resulting picture is formed as a consequence of a whole series of thermohydrodynamic interactions of different intensities, occurring in a very broad range of temporal and spatial scales and resulting in a rather complex hierarchical structure.

Despite this obvious physical evidence, the approach involving the intentional apportionment and separation of the unitary global tropical cyclogenesis process into two (or several) timescales (daily, monthly averaged, or yearly averaged) is used widely (e.g., see Gray *et al.*, 1997; Wilson, 1997; Landsea *et al.*, 1999; Smith, 1999; Elsner and Kara, 1999). We have also used this approach in the study of the time series of global tropical cyclogenesis (see Sections 2.2–2.3 and 2.6). However, it is obvious that a number of timescales of interactions are entirely lost under these conditions. To ease comprehensive study of these difficulties, a mathematical method for processing time series can be used to perform the analysis across wide timescales.

Astafyeva *et al.* (1994a,b,c) proposed and developed a modern approach called the wavelet transform method for the purpose of processing time series of global tropical cyclogenesis and, thus, revealing the effective scales of interactions. The wavelet transform method consists of expanding the signal under study in terms of the hierarchical basis that is attractive for direct analysis of complicated signals.

As this approach for processing observational data has not gained widespread acceptance in remote-sensing and geophysical investigations, we consider it opportune to carry out a concise review of its main properties.

### 2.7.1 Main properties and examples of wavelet transform

The notion of a wavelet (literally, a small wave) began in the 1980s when Grossmann and Morlet applied it to analysis of the properties of seismic and acoustic signals (Chui, 1992; Astafyeva, 1996; Bouman and Newell, 1998). The family of analytical functions dubbed wavelets is being increasingly used to address problems in pattern recognition, in processing and synthesizing of various signals (e.g., speech); in the analysis of images of any kind (satellite images of clouds, a planet's surface, mineral-bearing rocks, etc.), in the study of turbulent fields, in the contraction (compression) of large volumes of information, and in many other spheres of interest.

The wavelet transform of a one-dimensional signal involves its decomposition over a basis obtained from a solution-like function (wavelet), possessing some specific properties, by means of dilation and translation. Each of the functions of this basis emphasizes both a specific spatial (temporal) frequency and its location in physical space (time).

Thus, unlike the Fourier transform traditionally used in signal analysis, the wavelet transform offers a two-dimensional expansion of a given one-dimensional signal, with the frequency and the coordinate treated as independent variables. As a result, the possibility emerges of analyzing the signal simultaneously in physical

(time, coordinate) and frequency spaces. All of this can readily be generalized to multidimensional signals or functions.

The area in which wavelets can be used is not confined to analysis of the properties of signals and fields of arbitrary nature obtained numerically, experimentally, or observationally. Wavelets are beginning to be used in direct numerical simulations as hierarchical bases that are well suited to describe the dynamics of complex non-linear processes characterized by the interaction of perturbations across wide ranges of spatiotemporal scales.

Many researchers refer to wavelet analysis as the “mathematical microscope”, as this term accurately conveys the remarkable capability of the method to offer good resolution at different scales (Astafyeva, 1996). The capability of this microscope to reveal the internal structure of an essentially inhomogeneous process (or field) and expose its local scaling behavior has been demonstrated through many classical examples such as fractal Weierstrass functions and the probability measures of the Cantor series, to mention a couple. Application of wavelet analysis to a turbulent velocity field in a windtunnel under large Reynolds numbers offered for the first time a vivid confirmation of the Richardson cascade. The analogy between the energy cascade and the structure of the multifractal inhomogeneous Cantor series was explicitly settled. Even more efficient was the application of wavelet analysis to the multifractal invariant measures of several well-known dynamical systems that model the transitions to chaos observed in dissipative systems (Nicolis and Prigogine, 1977; Kadanov, 1993; Dubois, 1998).

So, wavelet analysis can be successfully applied to solve various problems. It is, however, not widely known to researchers dealing with the analysis of experimental and observational data. In this section, an attempt is made to outline the main properties needed in practical applications of the wavelet transform to processing signals of various types.

For practical applications it is important to know the criteria that a function should satisfy in order to be a wavelet; we (following Astafyeva, 1996) present them here and consider, by way of examples, certain well-known functions by ascertaining whether they observe these criteria:

- *Localization.* Unlike the Fourier transform, the wavelet transform is based on a localized basis function  $\psi(t)$ . A wavelet must be localized both in time and frequency.

- *Zero mean*

$$\int_{-\infty}^{\infty} \psi(t) dt = 0 \quad (2.26)$$

In applications, it is frequently necessary to additionally have the first  $m$ -zero moments:

$$\int_{-\infty}^{\infty} t^m \psi(t) dt = 0 \quad (2.27)$$

Such a wavelet is referred to as an  $m$ -order wavelet. Wavelets possessing many zero moments enable us to ignore most regular polynomial components of signals and analyze their small-scale fluctuations and high-order features.

- *Boundedness*

$$\int |\psi(t)|^2 dt < \infty \quad (2.28)$$

Possessing these properties, the soliton-like function (wavelet) forms the basis for designing the necessary base for the family of functions, obtained from a single function  $\psi(x)$ :

$$\psi_{a,b}(x) = |a|^{-\eta} \psi\left(\frac{x-b}{a}\right), \quad a, b \in R, \quad a < G \quad (2.29)$$

A characteristic feature of a wavelet transform basis is its self-similarity. All wavelets of a given family  $\psi_{a,b}(t)$  have the same number of oscillations as the basis wavelet  $\psi(t)$ ; they are derived from it by scale transforms and translations. It is for this reason that the wavelet transform is successfully used in fractal analysis.

The continuous wavelet transformation of a one-dimensional function  $f(x)$  is of the form:

$$W(a, b) = C^{-1/2} a^{-1/2} \int \psi\left(\frac{x-b}{a}\right) f(x) dx \quad (2.30)$$

where  $C = \int |k|^{-1} |\psi(k)|^2 dk$  is a normalizing constant; and  $\psi(k)$  is the Fourier transform of  $\Psi(x)$ .

Decomposition of the analyzing signal on scales is realized by means of extending or compressing the analyzing wavelet before its combination with the signal. This brings about the fact that wavelet transformation has good agreement both on large and small scales.

If the analogy of a “mathematical microscope” is pursued further, then the translation parameter  $b$  fixes the focusing point of the microscope, the scale factor  $a$  the magnification, and finally the choice of the basis wavelet  $\psi$  determines the optical quality of the microscope (Astafyeva, 1996).

When performing calculations under these conditions the wavelet transform is reversible in so far as it can recover a function on its wavelet transform. The formula for reconversion is of the form:

$$f(x) = C^{-1/2} \int \psi\left(\frac{x-b}{a}\right) W(a, b) da db / a^2 \quad (2.31)$$

where  $da db / a^2$  is a surface element that does not change at either shift or zoom.

Let us write down the basic elementary properties of the wavelet transform of function  $f(t)$ —the designation  $W[f] = W(a, b)$  will be adopted for brevity:

- *Linearity*

$$W[\alpha f_1(t) + \beta f_2(t)] = \alpha W[f_1] + \beta W[f_2] = \alpha W_1(a, b) + \beta W_2(a, b) \quad (2.32)$$

It therefore follows that the wavelet transform of a vector function is a vector with components that are wavelet transforms of the respective components of the vector analyzed.

- *Translational invariance*

$$W[f(t - b_0)] = W(a, b - b_0) \quad (2.33)$$

This property leads to the commutativity of differentiation, in particular,  $\partial_t W[f] = W[\partial_t f]$  (here  $\partial_t = \partial/\partial t$ ). Together with the first property it implies permutability for vector analysis derivatives.

- *Invariance to dilations (contractions)*

$$W\left[f\left(\frac{t}{a_0}\right)\right] = \frac{1}{a_0} W\left(\frac{a}{a_0}, \frac{b}{a_0}\right) \quad (2.34)$$

This property makes it possible to determine whether the function analyzed has singularities and to investigate their character.

Apart from these three elementary properties, which are independent of the choice of analyzing wavelet, the wavelet transform has a few others. In our opinion, the most important and helpful among them is the following:

- *Differentiation*

$$W[\partial_t^m f] = (-1)^m \int_{-\infty}^{\infty} f(t) \partial_t^m [(\psi_{a,b}^*(t))] dt \quad (2.35)$$

So, if we ignore, for example, large-scale polynomial components and analyze singularities of higher order or small-scale variations of function  $f$  we may perform differentiation of either the analyzing wavelet or the function itself. This is a highly useful property, especially if we remember that the function  $f$  is often defined through a sequence of values while the analyzing wavelet is given by a formula.

For the wavelet transform there exists *an analogue of the Parseval theorem* and the identity

$$\int f_1(t) f_2^*(t) dt = C_\psi^{-1} \iint W_1(a, b) W_2^*(a, b) \frac{da db}{a^2} \quad (2.36)$$

Hence, it follows that the energy of a signal can be calculated in terms of amplitudes (coefficients) of the wavelet transform, in the same way it is computed through the components of the Fourier transform:

$$E_f = \int f^2(t) dt = \int |A(\omega) - iB(\omega)|^2 d\omega \quad (2.37)$$

The definitions and properties of the one-dimensional continuous wavelet transform can be generalized to multidimensional and discrete cases.

Since the wavelet transform is a scalar product of the analyzing wavelet, of the given scale and signal being explored, coefficients  $W(a, b)$  contain combined information on both the analyzing wavelet and the signal (similar to coefficients of the Fourier transform which bear imprints of both the signal and the sinusoidal wave).

The choice of analyzing wavelet is, as a rule, dictated by the type of information to be derived from the signal. Every wavelet has specific features in time and frequency domains and sometimes—by applying different wavelets—we may reveal more fully or emphasize one or other of the signal’s characteristics.

Real-valued bases are frequently constructed from the derivatives of Gaussian functions:

$$\psi_m(t) = (-1)^m \partial_t^m [\exp(-t^2/2)] \quad (2.38)$$

$$\psi_m(k) = m(ik)^m \exp(-k^2/2) \quad (2.39)$$

where  $\partial_t^m = \partial^m[\dots]/\partial t^m$ ,  $m \geq 1$ . Higher derivatives have more zero moments and allow us to retrieve information about the features of higher orders contained in the signals.

Because of their shape, these functions came to be known, respectively, as the WAVE wavelet and the MHAT wavelet or the “Mexican hat” (looks like a sombrero).

The MHAT wavelet, with its narrow energy spectrum and two zero moments (zeroth and first), is well suited to analyze complex signals. Generalized to the two-dimensional case, the MHAT wavelet is frequently used to analyze isotropic fields. If the derivative is taken in one direction, an anisotropy basis can be obtained, with good angular resolution.

The wavelet transform, owing to its hierarchical basis, is well suited to analyze those cascade processes, fractal sets, and multifractal sets that have a hierarchical nature (Mandelbrot, 1977, 1982, 1989, 1998; Coniglio, 1987; Voss, 1989; Lovejoy and Schertzer, 1985; Lovejoy *et al.*, 1986).

We present an example concerning the analysis of a fractal set on the basis of a homogeneous triadic Cantor set. As is known, when constructing the first generation of this set, an interval is divided into three parts and the middle part is excluded; for the second generation the same procedure is excluded; for the third generation the same procedure is applied to the two remaining intervals, and so on at each subsequent stage up to infinity. Figure 2.27(a) displays the first stages of this construction.

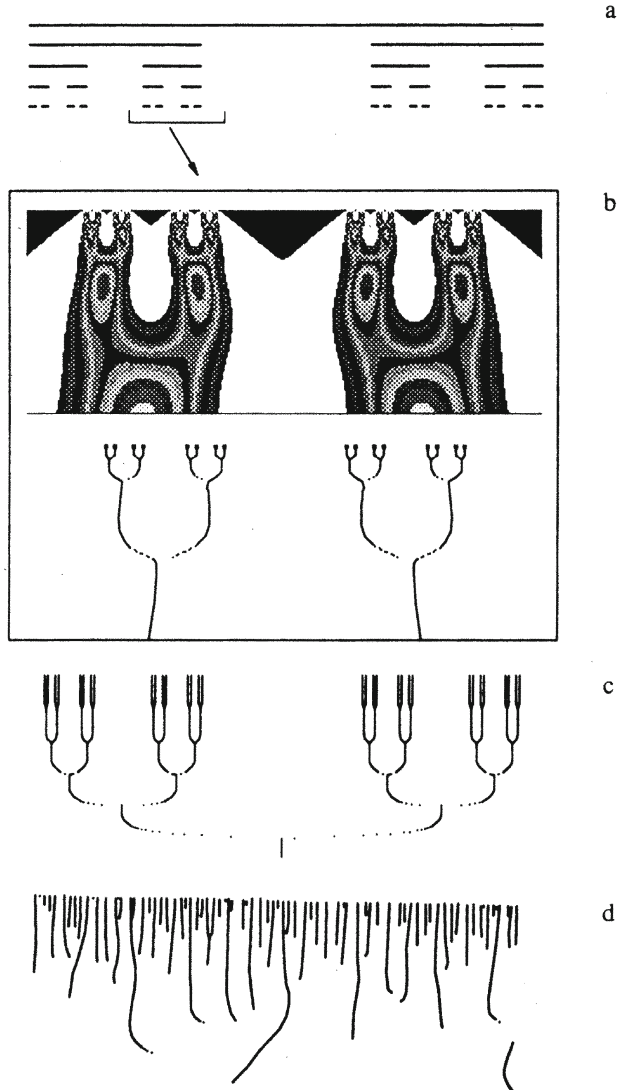
Based on the set constructed, the Cantor dust (a numeric set) is created from zeros and ones (zeros correspond to excluded parts of the interval).

Figure 2.27(b) presents the patterns of coefficients and local maximum lines. They are reasonably detailed; however, linear scale sweep does not allow a broad-scale range to be presented. To demonstrate the general character of the process, Figure 2.27(c) shows the skeleton in logarithmic axes.

The pattern of coefficients displays the hierarchical structure of the set presented. It is seen even more clearly in the patterns of local maximum lines. The skeleton not only reveals the hierarchical structure, but also shows how the fractal measure—on which the set is formed—was constructed.

At every stage of the cascade process, every scale subdivision is marked off on the local maximum pattern by branching giving the appearance of a peculiar “fork”: the line marking the local maximum position bifurcates into two independent local





**Figure 2.27.** First generations of a homogeneous triadic Cantor series (a), fragments of the patterns of coefficients and local maximum lines (b), pattern of local maximum lines for a triadic homogeneous Cantor series (c), and a random process (d) on the logarithmic scale (from Astafyeva, 1996).

maximum lines. This is the invariably recurrent feature since the measure is self-similar and monofractal.

It is known that the fractal dimension or self-similarity dimension of the homogeneous Cantor set  $D_f = \ln m / \ln s$ , where  $m$  is the branching rate and  $s$  is the scale factor. In the case of the triadic set  $D_f = \ln 2 / \ln 3$ . Using wavelet transform coefficients as the limit (with the scale going to zero) we can also assess

the dimension of the ratio  $\ln N(a)/\ln a$ , where  $N(a)$  is the number of local maxima. The higher the order of generation used for the Cantor set, the more accurately can its dimension be determined; for the 10th–11th generations the value computed by wavelet transform coefficients practically coincides with that found analytically.

For comparison, Figure 2.27(d) pictures local maximum lines of a random process. We can see how different, even qualitatively, the tree-like structure of the skeleton of the cascade process and the grass-like skeleton of the random process are (they could be likened to periodic skeletons of harmonic functions and bushes of lines marking off the singularities of signals).

Numerous examples of using the wavelet transform are described by Astafyeva (1996). Let us look at one of them that relates to the transformation of the “devil’s staircase”—a well-known and nearly differentiable function, built on the basis of the uniform Cantor set (Astafyeva *et al.*, 1994b). Figure 2.28 displays the typical “devil’s staircase” (Figure 2.28a), the pattern of wavelet transforms  $W(a, b)$  (Figure 2.28b), and a corresponding picture of local maximums of factors  $W(a, b)$  (Figure 2.28c).

In Figure 2.28(b) several ranges of the values of factors  $W(a, b)$  of wavelet transforms are marked by different tones. On the axis of abscissa a change to coordinate  $b$  is plotted and coordinate  $a$  is laid off on the axis of ordinates. So that details can be seen more clearly, only part of the picture showing the factors of wavelet transforms being changed is presented. The picture of the wavelet transform shows a hierarchical structure of the analyzing set (i.e., the “devil’s staircase”).

Nowhere else is it seen more clearly than in Figure 2.28(b) where the local maximums of wavelet transform coefficients are marked. The picture of local maximums reveals not only the hierarchical structure of the analyzing set, but also the way of building the fractal set to which it is connected. As is well known, on building the first generation of a uniform Cantor set, the length is divided into three parts, the average of which is rejected. On building the second generation such a procedure is performed using the two remaining lengths at each following stage, and so on.

Each such “crushing” scale is marked on the picture of local maximums by branching giving the appearance of a “fork” that notes the position of the local maximum, where the line bifurcates and separates into two independent local maximums. This can be repeated on all scales, since the process is fractal and possesses self-similar characteristics.

It should be noted that the “devil’s staircase” has been successfully employed in describing the hierarchical oscillator system, showing evidence of the phase transition from aperiodicity to a chaotic regime (e.g., like ENSO; Jin *et al.*, 1994, 1996).

To summarize, the examination of wavelet patterns has much potential for yielding information about the possible type and quantitative characteristics of dynamical systems. By this expedient we can clearly identify the different types of dynamical systems like the “pure” random oscillator (e.g., Poisson type or Brownian motion model), the harmonic oscillator (e.g., van der Pol model), aperiodic and pulsed oscillators (e.g., multivibrators), the intermittent oscillator (e.g., trigger type and “irregular burst” type), the hierarchical system (e.g., Cantor set type and

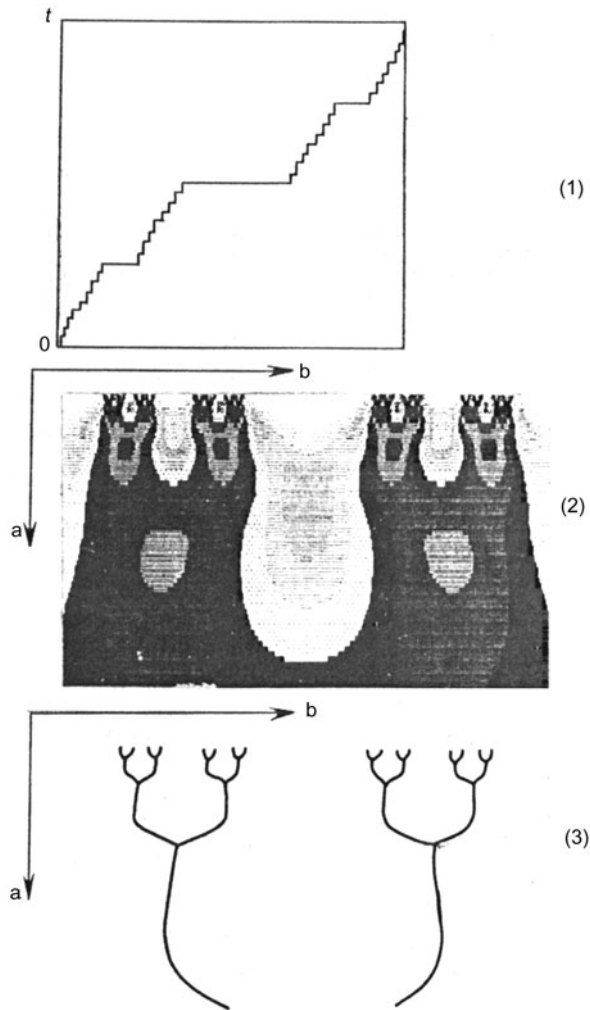


**Figure 2.28.** The “devil’s staircase” function (1), the pattern of the wavelet transform (2), and corresponding local maximum lines (3) (from Astafyeva *et al.*, 1994b).

Sierpinski gasket type), and the dynamical system near the transition point from order to chaos (e.g., Lorenz’s system and Duffing’s system).

The useful information on the structure and the temporal behavior of the simulation of (theoretical) dynamical systems can be obtained from many publications (e.g., Schuster, 1984; Landa, 1996; Kadanov, 1993; Chen and Dong, 1996; Gilmore, 1998; Dubois, 1998).

Of course, the identification of contrasting types of dynamical system, like the harmonic oscillator and the multivibrator, can be performed more simply by examining the time series of these processes without resorting to the wavelet procedure.

However, naturally complex systems (e.g., physical, geophysical, biological, and economic) usually consist of many subsystems. While subsystems can interact with each other, they also interact with an external environment. These combined effects give rise to both the non-linear and chaotic behavior of the system as a whole (e.g., Jin *et al.*, 1996; Jensen, 1998; Schweitzer, 1997; Gohara and Okuyama, 1999; Boccaletti *et al.*, 2000). All of this means that the successful analysis of such dynamical systems can be performed only by a processing procedure that considers wide ranges of temporal scales and has good resolution at different scales simultaneously. One such method is the wavelet transform procedure. In Section 2.7.2 we will use this approach to study the hierarchical structure of global tropical cyclogenesis as a complex natural system.

### 2.7.2 Wavelet patterns of global tropical cyclogenesis

The methodical basis of forming a time series of observational data of global tropical cyclogenesis offers up the idea of shaping and studying probabilistic features of the intensity of tropical cyclogenesis as signals having a complicated structure (type of telegraphic process) with the help of the mathematical device of the theory of random flows (see Section 2.1).

In accordance with this approach, the process being analyzed develops as follows. Leaving to one side the details and track record of individual tropical structures, we shall place each TD on the time axis as a pulse of single amplitude with a duration equal to the TC lifetime. The number of received pulses (indistinguishable events) in a single time interval (for us it is a day) is a natural physical parameter: the intensity of global tropical cyclogenesis.

The sequence of pulses formed by this method, with corresponding duration and amplitude, is simply the integer random time flow of indistinguishable events.

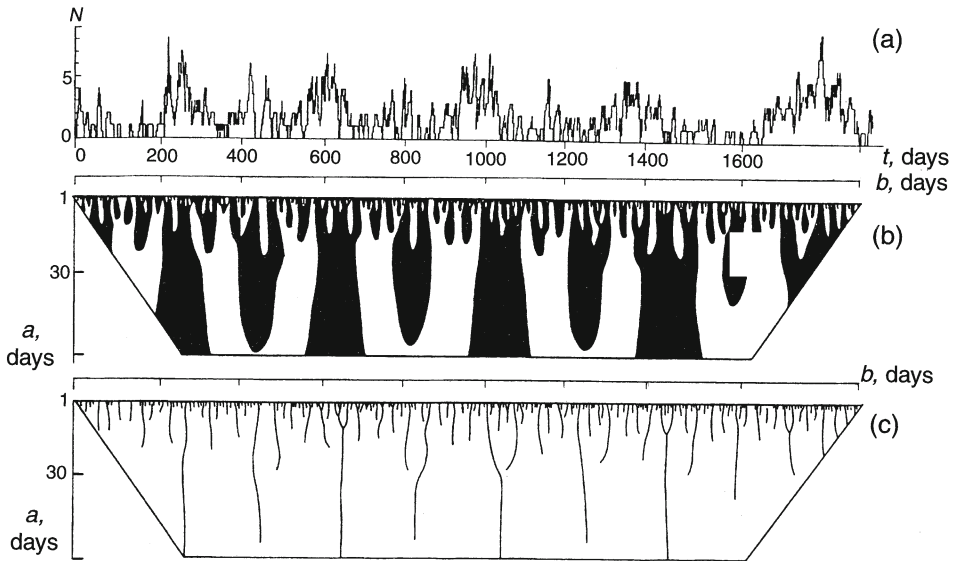
Figure 2.29a shows the time series formed by the method described from 5-year observational data, which reveals the changing intensity of global tropical cyclogenesis in the period 1988–1992.

Figure 2.29b, c presents the results of using the wavelet transform to obtain the time series (its length is 1,827 days).

As already noted, the wavelet transform of a one-dimensional signal shows us its two-dimensional expansion in temporal and spectral space  $W(a, b)$ . On the axis of abscissas changing time in days  $b$  is plotted and on the axis of ordinates the scale parameter  $a$  is presented on the linear scale. In order not to complicate the picture, obtained as a result of the wavelet transform, no different ranges of values of coefficient  $W(a, b)$  are shown, just its positive values in black.

The pattern of the wavelet transform coefficient reveals the periodic behavior of analyzing the process on average scales: annual and semi-annual periods clearly stand out. Figure 2.29c presents the corresponding picture for focal maximums. It is proposed that semi-annual and annual features of the intensity of global tropical cyclogenesis are independent.

The part of the surface (three-dimensional image) described by coefficients  $W(a, b)$  from 300 up to 1,500 days is shown in Figure 2.30. Six large-scale



**Figure 2.29.** Time series of the intensity of global cyclogenesis ( $N$ ) (a), the pattern of the wavelet transform (two-level) (b), and corresponding local maximum lines (c) for 1988–1992 (from Astafyeva *et al.*, 1994b).

“hunches” with approximately semi-annual period stand out sharply against the random noise: the three smaller ones are connected with increasing global tropical cyclogenesis in February and March, the three larger ones are connected with activity in August and September.

Figure 2.31 presents the changing intensity of global cyclogenesis (Figure 2.31a), the pattern of the wavelet transform (Figure 2.31b), and the pattern of local maximums (Figure 2.31c) for that part of the signal noted in Figure 2.29. These detailed results allow us to analyze the finer structure of the signal on small scales. Note the “forks”—which are an integration (bifurcation) of scales and the truth—are unlike the ones for the fractal set described above.

The pattern of the wavelet transform and the picture of local maximums, obtained with the fast-rising “hat” that reveals the properties of the process on greater timescales, do not allow us to reach an unambiguous conclusion about the appearance of “forks” resulting from the merging of annual local maximum lines. From the 5-year data we have been unable to ascertain whether a hierarchy of scales on the time order of several years exists.

We believe that the main result of scientific studies should be aimed at finding the hierarchical time structure of global tropical cyclogenesis. Such a result would allow a more goal-directed approach to building stochastic evolution models of tropical cyclogenesis (e.g., separate thermodynamic and kinetic physical factors that stipulate the developmental particularities of cyclogenesis).

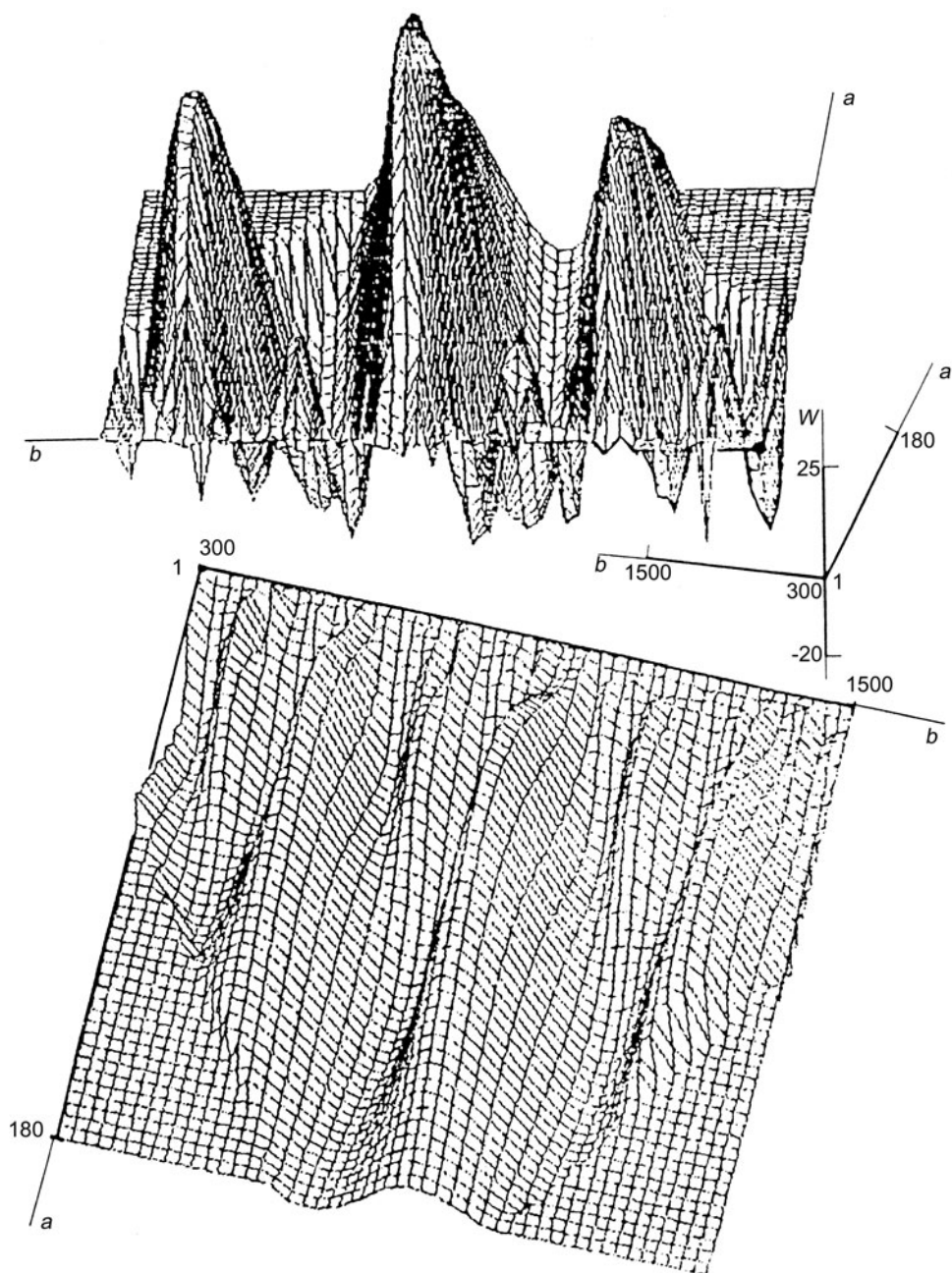


**Figure 2.30.** Three-dimensional pattern of the wavelet transform for time intervals from 300 to 1,500 days. The time series is given in [Figure 2.29](#) (from Astafyeva *et al.*, 1994a).



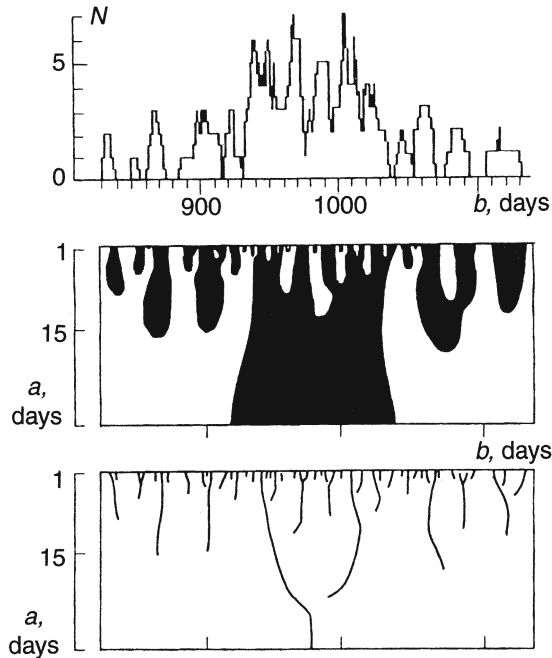


**Figure 2.31.** Time series of the intensity of global cyclogenesis ( $N$ ) (a), the pattern of the wavelet transform (b), and corresponding local maximum lines (c) for the time interval marked in Figure 2.29 (from Astafyeva *et al.*, 1994b).

As is well known, natural systems form as a result of the interactions of a number of processes that have their own energy, timescales, and spatial sizes, which can noticeably differ. Accordingly, the hierarchical structure of a natural system is connected with the presence of several distinctive temporal and spatial scales.

In this case, tropical cyclogenesis can involve, at least once, three timescales, which are characterized by their own particularities. So, on timescales of the order of 1–6 days a system of global cyclogenesis presents itself (on first approach) as an object of Poisson type (e.g., volume of ideal gas by fluctuations of density). The main role here is played by the kinetics of the processes of birth and death of the elements of a structured system. In other words, there are processes leading to the generation, evolution, and dissipation of individual TCs that behave like non-interacting Brownian particles under a restoring interaction (see Section 2.2.4).

When turning to timescales of the order of 1 month, non-linear interactions are included in the mechanism of global cyclogenesis operation. These interactions form sorts of bifurcation “forks” with the integration of scales. Non-linear interactions are most likely caused by internal feedbacks in the global ocean–atmosphere system. In turn, internal feedbacks can be arranged by circulating the particularities of atmospheric macroflows.

On half-yearly timescales the system of global tropical cyclogenesis is obviously linearized—we nearly have a harmonic signal. The maximums of global cyclogenesis activity are connected with significant activity in August and September in the northern part of the Pacific Ocean and in the Atlantic, as well as in February and March in southern parts of the Indian and Pacific Oceans. Analysis of the pattern of the wavelet transform shows that cyclogenesis in different hemispheres (north and south) has an independent individual nature.

For greater timescales (of the order of several years) we can expect a new generation of bifurcation “forks” as a result of interannual interactions, which can turn out to be “north” maximums of activity of global cyclogenesis in August and September (the influence of “south” maximums on such greater timescales is not known). The physical reasons for such correlations will become clearer when the external influences are known. It may be possible to explain this by cosmic factors: solar–terrestrial relationships and magnetosphere–troposphere interactions.

Analysis leads us to expect global tropical cyclogenesis to behave, strictly speaking, like a non-equilibrium system with elements of kinetics, diffusions, and non-linear interactions.

## 2.8 HIERARCHICAL STRUCTURE OF POPULAR SERVICE SYSTEMS

Considerable recent attention has been focused on using the principles and methods of non-linear dynamics to resolve geophysical, physicochemical, and socioeconomic problems (Polak and Michailov, 1983; Coniglio, 1987; Kadanov, 1993; Jin *et al.*, 1994, 1996; Diaz and Margraf, 1993; Holdom, 1998; Dubois, 1998; Jensen, 1998; Roberts and Turcotte, 1998; Chen and Dong, 1996; Chang *et al.*, 1996; Ivanitskii *et al.*, 1998; Branover *et al.*, 1999). By applying the approaches of dynamic chaos, some interesting and important aspects of such physical systems have come to light. First, it should be pointed out that new auto-model features and hierarchical structures in the functioning of such physical systems have been detected. In other words, the heart of the problem is the internal multiscale interaction by virtue of both its physical reasons and structural topological features.

Recently, Astafyeva and Sharkov (1998) have demonstrated the striking fact that the hierarchical structures of two distinctly different processes—global tropical cyclogenesis and railway traffic—are closely analogous. It is normal to expect many natural objects, consisting of independent individual elements with weak “distant” correlations, to possess a hierarchical structure similar to the one considered above and to comprise the “Poisson” area, non-linear and linear areas of scales of interactions. In addition to natural objects, transport service systems (e.g., land, air, and sea), multicomponent socioeconomic processes (e.g., the correlation between demand and marketing, or market-related economic models at different stages of capital accumulation) (Samuelson, 1961; Travis, 1964; Fischer *et al.*, 1988; Holdom, 1998; Schweitzer, 1997; Grassia, 2000; Ponzi and Aizawa, 2000) fit into this group.



As the analogy between natural and social phenomena is not only of scientific but also of public interest, it would be well to consider the work by Astafyeva and Sharkov (1998) in more detail.

### 2.8.1 Critical parameter of traffic services

One of the important aspects of the study of a transport system (in particular, of railway traffic) is the consequences of natural or artificial malfunctions (interruptions, delays, and cancellations) of the traffic. The time it takes to get traffic back to normality (i.e., the reconstruction or correction period) and restore the timetables of the traffic will, to a considerable extent, be defined by how the traffic service is managed, and the exact details of the reconstruction period will be a factor (though possibly not directly) of such management. Knowledge of the objectives of the reconstruction period (in particular, its inerrancy, degree of non-linearity, hierarchy, etc.) will adequately influence the transport system and, in particular, give more reliable forecasts about volumes of transportation which is one of the most important factors in the efficient functioning of the whole transport system.

Despite significant efforts by train services to keep records of malfunctions (i.e., disruptions of services) of the traffic, the reconstruction period, particularly its temporal features, remains little explored. This is bound, on the one hand, by the absence of corresponding mathematical facilities for studying complex hierarchical systems and, on the other hand, by the absence of a united approach to the mathematical description of the process of malfunctions of the traffic and of the reconstruction period.

The mathematical description proposed in Astafyeva and Sharkov (1998) allows us to use a very effective goal-directed approach to the study of the transport system of rail traffic on different timescales.

We use wavelet analysis to study the timescale characteristics of the process of malfunctions.

### 2.8.2 Forming a time series for the traffic process

Studying probabilistic features of a signal of complex structure is conducted with the help of the mathematical technique of the theory of random flows.

In accordance with this approach, data about the analyzed process can be accumulated as follows. Notwithstanding the detailed structure and track record of individual malfunctions, we shall present each traffic malfunction on the time axis as a pulse of single amplitude with duration equal to the lifetime of the event (in other words, the whole reconstruction period before restoration of the service). It is possible to show that this simplification—at first glance at least—will not introduce principal changes to the general picture of the phenomena. The number of pulses (i.e., indistinguishable events) received in a single time interval (for our experimental data this value was formed after half an hour) is a natural physical parameter, a sort of instant intensity of traffic malfunctions (in other words, a break in traffic intensity).

In the language of statistical procedures, this approach is identified as a method of calculating the number of events with provision for their lifetime (Cox and Lewis, 1966; Apanasovich *et al.*, 1988).

A mathematically proposed procedure for accumulation of a signal can be described as:

$$N(t) = \sum \Theta(t - t_i; \tau_i) \quad (2.40)$$

where  $N(t)$  is the “instant” intensity of traffic malfunctions (number of delays lasting half an hour); and  $\Theta(t)$  is the Heaviside limited function:

$$\Theta(t - t_i; \tau_i) = \begin{cases} 1, & t_i \leq t \leq \tau_i \\ 0, & t_i + \tau_i < t < \tau_i \end{cases} \quad (2.41)$$

where  $\tau_i$  is the time “existence” of the traffic malfunction (i.e., the length of disruption before restoration of the service; in other words, the rebuilding period);  $t_i$  is the time of origin of the traffic malfunction;  $t_i + \tau_i$  is the time of liquidation of the traffic malfunction. The sequence of pulses formed by a similar image with corresponding duration and amplitude is the integer casual time flow of indistinguishable events. In this way, we have presented the time sequence of malfunctions as a statistical signal of complex structure.

Of course, this approach is greatly simplified (e.g., the danger of the event, material losses, the degree of financing involved in the reconstruction period, and other particularities are not taken into account). However, we can show that such an approach (and we will demonstrate this below) allows us to ascertain the important statistical regularities of traffic malfunctions to reveal its temporal variability, hierarchical, round-robin, or other structured particularities of the process under study. Moreover, particularities of the signal structure can turn out to be highly different on different timescales. Raw data on disruption to the timetables were obtained from the systematized archive of the Federation Traffic Service (Russia).

### 2.8.3 Wavelet patterns of disruption to traffic intensity

Figure 2.32 presents a time series of the intensity of traffic malfunctions (i.e., disruptions to services) that occurred on the North Railway Service (Russia) from 1992 till the middle of 1995. The time series of analyzing data involves 61,135 samples of the intensity of traffic malfunctions obtained by sampling every 30 minutes (Figure 2.32 presents 7.5 hours of data from 15 locations). In the lower part of the drawing the beginning and duration of each season (winter, spring, summer, fall) are defined. As expected, the intensity of traffic malfunctions is described by the signal peculiar to the telegraphic process.

The time series of the intensity of traffic malfunctions demonstrate the following distinctive particularities. The most powerful maximums of the intensity of traffic malfunctions are observed at the end of winter/beginning of spring (March) and in the summer. This phenomenon is associated with complex weather conditions at the beginning of spring and intensive transportation during summer. The maximum intensity of traffic malfunctions occurred in January 1995 and deserves further

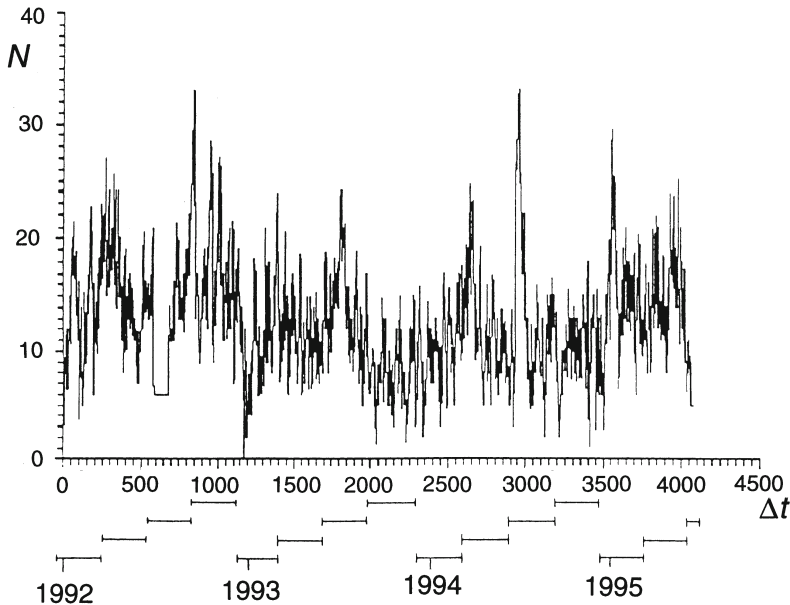


**Figure 2.32.** Time series of interruptions to railway traffic from January 1, 1992 to June 20, 1995 on a timescale ( $\Delta t$ ) equal to 7.5 hours. Straight line segments represent quarters of the given year (from Astafyeva and Sharkov, 1998).

attention. Looking at the process for 1992–1994 this extremum is shown to be typical. We should also point out that the reduction in the intensity of malfunctions in the autumn–winter period is general for the whole analyzed set.

More fine particularities and regularities of the temporal flows obtained are shown by means of wavelet analysis. [Figure 2.33](#) presents the results obtained by using the wavelet transform to describe the temporal set.

As already noted, the wavelet transform of a univariate signal provides a two-dimensional pattern in temporal and spectral spaces  $W(a, b)$ . On the axis of abscissas a change in time  $b$  is plotted and on the axis of ordinates the scale parameter  $a$  is presented (the scale decreases). To facilitate the collation of results, the time axes on [Figure 2.32](#) (for the raw dataset) and on [Figure 2.33](#) (for pictures of the factors of wavelet transforms) are alike. Dark areas on the pictures correspond to positive values of the coefficients of the wavelet transform and light areas negative values. The areas with different tones of gray reveal several ranges of the values of coefficients  $W(a, b)$ .

In [Figure 2.33a](#) the picture of factors of the wavelet transform is shown in such a range of scales as to compensate for the large-scale temporal dependence of the analyzing process. Here the scale changes every year. It is not difficult to see that the process demonstrates regular behavior on timescales from approximately 3 months up to 1 year (we call this range “large scale”). The round-robin annual cycle clearly stands out (particularly in the middle of the time range) with

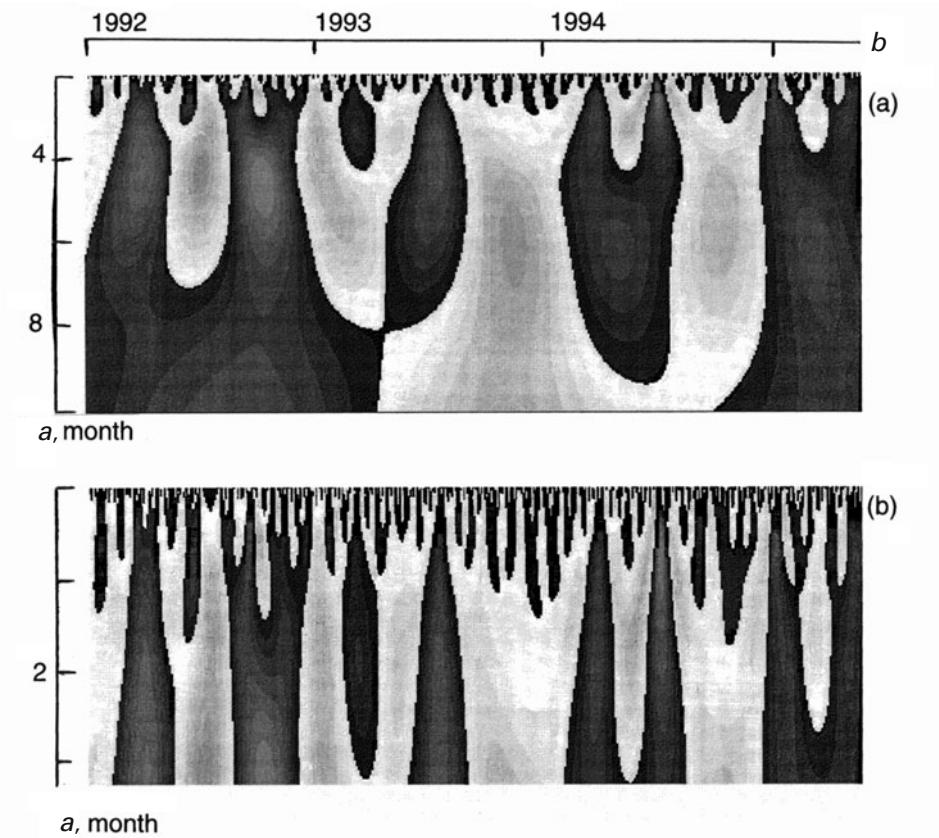


**Figure 2.33.** Wavelet transform two-dimensional patterns of a time series of railway traffic disruption (Figure 2.32) on timescales of up to 12 months (a) and up to 3.5 months (from Astafyeva and Sharkov, 1998).

intensity maximums in spring and summer and minimums in autumn and winter clearly defined.

In Figure 2.33b the small-scale part of the process (increased higher part of pictures shown in Figure 2.33b) is displayed using the most sophisticated treatment. Here the scale changes every 3 months for half of the months. We can see that the behavior of the process is sharply different from the large-scale one described above. A greater number of bifurcation “forks” are apparent, caused by non-linear internal mechanisms in the system on timescales of approximately 2 weeks up to 1 month (we call this range “average scale”).

We consider more detailed analysis of the data for the first half of 1995 may be particularly revealing. Figure 2.34 presents a time series of the intensity of traffic malfunctions for this period. The lower part of the drawing shows (as steps) the duration of months (in the analyzed range of time) from January to May and 20 days in June.

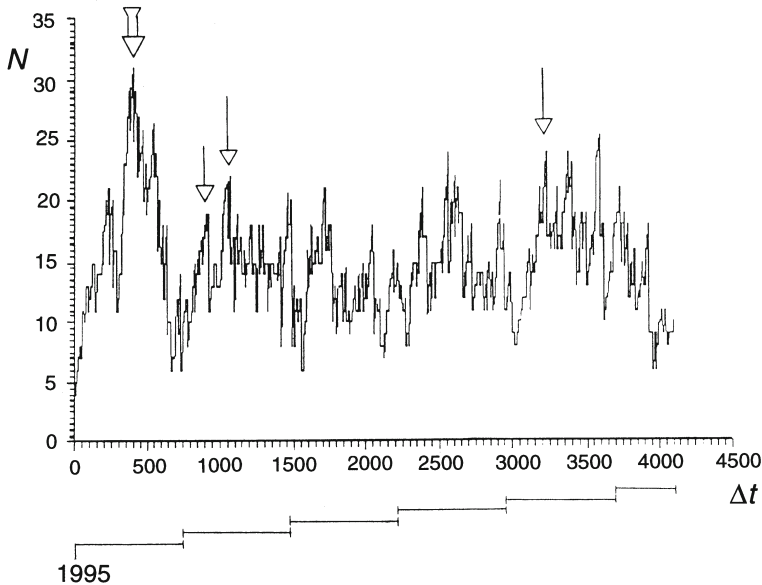


**Figure 2.34.** Time series of railway traffic disruption from January 1, 1995 to June 20, 1995 on a timescale ( $\Delta t$ ) equal to 1 hour. Straight line segments represent months of the given year (1995) (from Astafyeva and Sharkov, 1998).

Note that the data demonstrate the presence of intensity maximums of the process of traffic malfunctions of at least one of the two types. Maximums having an accumulative period (i.e., indicated by arrows in [Figure 2.34](#)) can be seen, as can the maximum time of relaxation (indicated by the double arrow).

[Figure 2.35](#) shows the pattern of the wavelet transform but this time with different scale values: here the scale changes every 1.5 months, whereas in [Figure 2.34b](#) it was every 11 days.

An important particularity of the process of traffic malfunctions follows from analysis of [Figure 2.35](#). There is a whole family of small-scale events with very short times of relaxation (short “memory”). On the picture of coefficients they are presented as separate black lines. Relaxation processes can take (on evidence from wavelet analysis) from a fraction of an hour up to several (2–3) hours (we call this range “small scale”). On the other hand, events with distant time correlations exist (conditionally called “long memory” they occur every 1.5 months or so, as shown in [Figure 2.33](#)).

#### 2.8.4 Possible physical models

The main result of using wavelet analysis to study the observational data of the process of railway traffic disruption is discovering the complex hierarchical time structure of the initial process. This allows a more goal-directed approach to

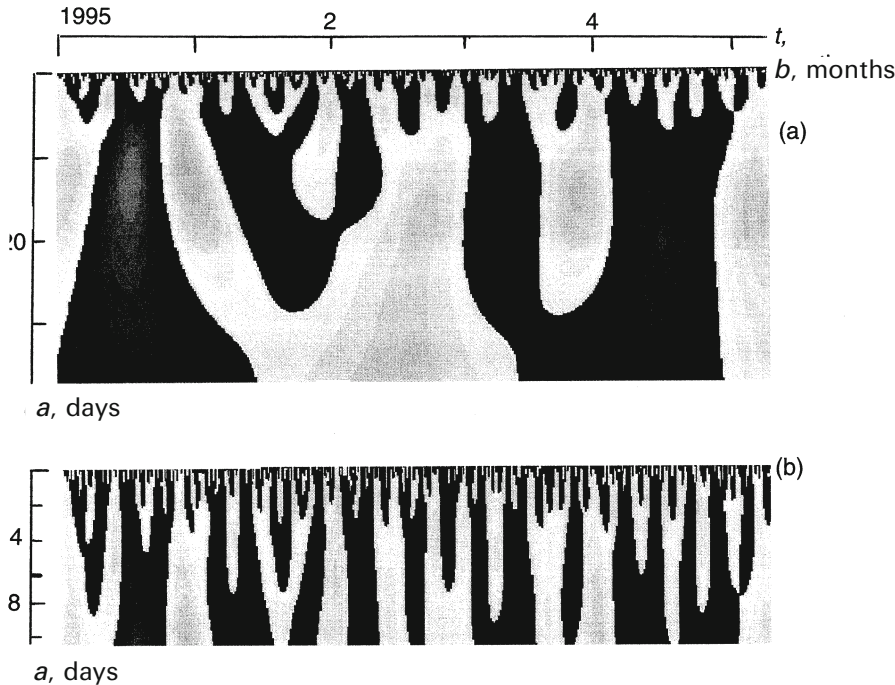


**Figure 2.35.** Wavelet transform two-dimensional patterns of a time series of railway traffic disruption (Figure 2.34) on timescales of up to 1.5 month (a) and up to 11 days (b) (from Astafyeva and Sharkov, 1998).

forming stochastic models of the process of traffic malfunctions (e.g., we can separate out the influence of technical, economic, and management factors that affect one or more particularities of the reconstruction period).

As is well known, the hierarchical structure of complicated systems is connected with the system having several different timescales, on the one hand, and having non-linear interactions affecting the time correlations of different scales, on the other hand.

As for the intensity of traffic malfunctions, we can choose at least one of three ranges of timescales, which are characterized by their own physical particularities. So, on small timescales of the order of several (2–3) hours the system of traffic malfunctions presents itself as a Poisson-type physical object (with independent events). Broadly speaking, this would be expected, because the reasons causing individual traffic malfunctions on these timescales clearly have no correlation with the traffic malfunction itself. In other words, the processes leading up to the events occurring (i.e., traffic disruption), their changes, and liquidations (i.e., the reconstruction period) in each concrete event behave like non-interacting Brownian particles in spring interaction models. For these timescales we can use the model of Brownian motion to move the particles from the viscous ambience into the system

of finite sizes. The process is described by the well-known one-dimensional Langevin equation (Nicolis and Prigogine, 1977; Klimantovich, 1982; Polak and Michailov, 1983).

In the considered event it is necessary to note that a very quick reconstruction period for suppressing the majority of events exists. This can be a quantitative criterion of working a managerial system on primary levels.

When we consider average timescales (from 5–10 days up to a month) in the physical mechanism of how traffic malfunctions operate, we include the non-linear modes of operation of the managerial system, which refines the reconstruction period of traffic malfunctions. The analysis of wavelet diagrams shows non-linear modes forming bifurcation “forks” as timescales integrate. This can be interpreted as timescale integration of interactions in the managerial system. Most likely this occurs because of the presence in the managerial system of non-linear feedbacks which “work” at highly decelerated rates in both space and time.

On greater timescales (from a month up to a year) the physical system of traffic malfunctions is clearly linearized and presents itself almost as a harmonic signal. The activity maximums of this process prevail at the beginning of spring and summer every year.

The limited length of the time series does not allow us to pronounce on larger scales (e.g., interannual interactions) with any degree of confidence. However, it is highly probable that the interannual interaction (and connected bifurcation “forks”) can be allied to standing management procedures (orders, instructions, etc.).

It follows from this that the process of traffic malfunction is a non-equilibrium system with elements of kinetics, diffusions, and non-linear interactions. On different timescales the sources of traffic malfunctions (disruption) and their liquidations (service restoration) are naturally determined by absolutely different physical processes: external influences (basically artificial) on timescales of sampling raw data (0.5 hour); inadequate management procedures on timescales of several hours up to 10 days; natural factors (floods, precipitation) and permanent management procedures and seasonal public–economic particularities (e.g., increasing intensity of transportation in summer) on timescales of several months up to a year.

On a broad range of timescales such factors as technical equipment of the railway network and non-linear feedback in the managerial system should be considered. We believe that the influence of these factors can be studied using wavelet analysis of the data for different railroads on different ranges of time and sampling.

## 2.9 MAGNETOSPHERE PROCESSES AND GLOBAL TROPICAL CYCLOGENESIS

The tropical zones of the global atmosphere–ocean system play a crucial role in the dynamics and evolution of synoptic and climatic meteorological processes on Earth. In this connection, any outer (Earth troposphere) interaction bringing additional influence on turbulent exchange in the tropical ocean–atmosphere system invites close investigation. Over the past 20 years, the findings of investigation into



solar–terrestrial linkages demonstrate that statistical plausible components of tropospheric processes considered on the synoptic scale result from solar activity (Loginov, 1973; Danilov *et al.*, 1987; Raschke and Jacob, 1993; JSTC, 1995; King, 1999; WMO, 1999; Svensmark and Friis-Christensen, 1997; Bochnicek *et al.*, 1999; Gabis and Troshichev, 2000).

On the other hand, it is interesting to note that it was long proposed (at the end of the 19th century) that cyclic recurrences in solar activity can affect the frequency of individual TC generation in various ocean basins (see references in Tchijsky, 1976 and the historical review in Elsner and Kara, 1999). Similar work has been carried out recently. In substance, the main experimental procedure in these investigations is called “the method of the superposition of epochs” (Tchijsky, 1976). Despite this approach being used over a protracted period of the last 100 years, it is not mathematically valid. Alternatively, the results of an investigation into the cross-correlation between sunspots and North Atlantic hurricane activity (e.g., see fig. 10.15 in the book by Elsner and Kara, 1999) do not contain estimates of confidence levels of the correlation values observed. Thus, rigorous treatment for statistical procedures is lacking. Because of this, final conclusions cannot be reached re-garding the relationship between longer term solar activity and tropical cyclogenesis.

As for global tropical cyclogenesis, such observational attempts have long not met with success. This is primarily due to the fact that comprehensive data on global tropical cyclogenesis are lacking (see Chapter 5). It is only over the past 10 years that progress has been made in developing comprehensive datasets on global tropical cyclogenesis. This makes possible more solid investigations of solar–terrestrial links with “fast” (on the timescale of a day) interactions.

On the basis of what is currently known about climatic interactions, Bochnicek *et al.* (1999) point to the necessity of studying extraterrestrial–weather linkages on substantially shorter time intervals (i.e., a few days).

Gdalevich *et al.* (1994) present experimental evidence for the possible existence of new physical mechanisms providing “fast” interconnections between magnetosphere variability and the time evolution of global tropical cyclogenesis.

In this section, global tropical cyclogenesis is represented in simple form as a discrete Markov (“telegraph”) process (see Section 2.2). By the “quantitative parameter of the activity of global tropical cyclogenesis” we mean the number of operating TCs in the World Ocean per day taking due account of the lifetime of individual TCs. So, the signal structure is the integer-numbered random time series of non-distinctive events (random impulse regime) (Figure 2.36). The characteristic, thus defined, determines the energy interaction in the ocean–atmosphere system and may be considered as the geophysical parameter needed to reveal the stability of the global ocean–atmosphere system (for the tropics).

Geomagnetic  $D_{st}$  variation is the global reduction in intensity of  $H$ -components in the terrestrial magnetic field, registered simultaneously by equatorial stations around the Earth. In accordance with the developing physical concept (see below), the quantitative features of geomagnetic variation reviewed for this study will be an integral of variation intensity within the current day and so  $W = \int_{\Delta t} \Delta D_{st} dt$  where



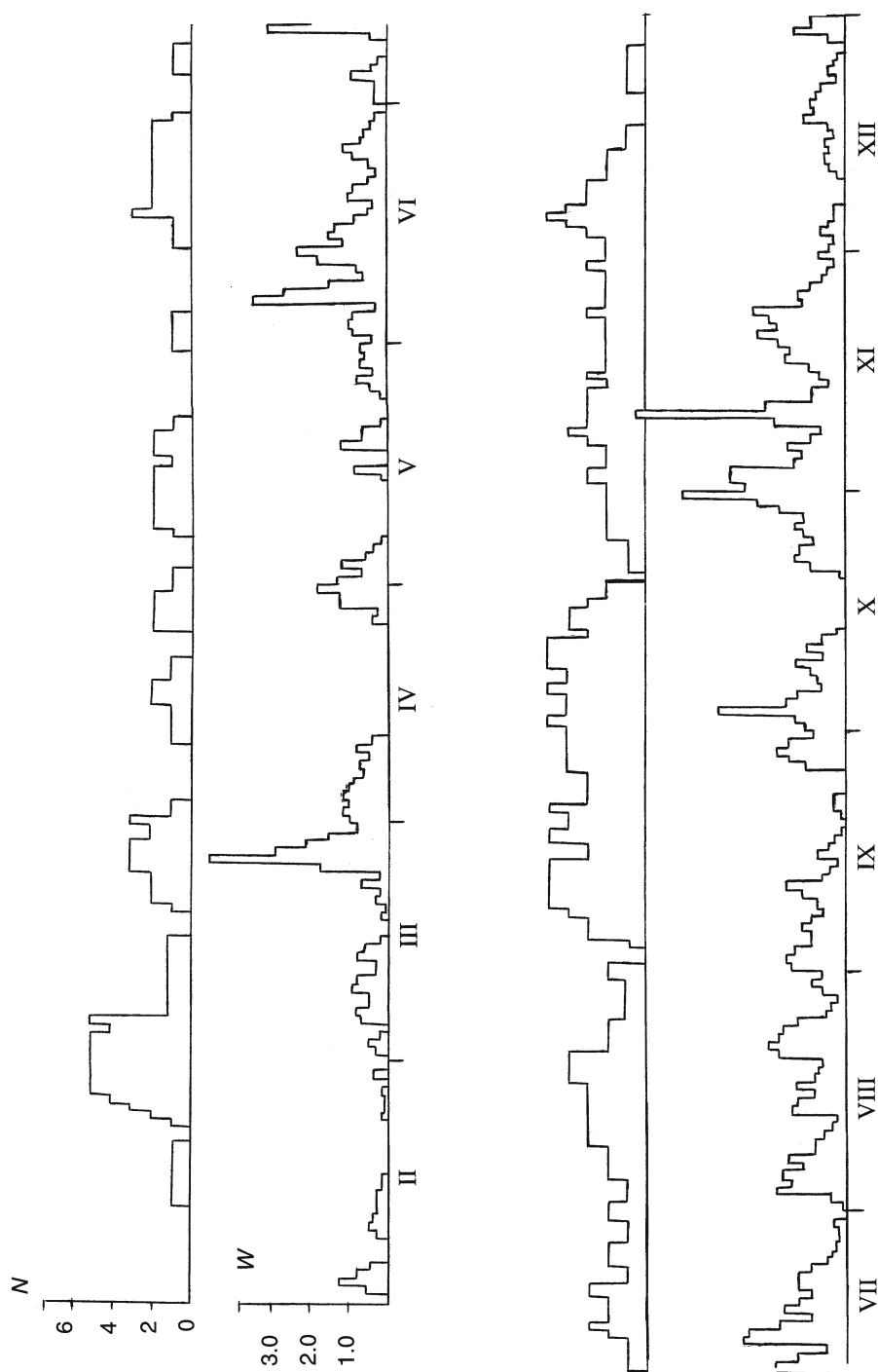


**Figure 2.36.** Annual (February–December 1991) time series of the intensity of global tropical cyclogenesis ( $N$ ) and of the intensity of magnetospheric variability ( $W$ ) (from Gdalevich *et al.*, 1994).

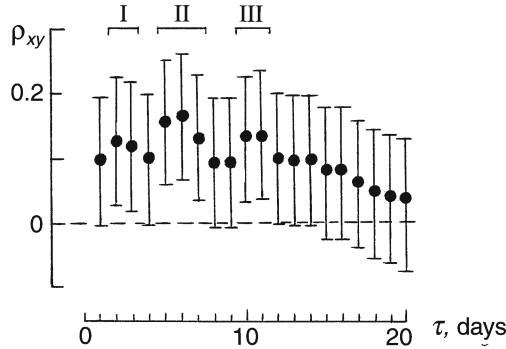


**Figure 2.37.** Cross-correlation coefficient  $\rho_{xy}$  of the intensity of magnetospheric variability and of the intensity of global tropical cyclogenesis. The  $\log(\tau)$  is in days. Vertical line segments are 95% confidence levels. Black dots are sampling values of the normalized cross-correlation coefficient. The sample run is 365 days (Gdalevich *et al.*, 1994).

$\Delta D_{st}$  is the negative contrast between the non-perturbed and terrestrial magnetic field outraged by the condition of  $H$ -components of the terrestrial magnetic field; and  $\Delta t = 24$  hours. In the physical sense  $W$  can be interpreted as a value proportional to the energy in the unit of time (power) of a geomagnetic storm.

The respective time series of parameter  $W$  are shown in Figure 2.36. Analysis of Figure 2.36b reveals the presence of all stages of a geomagnetic outbreak from the moment the main phase storm develops (“splash” of  $W$ ) to phases of reconstruction (extended “tail” of the disturbance).

Experimental material was subjected to cross-correlation processing with a timestep (timelag) of 1 day, and, on the strength of supposed physically stipulated relationships between processes, temporal writing of the integral  $W$  “was shifted” onwards. Sampling values of the normalizing factor of cross-correlations with timelags from 1 up to 20 days are shown in Figure 2.37.

Statistical analysis of the validity of this probabilistic procedure, connected with the calculation of cross-correlations, was considered using two (generally speaking, independent) approaches. One considered the building of confidence-level intervals using a normalizing Fisher transformation with confidence-level probability of 0.95% (level of value 0.05). The other checked the truth of these statistical (“zero”) hypotheses:  $H_0[\rho_{xy} = 0]$ , where  $\rho_{xy}$  is the truth factor of cross-correlations under different time shifts (from 1 up to 20 days).

The results of the first approach are shown in Figure 2.37 in the construction of confidence-level intervals of 0.95% for the truth factor value  $\rho_{xy}$ .

Figure 2.37 shows there are three time shifts (2–3, 5–7, and 10–11 days) when confidence-level intervals do not include  $\rho_{xy} = 0$  and, hence, are responsible for the difference of  $\rho_{xy} = 0$  in this temporal range from zero.

The second approach (i.e., checking the truth of hypothesis  $H_0$ ) ends by building a selective function  $t = r_{xy}(n - 2/1 - r_{xy}^2)^{1/2}$ , where  $r_{xy}$  are the sampling values of cross-correlations, and  $n$  is the full volume of samples. Moreover, sampling statistics

$t$  comply with the Student  $t$ -distribution with  $f = n - 2$  degrees of freedom. Evaluation of selective functions  $t$  for shifts from the areas specified above gives a value of  $t$  equal to 2.7 here with the critical value of statistics of  $t_{0.05;364} = 196$  (in the  $\alpha = 0.05$  and  $f = 364$  forms). We can see that  $t > t_{0.05;364}$  and the  $H_0$  hypothesis for specified temporal shifts must be rejected and, hence, the empirical value of factor cross-correlations differs substantially from zero. On the other hand, evaluation of functions  $t$  for other time shifts satisfies the inequality  $t < t_{0.05;364}$  and, hence, hypothesis  $H_0[\rho_{xy} = 0]$  can be accepted. In other words, deflections of the empirical factor  $r_{xy}$  from zero have a purely random nature.

This result can be interpreted as follows. During geomagnetic storms in the magnetosphere, energy ( $10^{23}$  erg) is released. This energy disperses on creation or reinforcement of the recirculating current—heating Arctic regions and exciting different waves. Variation of the magnetosphere current (World geomagnetic storms) disturbs ionospheric layers, which, in turn, generate infrasonic waves reaching the troposphere and disrupting the geostrophic balance. This can greatly transform spatial features of mesoscale turbulence (intensity and helicity) and, in accordance with the concept of the vortical dynamo (Chapter 4), will change the rate of generation and time of operation of tropical structures. Note that there may well be more than one interaction chain. Thus, it causes the presence of several timescales of efficient interactions. These considerations allow us to reach the non-trivial conclusion of the likely existence of a stochastic physical mechanism that is responsible for the generation of TDs by these teleconnections.



<http://www.springer.com/978-3-642-13295-7>

GLOBAL TROPICAL CYCLOGENESIS

Sharkov, E.A.

2012, XLIV, 604 p., Hardcover

ISBN: 978-3-642-13295-7